frontiers | Frontiers in Earth Science

TYPE Original Research
PUBLISHED 16 April 2025
DOI 10.3389/feart.2025.1549274



OPEN ACCESS

EDITED BY
François Fournier,
Aix-Marseille Université, France

REVIEWED BY
Luigi Jovane,
University of São Paulo, Brazil
Simon Mitchell,
University of the West Indies, Jamaica

*CORRESPONDENCE
Johanset Orihuela,
jorih003@fiu.edu

RECEIVED 20 December 2024
ACCEPTED 20 March 2025
PUBLISHED 16 April 2025

CITATION
Orihuela J, Melinte Dobrinescu MC and Maurrasse FJ-MR (2025) Characterization of the Weissert oceanic anoxic event in lower Cretaceous limestones of the Guaniguanico terrain, Sierra de los Órganos, Western Cuba. *Front. Earth Sci.* 13:1549274. doi: 10.3389/feart.2025.1549274



# Characterization of the Weissert oceanic anoxic event in lower Cretaceous limestones of the Guaniguanico terrain, Sierra de los Órganos, Western Cuba

Johanset Orihuela[1]*, Mihaela C. Melinte Dobrinescu[2] and Florentin J.-M. R. Maurrasse[1]

[1]Earth and Environment, Florida International University, Miami, FL, United States, [2]National Research and Development Institute for Marine Geology and Geoecology, Bucharest, Romania

The breakup of Pangea started in the Late Triassic when the new Tethyan domain developed into diverse sub-basins which began as shallow-water passive margins progressing into deeper foreland basins. Our study presents a high-resolution chemostratigraphic assessment of Lower Cretaceous organic-rich hemipelagic limestones from Sierra de los Órganos, Pinar del Río, Western Cuba, to assess the redox conditions in the Pro-Caribbean with respect to the dominant coeval global forcing factors in the Valanginian stage. To characterize presumed deoxygenation conditions associated with the Cuban deposit high-resolution lithostratigraphy, carbon geochemistry, trace element analysis, and biostratigraphy were performed on a ~3-meter interval at the base of a 30-meter quarry outcrop located near the city of Pons. The succession consists of alternating thin grayish black (N2) chert-bearing carbonaceous marlstones and medium dark gray (N5) limestones. The carbonaceous marlstones yield a total inorganic carbon content (TIC) ranging from 44.7% to 77.3% and total organic carbon content (TOC) fluctuates between 3.5% and 10.82%. By contrast, the medium dark gray limestones have TIC values exceeding 90% and an average TOC of 2.3%. Petrographic analyses, radiography, and scanning electron microscopy imaging (SEM-EDS) revealed an isotropic fabric throughout the lighter micritic limestone, with a bioturbation index (BI) greater than 3, whereas the carbonaceous layers show BI consistently less than 2 and include single framboids and bundles of cubic pyrite. The carbon isotopic (δ13Corg) analysis gives an average value of approximately −27.3‰, with a main peak reaching around −25.56‰, corresponding to a ~1.7‰ excursion. This carbon isotope excursion (CIE) correlates with the late Valanginian nannofossil subzone NK3B, as indicated by the presence of Calcicalathina oblongata and the disappearance of Rucinolithus wisei. The occurrence of calpionellids Tintinnopsella carpathica and Calpionellites cf. darderi supports the correlation up to the earliest Hauterivian. Enhanced values of redox-sensitive trace elements (V, Ni, Cr, Mo, Tl, U, and S) correlative with highest TOC suggest severe deoxygenation conditions during the δ13Corg CIEs archived in this section. These excursions also coincide with increased enrichment of major elements (Al, Si, Li, and Ti), thus indicative of enhanced terrigenous fluxes at these intervals. The results provide robust evidence supporting the occurrence of distinct deoxygenation conditions in the deposits of Western Cuba originated from the Proto-Caribbean Seaway-Basin.

They are coeval with the global Valanginian Weissert oceanic anoxic event. Thus, these results significantly enhance our comprehension of oxygen-deficient conditions as archived in this sub-basin and linked to the global event.

KEYWORDS

**Weissert OAE, organic matter, terrigenous input, RSTEs, dysoxia, proto-caribbean, ocean anoxic event**

## Introduction

The Cretaceous sedimentary archive includes widespread deposition of discrete intervals of organic-rich strata indicative of significant oceanic oxygen depletion coined oceanic anoxic events (OAEs) (Schlanger and Jenkyns, 1976; Weissert, 1979; 1981; Scholle and Arthur, 1980; Arthur and Premoli Silva, 1982; Jenkyns, 1980; 2012; 2018). These events reflect major disruptions in the global carbon cycle, often marked by pronounced carbon isotope excursions (CIEs), increased bioproductivity, and profound ecological impacts on marine biota (Scholle and Arthur, 1980; Arthur et al., 1985a; b; Weissert, 1989; Weissert et al., 1985; Percival et al., 2025).

The hallmark of these perturbations is a characteristic worldwide carbon isotopic signature (e.g., Weissert et al., 1998; Lini et al., 1992; Jarvis et al., 2002; Herrle et al., 2003; Gröcke et al., 2005; Bodin et al., 2007; González-Arreola and Barragán, 2007; Michalík et al., 2012; Thöle et al., 2020; Cavalheiro et al., 2021). These events simultaneously affected marine biota, leading to faunal turnovers and extinctions, highlighting their profound ecological impacts (Bornemann and Mutterlose, 2008; Price et al., 2020). As the resulting lithologic sequences encapsulate the overall biochemical dynamic states of ancient oceans, they provide invaluable insights into marine ecosystem response under such environmental fluxes.

Hence, the Weissert Event which is the first recorded major carbon cycle perturbation of the Cretaceous is also marked by a significant CIE associated with important marine crises (Lini et al., 1992; Channell et al., 1993; Erba et al., 2004; Erba and Tremolada, 2004; Weissert et al., 1998; Weissert et al., 2008; among others). The event reflects an interval of intensified organic carbon burial linked to variations in enhanced productivity, hyperthermal conditions, and nutrient fluxes (e.g., Erba et al., 2004; Weissert et al., 2008; Gréselle et al., 2011; Kujau et al., 2012; 2013). Its estimated duration ranges from ~2 million years (Ma) to ~5 Ma, based on a combination of biostratigraphic and isotopic data (Erba et al., 2004; Kujau et al., 2012; Martinez et al., 2015; Martinez et al., 2023; Aguirre-Urreta et al., 2017a; Aguirre-Urreta et al., 2017b; Percival et al., 2023; Percival et al., 2025).

It is argued that the onset of the Weissert event could be attributed to volcanic outgassing from the Paraná-Etendeka large igneous province (LIP) and increased oceanic crust production during Gondwana's fragmentation, contributing to atmospheric $pCO_2$ accumulation and heightened global nutrient supplies (Lini et al., 1992; Kerr, 1998; Larson and Erba, 1999; Leckie et al., 2002; Weissert and Elba, 2004; Föllmi, 2012; Charbonnier et al., 2016; Charbonnier et al., 2017; Charbonnier et al., 2020; Charbonnier et al., 2020; Cavalheiro et al., 2021). However, recent data suggest that the Weissert OAE and the onset of the Paraná-Etendeka LIP are not strictly synchronous (Rocha et al., 2020; Percival et al., 2023; Percival et al., 2025). Furthermore, sedimentary records indicate that these events triggered synchronous geochemical responses, but divergent sedimentary facies across different marine environments. As recognized in the published literature, in marine realms the Weissert Event is associated with diminished carbonate deposition and a crisis in carbonate-producing biota (e.g., Erba, 1994; Erba et al., 2004), while terrestrial records suggest shifts in the flora and intensified weathering (Price et al., 2000; Price et al., 2020; Gröcke et al., 2005). Such diverse responses highlight the complex interplay of global forcing factors and regional conditions that may modulate oceanic chemistry, climatic dynamics, and biological ecosystems in different basins, as preserved in the geological record (Harris et al., 1993; Fo¨llmi et al., 1994; Weissert et al., 1998; Weissert, 2019; Percival et al., 2023; Percival et al., 2025).

However, significant knowledge gaps remain to be further elucidated concerning the expression of the Weissert event in different regions such as the Proto-Caribbean area in the westernmost Tethys. So far only a limited sedimentary succession is known from ocean drilling sites in the Gulf of Mexico (e.g., Patton et al., 1984; Cotillon and Rio, 1984; Lini et al., 1992; Bornemann and Mutterlose, 2008; Phelps et al., 2014), land outcrops in northwestern Mexico (Omaña et al., 2017), Cuba (Orihuela and Maurrasse, 2022), and northern Colombia (Silva-Tamayo et al., 2016). To further increase our knowledge of the event in the Proto-Caribbean the outcrop of the "La Lata" quarry section in the Sierra de los Órganos, western Cuba, offers a unique sedimentary succession to pursue this goal. Our study will help clarify how the local biogeochemical processes influenced regional organic matter preservation within the broader global context of the event. The results provide a high-resolution multiproxy data to characterize a Valanginian marine succession at the La Lata quarry (Figures 1A–C), which is a geologic terrane developed within the Proto-Caribbean Basin-Seaway since the Jurassic (Iturralde-Vinent and MacPhee, 1999; Iturralde-Vinent and Pszczółkowski, 2021). New lithologic and geochemical analyses, including carbon geochemistry (TOC, TIC, $\delta^{13}C_{org}$), SEM with EDS, major and redox-sensitive trace element analyses, together with composition and petrographic observations highlight regional responses to Valanginian carbon cycle perturbations and further our understanding of enhanced organic matter preservation in the Proto-Caribbean Basin during this stage (Orihuela and Maurrasse, 2022; Orihuela et al., 2023a; Orihuela et al., 2023b; Orihuela et al., 2024a; Orihuela et al., 2024b).

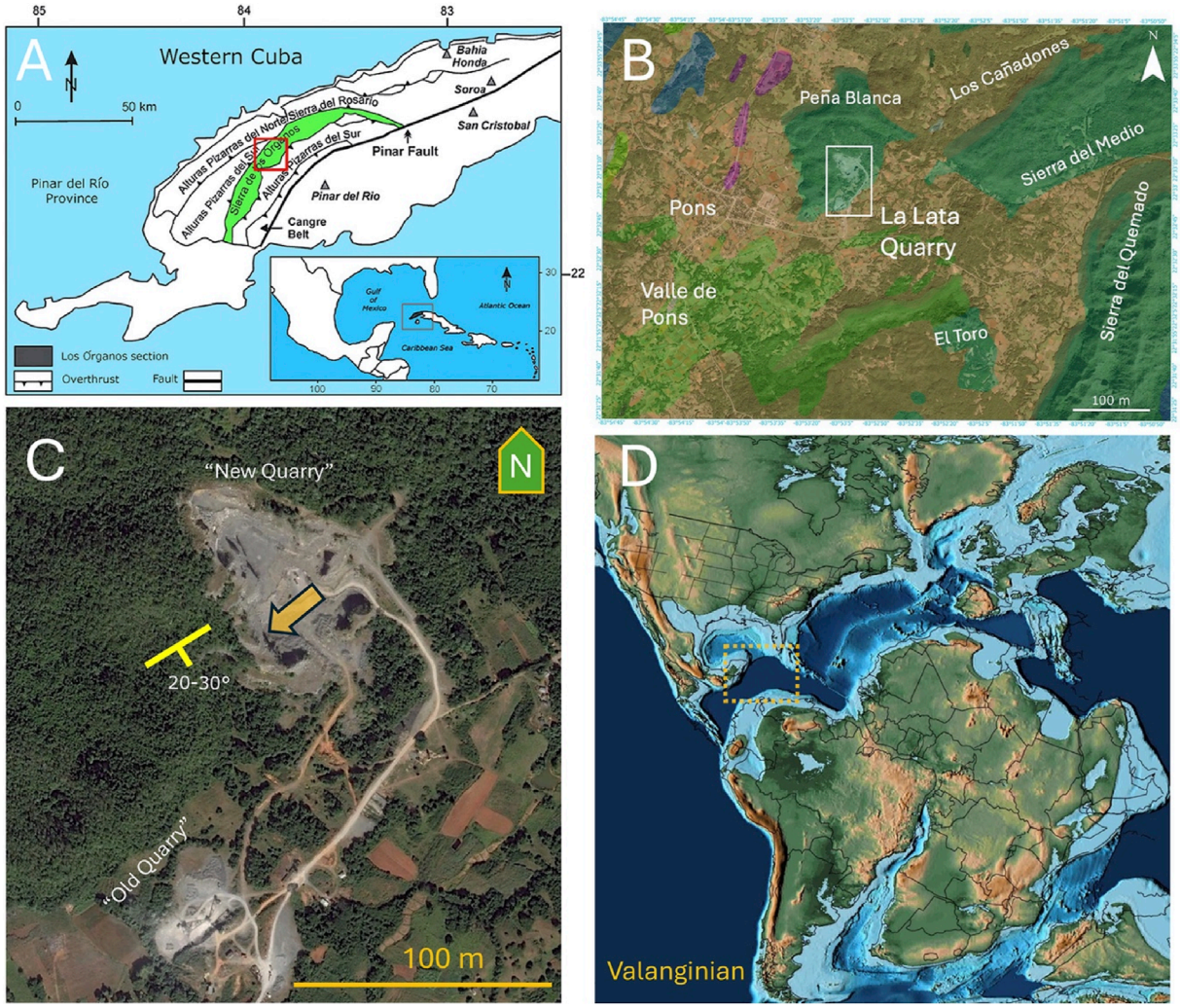


FIGURE 1
**(A)** Map of western Cuba showing the Guaniguanico terrains, with the Sierra de los Órganos highlighted in green. The study area is marked by a red square [map modified from López-Martínez et al. (2013)]. **(B)** Google Earth satellite image showing physiographic features around La Lata Quarry and the Valley of Pons (Valle de Pons). Geological formations are color-coded: the Pons Formation type section and outcrops are shown in light green, the Guasasa Formation (including the older Infierno Member, now classified within the lower Pons Formation) in dark green, ophiolite exposures in magenta, Jurassic terrains in blue, and younger Moncada Formation in uncolored areas (see Figure 2 for further details). **(C)** Satellite view showing the locations of the "new" and "old" La Lata quarries near Pons, with annotated dip and strike directions. The primary sample collection site is indicated by an arrow on the southwestern quarry wall. **(D)** Paleogeographic map illustrating the Proto-Caribbean Basin during the Valanginian stage (Early Cretaceous), with the estimated depositional area of Los Órganos sediments marked by an orange dotted square. Map adapted from Scotese PaleoAtlas v3 (2016).

## Geological setting

The Sierra de los Órganos is the largest of the geological stack units that make up the Guaniguanico terrain in Western Cuba (Iturralde-Vinent, 1994). This terrain, often referred to as the "Guaniguanico megaunit," consists of five primary tectonic sheets, each with distinct stratigraphic components, one belt of which is the Sierra de los Órganos (Hatten, 1957; 1967; Rigassi-Studer, 1963; Khudoley and Meyerhoff, 1971; Pardo, 1975; Piotrowska, 1976; Piotrowska, 1978; Piotrowska, 1993; Pszczółkowski, 1971; Pszczółkowski, 1978; Pszczółkowski, 1987; Pszczółkowski and Myczyński, 1999; Pszczółkowski and Myczyński, 2003; Draper and Barros, 1994; Cobiella Reguera, 2000; Cobiella Reguera, 2008; Pszczółkowski and Myczyński, 2003; 2010; Pérez et al., 2011; Iturralde-Vinent and Pszczółkowski, 2021) (Figure 1A).

Tectonically the Sierra de los Órganos comprises several stacked fold-thrust belt units identified as Norther and Southern Rosario and La Esperanza (Figure 1A). These nappes are the result of tangential, piggy-backed unit successions, developed during the tectonic evolution of the region since the Eocene (Danilewski, 1972; Piotrowska, 1976; 1978; 1993; Draper and Barros, 1994). Lithologically the Sierra de los Órganos includes a significant geological record of the complex sedimentary and tectonic history of the Proto-Caribbean region. It thus gives a semi-complete documentation of the evolution of the basin from the post-Pangea breakup and the subsequent formation

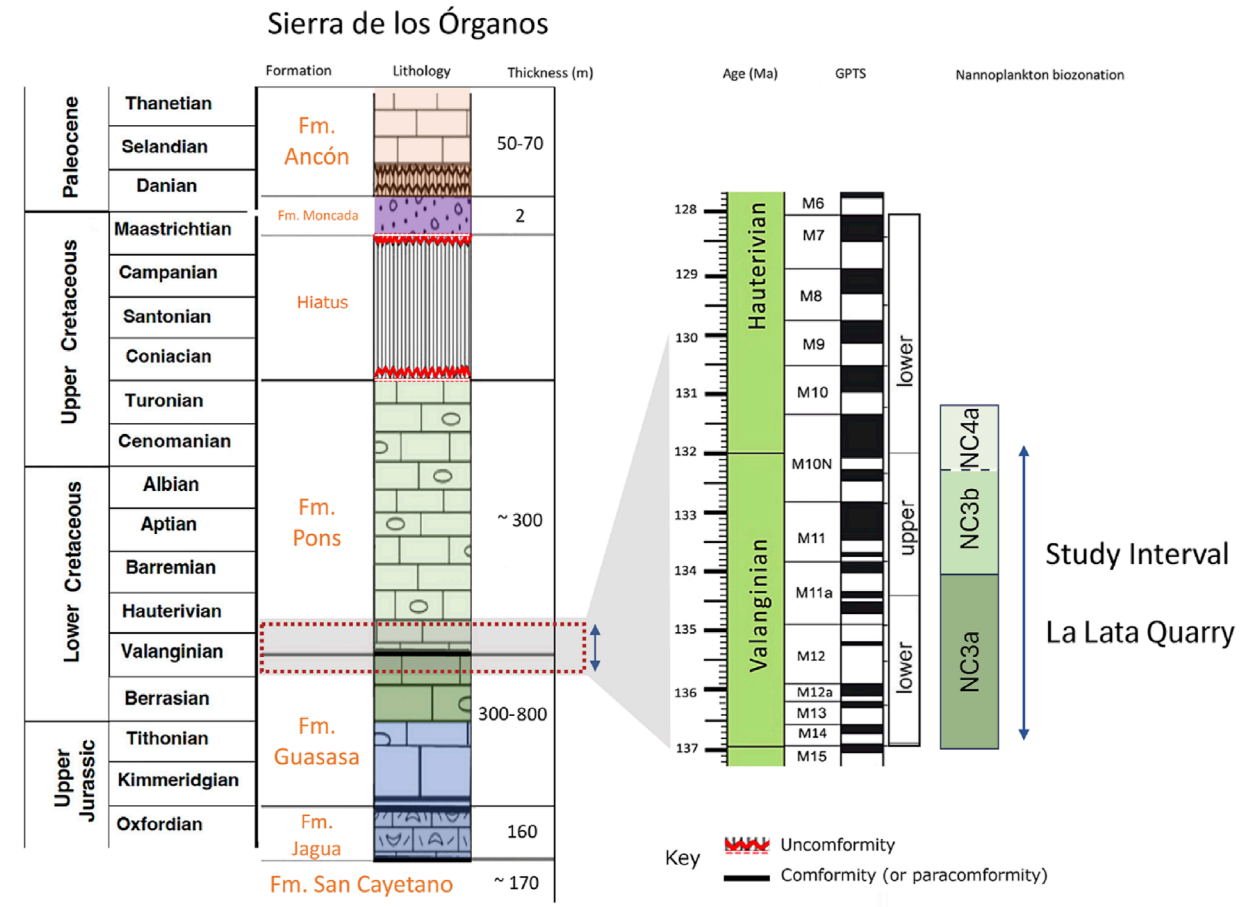


FIGURE 2
Generalized stratigraphy of the Sierra de los Órganos, showing lithostratigraphic units, formation thicknesses, and the geomagnetic polarity time scale (GPTS) from Ogg et al. (2016) and Cavalheiro et al. (2021) with formation data from Vázquez Torres et al. (2020). The study interval at La Lata Quarry is highlighted within the Valanginian to Hauterivian stages. Note that based on this schema, our studied section can include the transition between the Guasasa and Pons formations.

of a passive margin to foreland basin (e.g., Draper and Barros, 1994; Iturralde-Vinent et al., 2008; Pszczółkowski and Myczyński, 2010; Pindell et al., 2021a; Pindell et al., 2021b). The succession at Sierra de los Órganos includes the Guasasa Formation (upper Oxfordian–Valanginian) and Pons Formation (late Valanginian–Turonian) which together are reported to originate either along the Yucatan or the Bahamian passive margins and were later accreted into the Cuban arch during the Eocene as shown in Figure 2 (Pszczółkowski, 1978; Pszczółkowski and Myczyński, 1999; Pszczółkowski and Myczyński, 2003; Cobiella Reguera, 2000; Pszczółkowski and Myczyński, 2010; Pszczółkowski et al., 2013; Iturralde-Vinent et al., 2016).

## Site location and previous works

Our study site is located at the "La Lata" quarry, approximately 1 km northeast of the city of Pons, at the eastern terminus of the Sierra de Pan de Azúcar, specifically at an elevation known locally as Peña Blanca Alta (Figure 1B). This elevation consists of sedimentary rocks from the Pons Formation (Figure 2), which was originally classified as part of the Infierno Member of the Guasasa Formation (Pszczółkowski et al., 2013; Álvarez and Bernal, 2013). As such, it is considered an older, local overriding structure (Hatten, 1957; Rigassi-Studer, 1963). The Pons Formation, which is confined to the Sierra de los Órganos belt, is composed of grey to black micritic limestones with intercalated chert layers (Hatten, 1957; Herrera, 1961; Pszczółkowski et al., 1975; Piotrowska, 1976; Piotrowska, 1978; Álvarez Sanchez, 1981; Pszczółkowski et al., 2013) and is not expected to contain calpionellids (Pérez et al., 2011).

Previous biostratigraphic analysis of samples from uppermost levels at the La Lata quarry revealed a foraminiferal assemblage characteristic of the *Globigerinelloides algerianus* and *Hedbergella trocoidea* Zones. Reported calcareous nannoplankton includes *Nannoconus bonetii*, *N. colomii*, and *N. elongatus* indicative of a late Valanginian to late Aptian age (Pérez et al., 2011; Pszczółkowski et al., 2013). Thus, the biochronology of the succession permits to further explore the relationship between the dark limestones and their potential interrelation with the Valanginian oceanic anoxic event coined the "Weissert Event" (Erba et al., 2004).

The dark limestones of the Pons Formation have been generally interpreted as deep-water environments of oxygen-deficient to anoxic conditions based on their coloration (Hatten, 1957; Herrera, 1961; Pszczółkowski et al., 1975; 2013; Piotrowska, 1976; Pszczółkowski and Myczyński, 2010; Pérez et al., 2011). The presence of black "shales" and limestones, along with preliminary geochemical findings, suggested a high total organic carbon (TOC) content in the Pinar 1 core (Pendás-Amador, M., 2007), support the potential for enhanced organic matter preservation in the archive of the Sierra de los Órganos (Castro-Alfonso, 2015). However, published studies on organic-rich rocks in Cuba are still extremely limited (Moretti et al., 2003; Magnier et al., 2004), and many of these assumptions, some based on coloration alone, lack comprehensive geochemical data to support the interpretations. In this study, we present a detailed geochemical characterization of the Pons Formation outcrop at the La Lata quarry to further our understanding of the geological history of the Proto-Caribbean and its relevance to global Cretaceous oxygen-deficient conditions and carbon cycle perturbations during greenhouse periods.

# Methodology

## Field sampling

The lower 3-meter studied portion of the "New Quarry" section includes samples from the zero datum (at ~ 130 m above sea level) up to the first 2.61 m of a ~30 m, quarry cut wall section exposed to the southeast (Figures 1C, 3). The strike was 135° SE, with an undulating dip of 22–25°.

Overall, eighty ($n$ = 80) samples were collected in June 2015 and April 2016: 73 from the lowermost or oldest exposed section of the "new quarry" (22.552017 N, −83.884205 W, ~130 m asl) and seven from the top of the section of the "old quarry" (22.548661 N, −83.885495 W) (*sensu* Pszczółkowski et al., 2013) (Figures 1C, 3). All samples were carefully taken after removal of 5–10 cm of the exposed surface. Sampling resolution was ~14 samples per meter (~1:10 cm), targeting all lithological changes, with closer intervals in the greyish black to black beds (N2-1) (Figure 3). Colors used were acquired on wet samples following the color chart of the Geological Society of America (Goddard et al., 1963). Results of the first 25 samples are reported in this study.

## Petrography and microscopic analyses

The lithologic nomenclature follows (Sanchez-Hernandez and Maurrasse, 2014; Sanchez-Hernandez and Maurrasse, 2016) based on TIC values measured as total inorganic carbonate ($CaCO_3$) weight percentage (wt%), whereby limestone exceeds 70 wt%; marly limestones have between 60 and 70 wt%; argillaceous marls - marlstones <60 wt% (Figure 3). At least two thin sections and a smear slide were prepared for each hand sample collected. Microfacies analyses were conducted with transmitted light microscopy on an Olympus BH-2 microscope to determine skeletal fragments, mineral composition, and the bioturbation index which was assessed on a scale ranging from 0 to 6 (Taylor and Goldring, 1993). Computed Tomography (CT) X-ray imaging was used to further document bioturbation, internal structures, and heavy mineral content.

Scanning electron microscopy (SEM) imaging and Energy Dispersive X-ray Spectroscopy (EDS) analyses utilized a JEOL JSM 5900LV SEM at the Florida Center for Analytical Electron Microscopy (FCAEM) located at Florida International University. The selected samples were first cut into small cubes measuring approximately 1 $cm^3$ and partially polished to ensure optimal sample surface quality. To facilitate conductivity and reduce surface charging, a gold coating was applied to each sample using an SPI-MODULE sputter coater as described in Sanchez-Hernandez and Maurrasse (2014). SEM imaging of samples encompassed two primary modes of analysis: Secondary Electron Imaging for the determination of the matrix and Backscattered Electron Imaging offering insights into composition and structure.

Calcareous nannofossils were analyzed using simple preparation of the smear slides ($n$ = 17), on an Olympus LM (light microscope), with ×1,200 magnification. Biostratigraphy and taxonomic identification follow Roth (1978), Roth (1983), Bralower et al. (1989), and Bown et al. (1998).

## Geochemical analyses

### Total organic carbon (TOC) and total inorganic carbon (TIC) from modified standard loss on ignition (LOI) method

A water-cooled diamond-coated blade saw was utilized to cut specimens into cubes of ~1 $cm^3$ (equivalent to ~20–30 g). This procedure involved meticulous removal or avoidance of any carbonate cement fill within the samples. The cubes were allowed to air dry for 24 h at a temperature of 70°C (Sanchez-Hernandez and Maurrasse, 2014) and powdered using a Bell-Art micro-mill grinder equipped with a tungsten carbide chamber and blade. Each sample underwent grinding for 2 min, ensuring thorough pulverization. The micro-mill chamber, and blade were thoroughly cleaned between each sample to prevent any cross-contamination. Powdered samples were transferred into 5-dram (~18.5 cc) sterile glass (borosilicate) vials, then securely sealed and stored.

Total organic carbon (TOC) and total inorganic carbon (TIC) were determined by differential thermal analysis (DTA) using a modified standard "loss on ignition" (LOI) method yielding high accuracy, particularly for carbonate samples containing relatively minor clay content (Dean, 1974; Heiri et al., 2001; Llaguno, 2017; Herdocia and Maurrasse, 2022; 2023). The LOI identifies organic carbon (OC) loss by thermal oxidation between 200°C and 550°C, inorganic carbon (IC) loss from dolomite between 700°C and 750°C, and IC loss from calcium carbonate between 800°C and 850°C, extending to temperatures up to 1,000°C (Dean, 1974).

Prior to the LOI operation, ceramic boats were carefully washed three times and placed in a drying oven for 24 h, then subjected to a 560°C burn for 2.5 h to eliminate organic material. Approximately 0.3 g of powdered sample was spread evenly in the ceramic boat and subsequently placed in the muffle furnace set at 105°C and allowed to dry for 24 h. Beginning with the initial dry samples, the weights were documented at each step after cooling and then returned to the muffle furnace. First step is 560°C for 2.5 h to ensure complete combustion of organic material. See formulas below. The

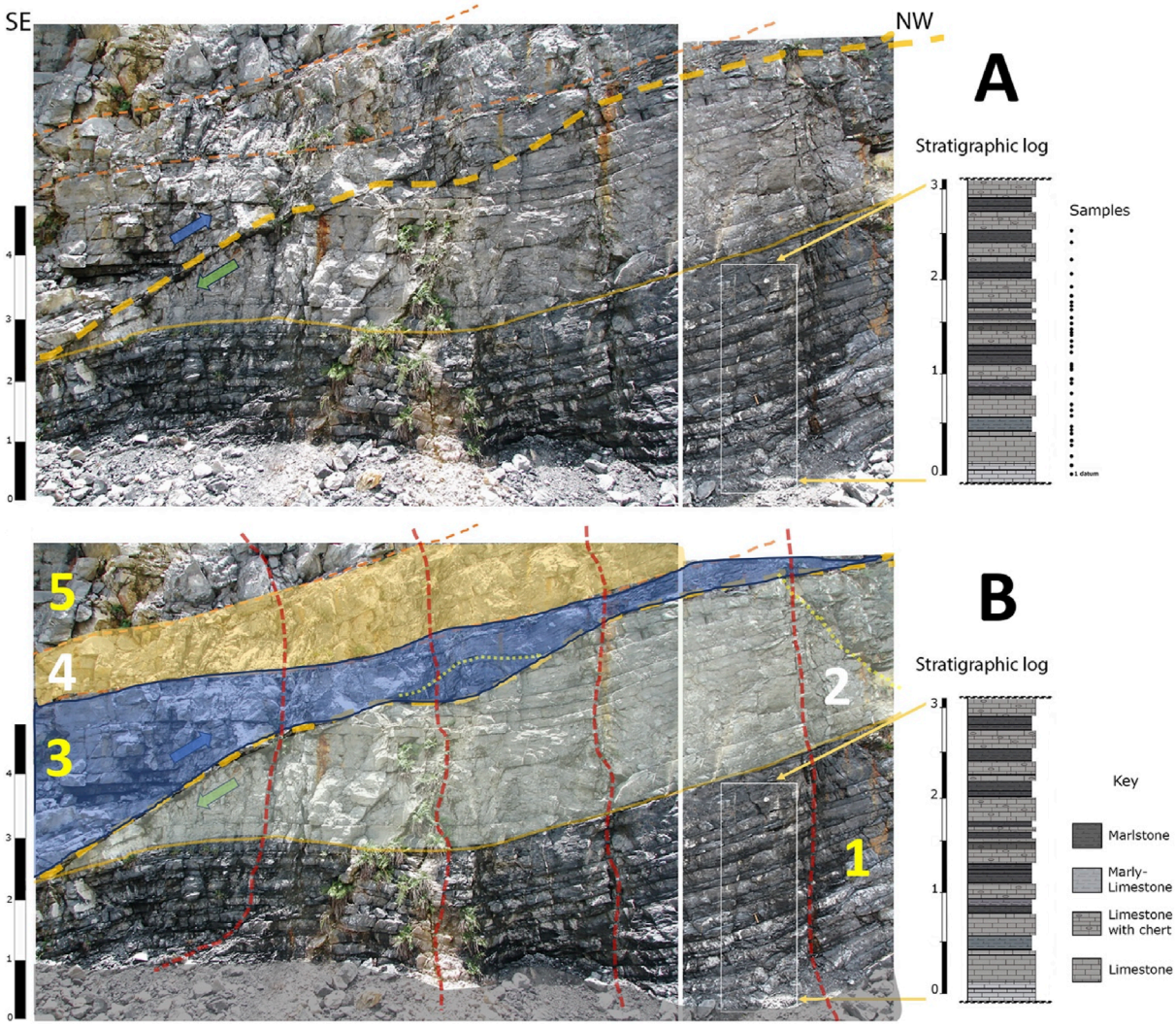


FIGURE 3
Stratigraphic section at the southwestern wall of the outcrop, oriented from southeast (SE) to northwest (NW), showing detailed layering and folding patterns **(A, B)**. Orange dashed lines indicate internal thrusts, while the yellow dashed line marks a major thrust with basal slip **(A)**. Note the slumped, semi-folded, cyclic dark and light beds with sharp contacts, labeled 1–5. The lowermost sheet may include the transition between the Guasasa (below 2) and Pons formation (above 2). The solid yellow line marks the main stratigraphic boundary. On the right is a simplified log of the lower 3 m showing the vertical sequence, sampling density, and lithological key.

difference in mass indicates TOC values in C weight percent (C wt%). The second step eliminates carbonate content as samples were combusted at 960°C for 4.5 h. Thus, TOC and TIC LOI values were determined using the following equations as described by Heiri et al. (2001) and Herdocia and Maurrasse (2023):

$$\mathrm{TOC\,(C\,wt\%)} = (\mathrm{DW_{105}} - \mathrm{DW_{560}}) / (\mathrm{DW_{105}}) \times 100$$

$$\mathrm{TIC\,(CaCO_3\,wt\%)} = ((\mathrm{DW_{560}} - \mathrm{DW_{960}}) / (\mathrm{DW_{105}}) \times 100$$

$\mathrm{DW_{105}}$ = sample weight after drying at 105°C.
$\mathrm{DW_{560}}$ = sample weight after combustion at 560°C.
$\mathrm{DW_{960}}$ = sample weight after combustion at 960°C.

Given the weight of 44 g $\mathrm{mol^{-1}}$ for carbon dioxide and 100 g $\mathrm{mol^{-1}}$ for calcium carbonate ($\mathrm{CaCO_3}$) ratio (100/44 = 2.27), the weight loss by LOI at 950°C multiplied by 2.27 should then theoretically equal the weight of the calcium carbonate in the original sample (Bengtsson and Enell, 1986; Llaguno, 2017; Herdocia and Maurrasse, 2022; 2023). Analytical precision fluctuated between 0.48% and 1.2% standard error ($n$ = 30; 1.08–2.8 standard deviation) based on controlled standards ($n$ = 5).

## Stable isotopes of carbon on bulk organic carbon ($\delta^{13}C_{org}$)

Bulk carbon isotope measurements on the organic fraction ($\delta^{13}C_{org}$) were performed on four samples and consists in the removal of $\mathrm{CaCO_3}$ following the method B of Schubert and Nielsen (2000). Approximately 1–2 g of powdered sample was placed in an 11-dram glass vial previously treated with 10% HCl and combusted at 560°C. Following acidification, samples were thoroughly mixed using a vortex mixer to ensure uniform

contact with the acid. The HCl solution was replaced as needed until complete dissolution of carbonate (Ponton-Guerrero, 2006; Sanchez-Hernandez and Maurrasse, 2014). Experimental control and use of pure calcium carbonate standards Fischer Scientific (Lot# 960058A), yielded an experimental error of <4 Wt% (mean 2.6 ± 0.6 Wt%). After effervescence ceased, each sample was rinsed with deionized water, dried at 40°C overnight, and later further homogenized using an agate mortar and pestle. The dried powder was later sealed in 0.5-dram glass vials in readiness for $C_{org}$-isotope analysis at the Stable Isotope Laboratory, Rosenstiel School of Marine, Atmospheric and Earth Science (RSMAES), University of Miami, utilizing an Elemental Analyzer coupled with an Isotope Ratio Mass Spectrometer (Finnigan MAT Delta C). Isotope values were reported relative to the international standard Vienna Pee Dee belemnite (V-PDB) (Gonfiantini et al., 1995). The analytical procedure used a Costech elemental combustion system coupled with a Thermo Scientific Delta V Advantage continuous flow isotope ratio mass spectrometer (Swart et al., 2019). A glycine and secondary standard were analyzed every 10 samples to ensure reproducibility of ±0.1‰. The results of the $\delta^{13}C_{org}$ values, with deviations (δ), are expressed per mil (‰) relative to the ratios $^{13}C/^{12}C$ of the Vienna Pee Dee belemnite (V-PDB) standard (Hoffman and Rasmussen, 2022). For the measurement of Nitrogen, atmospheric air (AIR) served as the reference standard for reporting delta $^{15}N$ ($\delta^{15}N$) values.

## Major, biolimiting, and redox sensitive trace elements (RSTEs)

Elemental concentrations were analyzed on 25 samples from the lowest 3 m of the section and included major elements, aluminum (Al), silicon (Si), titanium (Ti), and lithium (Li), biolimiting elements iron (Fe), phosphorus (P), and redox sensitive trace elements (RSTEs) vanadium (V), chromium (Cr), cobalt (Co), nickel (Ni), copper (Cu), molybdenum (Mo), thorium (Th), thallium (Tl), and uranium (U). Concentrations of Ba, Ca, K, and S were also analyzed.

The sample preparation is after Arroyo et al. (2009) with further adaptation in Sanchez-Hernandez and Maurrasse (2014), Sanchez-Hernandez and Maurrasse (2016) and Socorro and Maurrasse (2019), Socorro and Maurrasse (2020) using a Laser Ablation Inductively Coupled Mass Spectrometer (LA-ICPMS) at Florida International University's Trace Evidence Analysis Facility (TEAF). Sediment pellets were spiked with two internal standard solutions: first 350 µL of 1,000 ppm scandium oxide (1,000 ppm in 3% $HNO_3$ from Ricca Chemical Company, Lot#4711D63), and second 300 µL of 1,000 ppm indium metal (1,000 ppm in 3% $HNO_3$ from Accustandard, Lot#218115017). Instrumentation included a 266 nm Nd-YAG laser operating with a 200 µm spot size at a frequency of 10 Hz (Applied Spectra J200 Tandem at 20% output) and an ELAN DRC II quadrupole (Perkin Elmer LAS, Shelton CT United States) operating in standard mode. Each pellet underwent four ablations in distinct locations to ensure comprehensive data acquisition. Instrument performance was assessed by running three external sediment reference samples (SRM NIST2710 Montana Soil, which contains molybdenum, NIST 2704 Buffalo River Sediment, and PACS-2 Marine sediment reference material). Analytical precision was tested with standards introduced at the commencement, midpoint, and conclusion of the analysis. The precision of the major and trace element determinations ranged from 1.4% to 10.4%, with an average error of <0.2% relative to the standard reference materials. An average bias of <2% error for SRM 2710 and 2704 was also calculated. Data points were averaged for each sample based on the four ablations relative to their standard deviations. Elemental data were processed using GLITTER software (version 4.5) and expressed as absolute concentrations; major and biolimiting elements are reported in mg/g (i.e., mg $g^{-1}$ = ppm/1,000), and the RSTEs in parts per million (ppm) (Socorro and Maurrasse, 2019; Herdocia and Maurrasse, 2023).

In marine environments trace metals exist as detritus or dissolved ions and only the authigenic fractions are indicative of reducing conditions when associated with OM-rich sediments (Calvert and Pedersen, 1993; Jones and Manning, 1994; Achterberg et al., 1997; Morford et al., 2001; Tribovillard, 1998; Tribovillard et al., 2006). Therefore, to interpret redox conditions only the authigenic fraction of RSTEs should be evaluated. As commonly practiced in RSTEs, aluminum (Al) is used for normalization because it is a conservative element derived from silicates. Hence, detrital fractions are typically removed by normalizing RSTE concentrations to Al (as E/A) (Turekian and Wedepohl, 1961; Brumsack, 2006). Correlations between RSTEs and TOC assess redox conditions and trace element sources. However, in certain cases normalization may not be efficient and risks to yield false correlations when there is high coefficient of variance of the divisor (Pearson, 1896; Pearson, 1900; Van der Weijden, 2002; Socorro and Maurrasse, 2019; Herdocia and Maurrasse, 2023). Here RSTEs were not normalized to Al because of the high variance coefficient in Al (v = 173.7); Ti (v = 202.7); and Li (v = 163.7). To avoid spurious correlations caused by the high coefficients of variation in elements like Al, Ti, or Li, we did not normalize RSTEs to these elements. Instead, we used background elemental concentration based on means calculated from a total of fifteen samples of the original basin: eight samples from the four members of the Guasasa Formation (two samples from each: upper San Vicente, El Americano, Tumbadero, and Tumbitas); six from the Pons Formation stratotype section; and one from San Cayetano Formation (Orihuela and Maurrasse, unpub. Data). These data were used to calculate relative enrichments above a common detrital baseline, allowing us to better identify enrichment and/or reducing conditions. Instead, absolute values of RSTEs are utilized to assess paleo redox conditions for trace elemental ratios (V, Mo, U) and biolimiting trace metals (P, Fe) (Supplementary Tables S1–S9; Orihuela and Maurrasse, unpub. Data).

## Statistical tests

All statistical analyses were conducted with PAST Paleontological statistics software package, version 3 (Hammer et al., 2001). One-way and two-way ANOVA tests were conducted to detect overall differences among elements and correlation between them: between the independent variables (e.g., TOC and TIC) and the dependent variables (other elements). In cases where a one-way ANOVA was unpractical due to the sample size, tests were run separately for each variable. Post hoc comparisons through Tukey's Tests were used to compare groups or samples of unequal size and tested for pairwise differences among chemical species and stratigraphic level or lithology. Two-tailed *t*-tests were

further used to find significant mean differences between groups of variables (e.g., $\delta^{13}C_{org}$ vs. TOC; or lithologies). Significance levels were set at $p < 0.010$ for all Tukey Tests, plus $p < 0.010$ for all ANOVA (Supplementary Tables S1–S5).

Additional multivariate analyses, MANOVAs, were conducted under similar constraints. Canonical and Principal Component Analysis (PCA) were performed to visualize significant differences between groups and identify relationships between variables from the dataset. PCA $p$ was set at < 0.010 (Supplementary Tables S5–S8).

We used Pearson's correlation coefficient (r) to measure the strength and direction of the linear relationship between two variables (represented here by lowercase r). Values close to 1 or -1 indicate a strong linear relationship, while values close to 0 indicate a weak relationship (Pearson, 1900). We also included R-squared values ($R^2$) derived from the square of Pearson's correlation coefficient to indicate the proportion of variance in one variable that is predictable from the other variable. Higher values imply a stronger relationship (Myers and Myers, 1990). The $p$ was set at < 0.010 for their statistical analyses. Correlation strengths were interpreted following the guidelines of Mukaka (2012), as follows: weak or negligible (0.00–0.20); low to moderate (0.20–0.40); moderate to strong or high (0.40–0.60); strong (0.60–0.80); and very strong or very high (0.80–1.00) (Supplementary Tables S6, S7).

The facies code of the correlation analysis is a numeric representation of the various microfacies identified from thin section data (Supplementary Tables S2, S8) converted to distinct numerical codes to each unique facies type for correlation analysis. The three microfacies identified as A through D were coded 0, 1, 2, 3 and 4, respectively that allow for correlations with other numerical data. Elemental ratios have been computed and graphically represented to serve as supplementary proxies for evaluating redox conditions, following the methodologies described by Cramér (1946), Jones and Manning (1994) and Wignall and Myers (1988).

# Results

## Field description and petrographic analysis

At the field scale, the succession consists of thinner interbedded (1.5–7 cm) biomicritic greyish black (N2) to black (N1) carbonaceous marlstone showing fissile laminations with sharp, planar contact with much thicker (8–20 cm) medium dark grey (N5) limestone often containing small nodules of dark chert (N2) (1–5 cm). Stylolites and microfractures filled with sparry calcite were often visible, but without visible macrofossils. Overall, beds thickened upwards, with a 135-degree SE strike and dip angle ~22–25° (up to 30° in the basal folds), with compression deformation and some lateral gradation and pinch out. Internal thrust micro faults and upper and basal slip were observed. The first 5 m of the intercalating sequence lies just below the main basal slip and shows incipient semi-folding (Figure 3). Four microfacies were identified in the first 2.61 m of the section (Figure 4).

Microfacies A is a bioclastic limestone with >10% poorly sorted bioclasts showing isotropic fabric in a micritic matrix (Figures 4 A1–3). Allochems primarily consist of small planktic foraminifera (<50 µm, ~25%), radiolaria (~2–15%), calpionellids (<2%), rare calcispheres (~1%), and ostracods (<1%). Microstylolites and microfractures are rich in organic matter and kerogen, whereas larger veins are typically filled with blocky sparite, and pyrite (<2%) commonly found near or inside the bioclasts. SEM analysis revealed a calcareous matrix predominantly composed of abundant coccolithophores, such as *Watznaueria barnesiae*. The planktic foraminifera include *Globigerinelloides* spp., *Globigerinelloides* cf. *paragottisi*, *Conoglobigerina* cf. *gulekhensis,* and *Hedbergella sigali*. Benthic foraminifera were absent. Among the calpionellids, *Tintinnopsella* spp., *Tintinnopsella* cf. *carpathica*, and *Calpionellites* cf. *darderi* were noted. The nannoconids are represented by *Nannoconus kamptneri kamptneri* (Figure 5; Supplementary Figures S1, S2).

Microfacies B is a "shaley" biomicrite (Figures 4 B4–6), nearly barren of bioclasts (<1%), with an anisotropic, alternating, pseudo-laminated, wavy-lenticular fabric featuring ovoid calcareous lenses lighter in color with mottled structures. Brownish fibrous fragments were observed through optical microscopy and SEM. Pyrite in the form of concretions and framboids (~1 mm to micrometer), constitutes approximately 5% of the composition (Figures 4 B4–6). Calcite-filled microfractures and veins are also abundant (Figure 4B5). The rare bioclasts present are predominantly radiolaria, planktic foraminifera (*Globigerinelloides* sp. or *Hedbergella* sp.) (Figure 4B4), ostracods and/or calpionellid fragments. Benthic foraminifera are absent. The radiolaria and planktic foraminifera are often filled with blocky sparite, pyrite, or silica (Supplementary Figures S1, S2).

Microfacies C is a micritic limestone that is also almost barren of bioclastic content (Figures 4 C7–9). It has a high abundance of kerogen, organic matter, and pyrite, constituting over 25% of the overall components. The allochems content is less than 2% overall composition. Evidence of soft tissue debris which refer to small, often fragmented multi-cellular-like structures observed in thin section and SEM images, believed to be remnants of plant tissues, algae, or other organic material (Figures 4 C7–8). The presence of phyto debris interpreted plant-derived fragments, possibly indicating preserved plant material or organic matter in the samples as well as possible dinoflagellate cysts in these facies is corroborated by SEM analysis of the samples (see data below).

Microfacies D is unique as it is a predominantly sparse biomicrite (~5–10%) with a mottled structure characterized by a high organic content and allochems include small benthic foraminifera (mostly biserial), scarce radiolaria, rare microgastopods and echinoid fragments (Figures 4 D10–12). Bioclasts are poorly sorted in an isotropic fabric. As seen in SEM the matrix includes a significant amount of fine clay minerals (Figure 4 D12; Supplementary Figure S1). Dispersive pyrite is particularly abundant (>25%) in the matrix (Figures 4 D10–12) and within foraminifera tests (Figures 4 D10–11). Minute quartz and feldspars contribute an estimated 10%–15% to the overall composition. These grains are angular to subangular, and conspicuous dark areas constitute 1%–5% of the composition. Fibrous organic matter with seemingly cellular structure and amorphous kerogen constituted 1%–5% of coarse components.

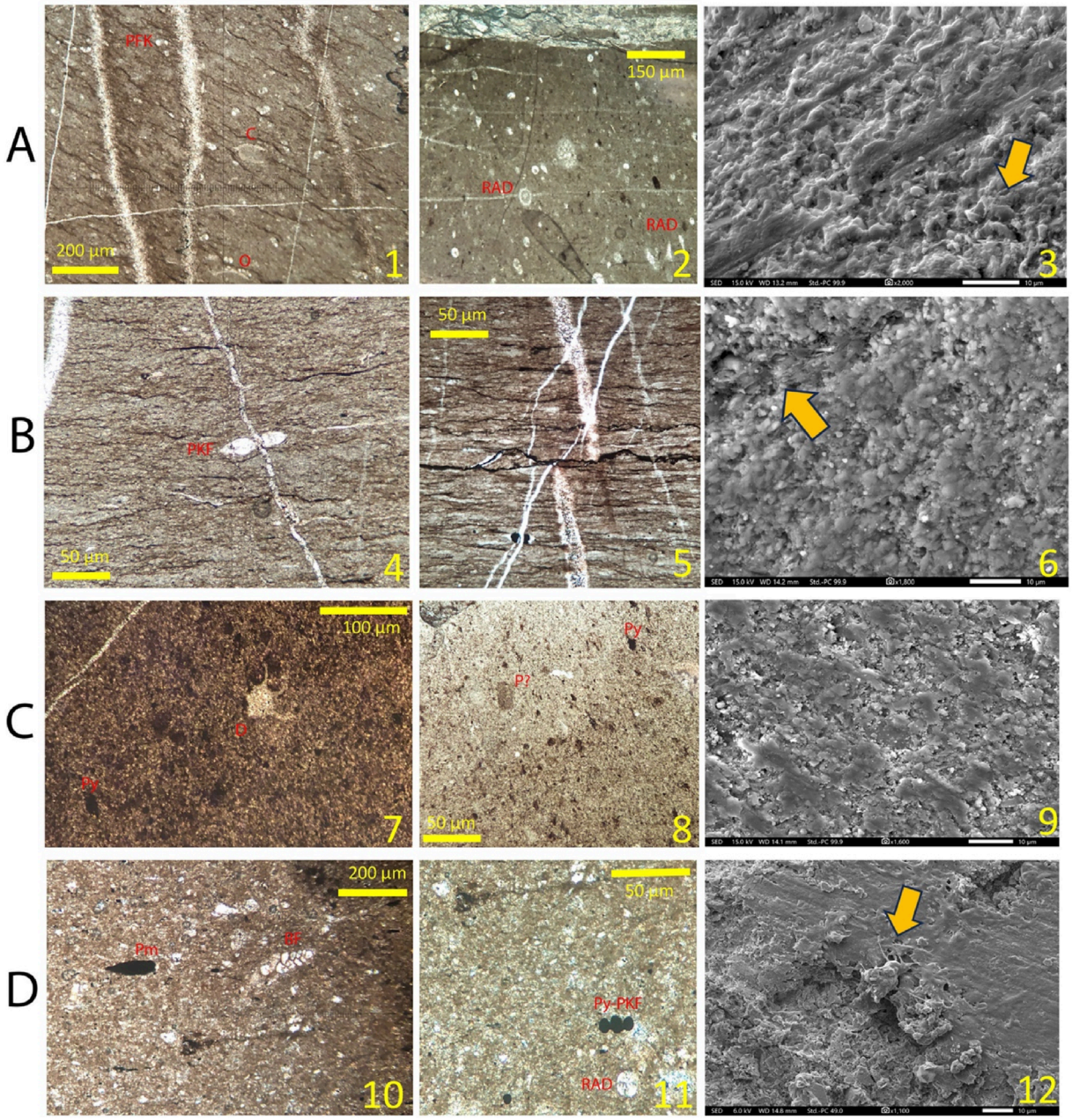


FIGURE 4
Four distinct microfacies **(A–D)** based on microstructural composition, shown with photomicrographs under plane polarized light, crossed polarized light, and scanning electron microscopy (SEM) images (left to right). Annotations include planktic foraminifera (PKF), benthic foraminifera (BF), possible dinoflagellate cyst **(D)**, pyrite (Py), calpionellid **(C)**, ostracod (O), and radiolaria (Rad). SEM arrows indicate dissolved nannofossils, clay minerals, and organic matter associated with pyrite. Sample details: **(A)**, Cu-PR-1 (A1), Cu-PR-3 (A2), Cu-PR-29 (A3); **(B)** – Cu-PR-6 (B4-5); **(C)**, Cu-PR-11 (C7-8), Cu-PR-12 (C9); **(D)**, Cu-PR-26 (D10-12). Note the shearing and structural alterations on B4 and 5.

## Micropaleontology

### Calcareous nannofossils

Several levels targeting the different microfacies were analyzed for their microfossil content which revealed a diverse calcareous nannoflora (total of 23 taxa) of typically oceanic environment and indicative of specific biozone within the Early Cretaceous, particularly the Valanginian stage (Figures 5–7; Supplementary Figures S1, S2). In temporal order the results are as follows:

Marlstone of microfacies B at stratigraphic level 0.41 m containes species such as *Calcicalathina oblongata*, *Conusphaera mexicana*, *Nannoconus bermudezii*, *Rucinolithus wisei*, *Cretarhabdus conicus*, *Retecapsa angustiforata*, *Micrantholithus obtusus*, *Nannoconus* spp., *Zeugrhabdotus embergeri*, *Z. noeliae* and *Watznaueria* spp., including *W. barnesiae* and *W. britannica*.

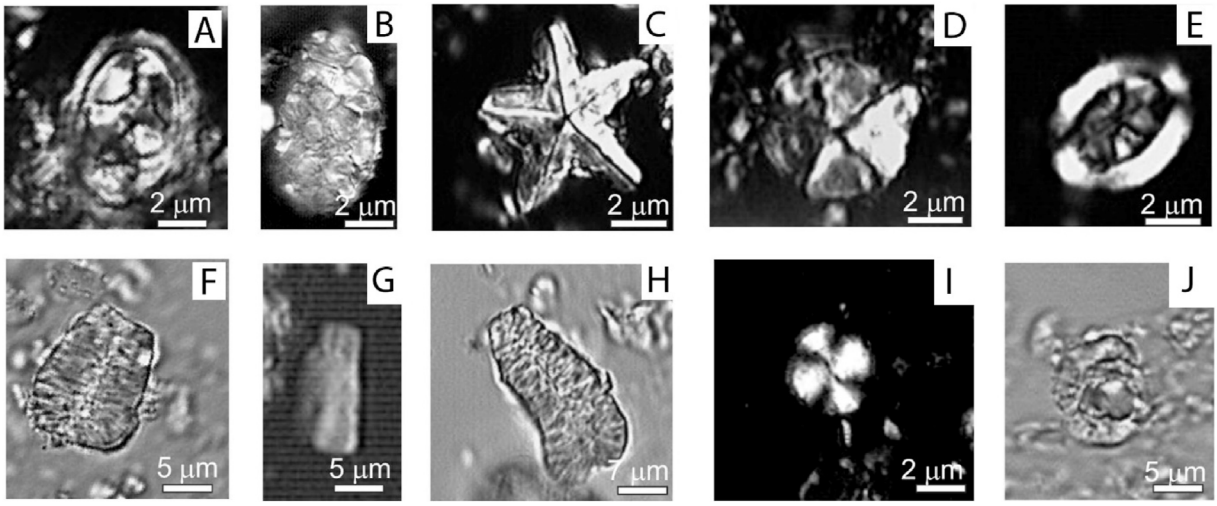


FIGURE 5
Calcareous nannofossils from La Lata Quarry: **(A)**, *Zeugrhabdotus embergeri*; N+, Cu-PR-6. **(B)**, *Calcicalathina oblongata*; N+, Cu-PR-11. **(C)**, *Micrantholithus obtusus*; N+, Cu-PR-29. **(D)**, *Micrantholithus hoschulzii*; N+, Cu-PR-12. **(E)**, *Retecapsa angustiforata*; N+, Cu-PR-29. **(F)**, *Nannoconus steinmannii* subsp. *steinmannii*; NII. **(G)**, *Conusphaera mexicana* subsp. *mexicana*; N+. **(H)**, *Nannoconus bermudezii*; NII, Cu-PR-11. **(I)**, *Watznaueria barnesiae*, N+. **(J)**, *Nannoconus globulus* subsp. *globulus*; NII, Cu-PR-29. Microphotographs taken at LM (light microscope), with ×1,200 magnification; scale bar in microns; N+ crossed nichols; NII light polarized light.

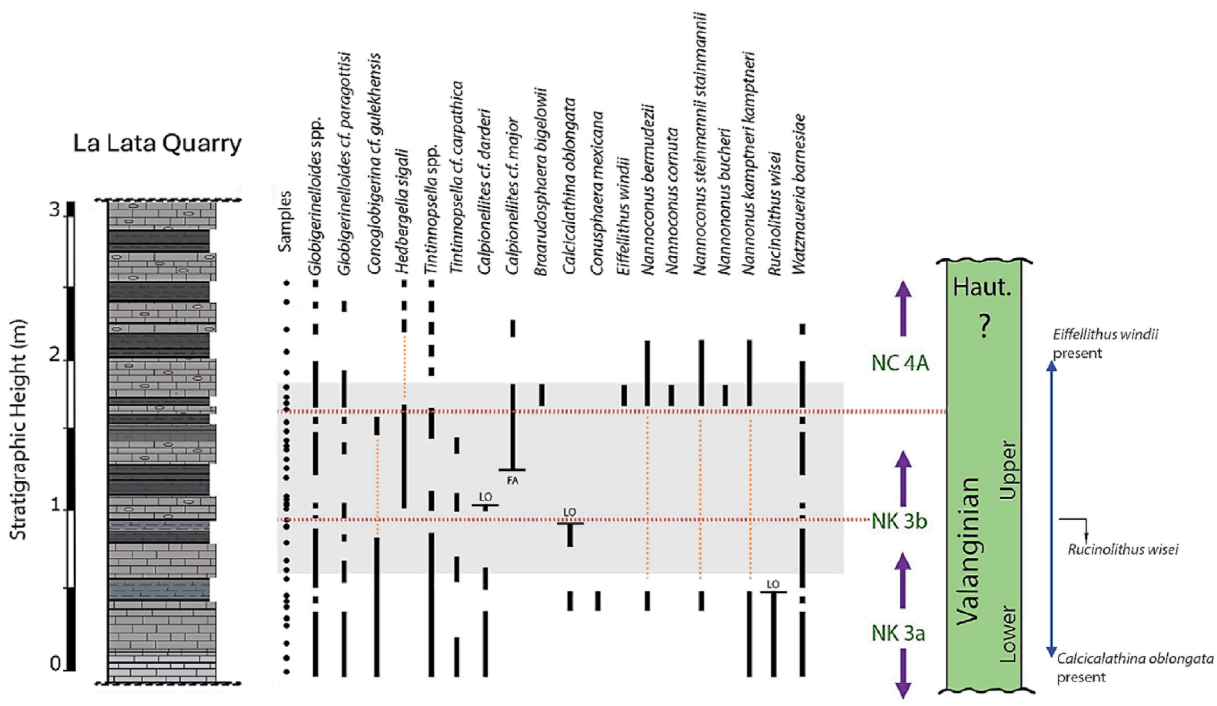


FIGURE 6
Stratigraphic distribution of microfossil species within the La Lata Quarry section, Pons, Western Cuba. The stratigraphic column on the left shows corresponding lithology. Microfossil occurrences are marked by black vertical lines at sample points, with potential but undetected levels shown as orange dotted lines. Nannofossil biozones NK3a (NC3a), NK3b (NC3b), and NC4A are labeled along their stratigraphic positions. The gray horizontal band highlights the interval of the Weissert Event, in the section correlated to the Valanginian (lower) up to possibly the lower Hauterivian stage. Refer to lithologic legend on Figures 3, 7.

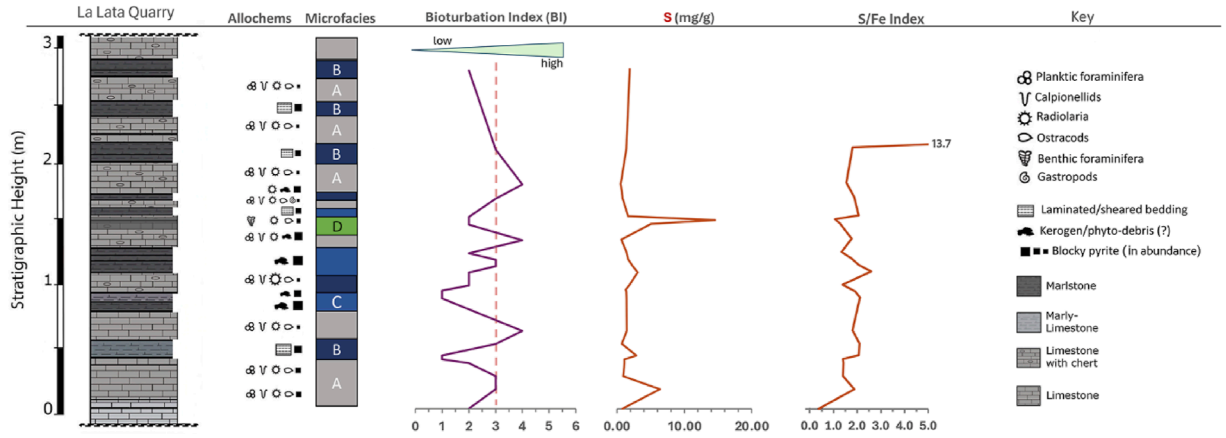


FIGURE 7
Stratigraphic profile of the first 3 m at La Lata Quarry showing bioturbation index (BI = 0–6), sulfur content (S), sulfur-iron (S/Fr) index, allochems, and microfacies distribution. Key symbols represent primary fossil groups, bedding features, and pyrite abundance. The dotted line on the BI indicates the intermediate-moderate value index.

Microfacies B at 1.73 m and 2.22 m also contains long ranging taxa and a similar assemblage as decribed above, including *Watznaueria barnesiae*, *W. ovata*, *W. britannica*, *Zeugrhabdotus embergeri*, *Nannoconus steinmannii* subsp. *stainmannii*, and *Nannonus kamptneri kamptneri* (Figure 5; Supplementary Figure S1).

Marlstone of microfacies C (0.85–0.90 m) shared several species with microfacies B at 0.41 m such as *Calcicalathina oblongata* and *Nannoconus bermudezii*, along with long-ranging species such as *Micrantholithus hoschulzii*, *Haqius circumradiatus*, *Helenea chiastia*, and *Zeugrhabdotus erectus*.

Limestone of microfacies A at 1.62 m comprises species such as *Conusphaera mexicana, Haqius circumradiatus, Helenea chiastia, Eiffellithus windii, Nannoconus cornuta, Nannoconus bucheri, Nannoconus steinmannii* subsp. *steinmannii, Nannonus kamptneri* subsp. *kamptneri Micrantholithus hoschulzii, M. obtusus, Retecapsa angustiforata*, *Watznaueria barnesiae, W. britannica, Zeugrhabdotus embergeri,* and *Zeugrhabdotus erectus*.

In general, preservation of the nannofossils is generally poor, only between 50% and 60% of nannofossils could be determined at a specific level due to recrystallization or overgrown (Figure 5; Supplementary Figures S1, S2).

### Foraminifera and calpionellids

Supplementary Figure S2 shows the diversity of these organism, and Figure 8 shows the stratigraphic distribution of characteristic microfauna. Among the planktonic foraminifers *Hedbergella sigali*, *Globigerinelloides paragottisi*, *Favusella hoterivica* and *Conoglobigerina* cf. *gulekhensis* are dominant throughout the section and most frequently in the limestone beds, particularly microfacies A (Figures 4 A1–3, 7; Supplementary Figure S2). Other globigerinellids were also represented but poorly preserved to be of diagnostic value. Several of them demonstrated abnormal growth of their test chambers (Supplementary Figure S2).

Calpionellids are in low diversity and poorly preserved throughout the section but are more abundant in the lower 1.5 m. They include *Calpionellites darderi*, *Tintinnopsella carpathica*, and *Tintinnopsella* aff. *longa*. *Calpionellites darderi* occurs up to 1.05 m (LAD) followed by the first record (FOD) of *Calpionellites major* (Figure 6; Supplementary Figure S2).

## Carbon and nitrogen geochemistry (TIC, TOC, $\delta^{13}C_{org}$, $\delta^{15}N_{org}$)

The TIC results from 24 samples show variations throughout the studied section (Figure 8) with an overall carbonate value between 44.7 and 97.7 wt% (mean 86.6 wt% and ±14.5 standard deviation (SD)). Three major decreases occur at 0.41 m, 0.90–0.94 m, and 1.42–1.45 m, respectively (Figure 8). TIC showed a high negative correlation with TOC (r = −0.85, moderately strong $R^2$ = 0.65, $p > 0.05$) (Supplementary Tables S6, S7). The $R^2$ values imply that approximately 65% of the variance in TIC can be explained by the variance in TOC.

The TOC is consistently high (>1.5 wt%) and ranges from 0.75 wt% to a high of 10.82 wt% (at level 0.915 m, Cu-PR-13) as it varies throughout the section yielding a mean of 3.7 wt% (±3.2 SD) (Figure 9). Three major peaks exceeding the background: the first at 0.41 m (9.0 wt%), coincide with microfacies B; a second at 0.85–0.95 m (6.2–10.2 wt%); and a third at 1.42–1.45 m (6.1–10.8 wt%) which coincides with marly levels and lower TIC (Figure 8; Supplementary Table S1).

The $\delta^{13}C_{org}$ profile of the 24 samples exhibits temporal variations from −27.7‰ (at 1.2 m, high TIC limestone, microfacies A) to −25.6‰ (at ~0.90 m, low TIC, high TOC carbonaceous marl level, microfacies C. This level has a range of 2.1‰), a mean value of −27.1‰ (background level), a standard deviation (SD) of ±0.4‰, and a standard error (SE) of 3.0‰. Three major carbon isotope excursions (CIEs) occur with the largest negative shift (−1.37‰) situated between 0.90 m and 1.0 m (Figure 8; Supplementary Tables S1).

The $\delta^{13}C_{org}$curve can be divided into five main segments: 1) 0–25 cm, (−26.6‰ to −26.8‰); 2) 25–85 cm, relatively stable (−27.1‰ to −27.2‰); 3) 90–95 cm carbonaceous marl which

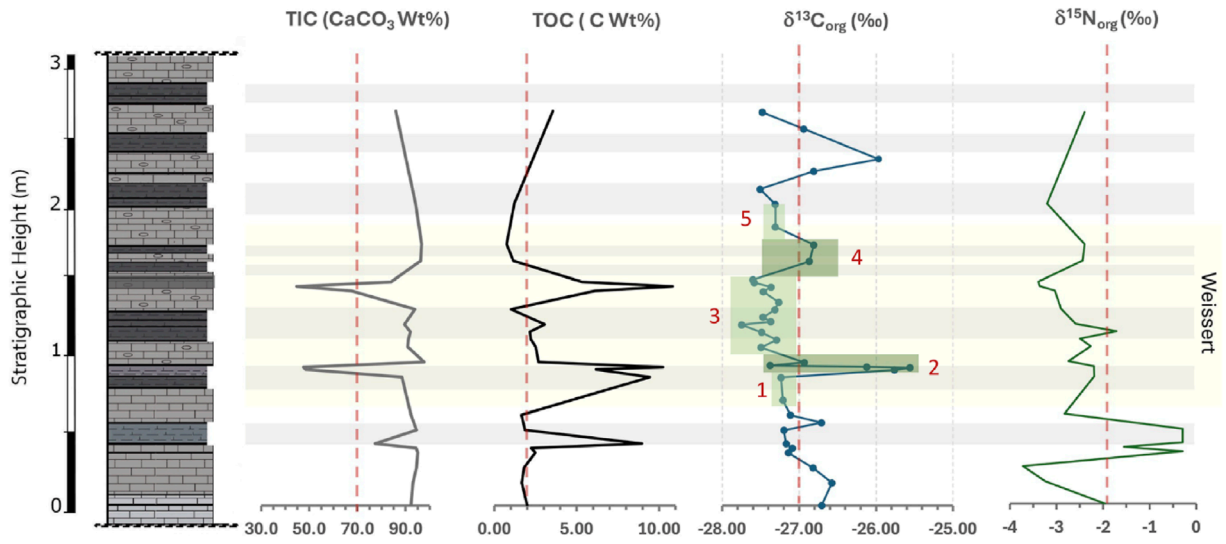


FIGURE 8
Stratigraphic height versus geochemical profiles of the studied section. The leftmost panel illustrates the stratigraphic column with distinct lithological units defined for this study, including limestone, limestone with chert, carbonaceous marly-limestone, and carbonaceous marls, denoted by variations in color and pattern. Center panels display the geochemical data: total inorganic carbon (TIC) as $CaCO_3$ (wt%), total organic carbon (TOC) as wt% of C, organic carbon isotopic composition ($\delta^{13}C_{org}$), and nitrogen isotopic composition ($\delta^{15}N_{org}$), with concentration and isotopic ratios plotted along the stratigraphic height. Red dashed lines correspond to the limestone line in TIC (>70 wt%), enrichment level in TOC (>2 wt%), and the isotope averages. The grey shaded bars correspond to the carbonaceous, organic matter-rich lithologies. Refer to lithologic legend on Figures 3, 7.

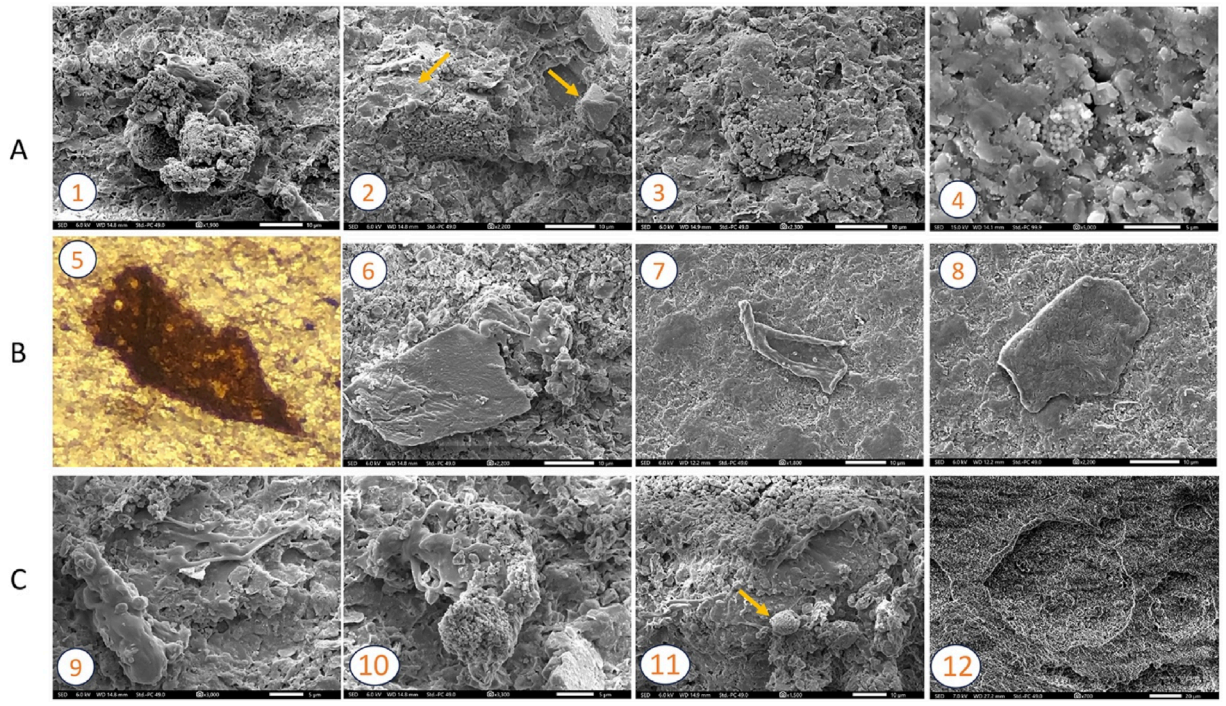


FIGURE 9
Scanning electron microscopy (SEM) images showing framboidal and euhedral pyrite [top row **(A)**], phyto debris and possible dinoflagellate cysts [middle row **(B)**], and organic matter associated with microbial, polymeric substances and cyanobacterial structures [bottom row **(C)**]. Top row samples 1–4: Cu-PR-19, 11, 12, and 16. Middle row samples 5–8: Cu-PR-6, 19, and 27. Bottom row samples 9–12: Cu-PR-19, 27, 35, and 36 respectively. Arrows on A2 point to euhedral pyrite and associated Illite clay minerals. Arrow on C11 indicates calcified coccoid structure with associated pyrite.

records the first and largest CIE (peaks at −25.6‰); 4) 1.0–~1.5 m (−27.3 to −27.6‰) where values are slightly lower than the background level; 5) 1.62–2.61 m comprises slightly more negative values (−26.9‰ to −27.3‰). The mean $\delta^{13}C_{org}$ value for limestone samples is −27.2‰, whereas it averages −26.5‰ for the marly-limestone, marlstone levels.

The nitrogen isotope values in the bulk organic fraction ($\delta^{15}N_{org}$) exhibit a complex temporal pattern with a minimum of −3.7‰ at 0.25 m (Figure 8; Supplementary Tables S1, S5–S8) and the highest values, ~0.3‰ at the low levels 0.41–0.5 m. The mean $\delta^{15}N_{org}$ value is −2.0‰ with a standard deviation (SD) of ±1.20‰ and a standard error (SE) of 0.24‰ Correlation analysis revealed a weak negative association between $\delta^{15}N_{org}$ and TOC ($r = -0.15$, $R^2 = 0.02$, $p = 1.0$), indicating a limited or indirect relationship between organic carbon and nitrogen isotopic composition, while the presence of a major shift between the first 35 and 50 cm sampled (~−0.3 to −1.6‰) indicates a more complex relationship (see discussion below).

## Scanning electron microscopy (SEM) with energy-dispersive X-ray spectroscopy (EDS) analyses

SEM/EDS analysis was carried out on fifteen samples representing different lithologies: limestones at 0.0 m, 0.5 m, 0.6 m, 0.95 m, 1.05 m, 1.62 m, and 2.61 m; marlstone at 0.41 m and from 0.85 to 0.90 m. Levels 1.15 m, 1.42 and 1.48 m were transitional, and exhibited significant TOC and $\delta^{13}C_{org}$, $\delta^{15}N_{org}$ excursions (Figure 9; Supplementary Figures S1, S3).

Limestones with high TIC contained abundant calcareous nannofossils (often poorly preserved, disaggregated plates, or partially dissolved) and dolomite rhombs (angular, equant, non-interlocking) within a compact, low porosity micrite matrix (Figure 4; Supplementary Figures S1, S2). Qualitative elemental composition analysis (EDS) confirmed the presence of high and low Mg calcite (44.3–52.4 mass%, Mg ~0.30–0.32 mass%) and microcrystalline quartz (21.1–53.9 mass%), with a minor presence of clay crystals (predominantly illite-smectite) (e.g., Figure 4 B6). Pyrite content was low (<2%) in these limestone microfacies. In morphology, pyrite was generally represented by sparse, blocky, and ovoid crystals (Figures 9 A1–4; Supplementary Figures S2, S3).

Similarly, low TIC, high TOC carbonaceous marl and marly-limestone levels (0.38–0.41 m, 0.85–0.90 m, and 1.40–1.45 m) consisted of a disaggregated calcareous nannofossil matrix, but microfacies B-D include higher frequency of phyto debris with other biogenic particles interpreted as possible dinoflagellate cysts (?), calcified remains of coccoid cyanobacteria, microbial structures associated with pyrite framboids (~5–10 μm) (comparable to those in Duque-Botero and Maurrasse, 2005; 2008), irregular pyrite lumps, and ovoid pyrite (Figures 4C, D, 9A1-4; Supplementary Figures S2, S3). Pyrite associated with calcareous microfossils and phyto remains typically presented as truncated cubic to cubic and octahedral microcrystals, averaging less than 10 μm in diameter. Larger pyrite aggregates associated with clays, calcite crystals, and microbial structures (biofilms and fibers), are notably abundant at 1.05 m, 1.15 m, 1.42 m, 1.45 m, and 1.48 m, respectively (Figures 9 C9–12). A sample between microfacies C and B (1.15 m) has enrichment in pyrite framboid bundles conjointly with illite-smectite clay textures, chlorite crystals, and a rare echinoderm spine fragment. Microfacies D (1.42 m–1.45 m) is remarkable because of its higher content of minute siliciclastic particles, abundant pyrite, phyto debris, dinoflagellate cysts (?), cyanobacterial (?) and microbial structures associated with pyrite framboid aggregates (Figures 4 D10–12 and 9 C9-12).

### SEM-EDS analysis of phyto debris and microbial structures

SEM micrographs revealed a complex matrix rich in micrite interspersed with a fine-grained, clay-rich substrate (Figures 4, 9; Supplementary Figure S1) including possible plant fibers, dinoflagellate cysts, and other undetermined biological detritus (Figures 9 B5–8). Qualitative energy dispersive spectroscopy (EDS) analyses for these samples i.e., Cu-PR-25, 26, and 27 disclosed varying mass percentages of carbon (50.4–15.41), chlorine (3.24–6.86 only Cu-PR-26 and 27), potassium (6.67), nitrogen (4.01–3.09), sodium (1.05–1.58-only on Cu-PR-27), calcium (~2.62), and sulfur (~0.65).

### Bioturbation analysis

The bioturbation Index (Taylor and Goldring, 1993) ranges from 1.0 to 4.0 and fluctuates across the 2.61 m studied interval with an average of ~2.6 (Figure 8). The distribution of BI values exhibit multiple peaks, between 2 and 3. Temporal variations in BI show that microfacies A and B have the most variant BI (1–3), whereas microfacies C and D yield the lowest and least variable indices (1–2). At the 0.0 m level the average BI is 2.0, and at 0.15 m it is 3.0. Upwards a BI of 4.0 occurs at 0.55 m, 0.60 m, and 0.70 m, respectively. The lowest BI of 1.0 occurs at intermittent levels: 0.41 m, 0.85 m, 0.90 m, and 0.95 m with an upward stabilization towards intermediate values (~2.5). Facies A, B, C include a relatively narrow range of BI values, whereas others transitional levels (B-A and C-B) exhibit more variability (Supplementary Table S1). X-ray imaging revealed additional inconspicuous bioturbation in samples with low BI (microfacies B and C, levels 0.41 m, and 0.95 m) which also show irregular voids, vugs, and linear structures not related to fractures that differ from the surrounding matrix (Supplementary Figure S3).

## Elemental concentrations: major, biolimiting, and redox sensitive trace elements (RSTEs)

Elemental values for major terrestrially derived components (Al, Si, Ti, Li), RSTEs (V, Ni, Co, Cr, Cu, Mo, Th, U) of the "La Lata" quarry outcrop are summarized in Figures 10–12 (and Supplementary Tables S2–S4; Supplementary Figure S4) which show two major episodes of enrichment: one at 0.90 m–1.15 m and a second, larger at 1.42 m and 1.45 m. Characteristically, major elements and RSTEs yield increasing values associated with marly and argillaceous limestone layers. Al and Si show similar trends in relationships with TIC and TOC (Supplementary Tables S5, S6; Supplementary Figure S4). Al and Ti are perfectly correlated (r =

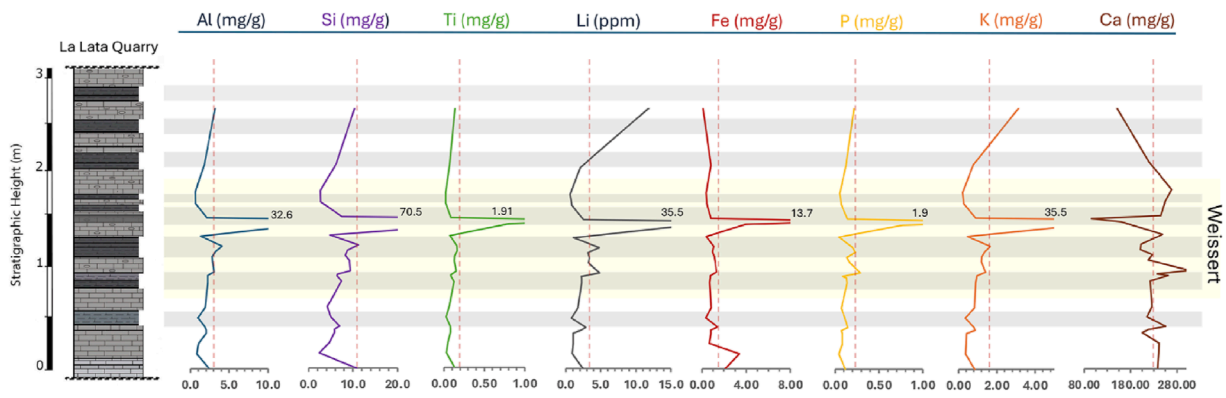


FIGURE 10
Stratigraphic variation in major and biolimiting trace elements correlated with lithology. The red dashed line corresponds to the average value from the dataset of this section. The yellow shaded area highlights the Weissert horizon, with corresponding geochemical signatures. The grey shaded bars correspond to the carbonaceous, organic matter-rich lithologies. Refer to lithologic legend on Figures 3, 7.

1.0). Al exhibits low variation from 0 m to approximately 1.40 m, ranging from 0.80 mg/g to 4.0 mg/g with a slight peak between 0.41 m and 0.5 m and a major enrichment level at 1.2 m. Upwards, between 1.42 m and 1.45 m, Al reaches values of 15.5 and 32.6 mg/g, an enrichment significantly greater than the average. Concentrations revert to below-average values towards the top of the studied interval of the section (Figure 10) but shows low to moderate positive correlations with TOC (r = 0.54, $R^2$ = 0.40, $p$ = 1.0) and a strong negative correlation with TIC (r = −0.72, $R^2$ = 0.52, $p$ < 0.010) (Supplementary Figure S4). Fe and P show a trend of enrichment correlative with the major elements (Figure 10). Fe enrichment (section average > 1.6 mg/g) reaches a peak between 1.42 and 1.45 m. Fe and P vary temporarily at levels 0.41 m, 1.42, and 1.45. At level 0.41 m, they are near concomitant with the lowest observed carbonaceous marly-limestone level with TOC enrichment and low TIC. Fe and P show a moderate positive correlation with TOC (r = 0.50 and 0.54; $p$ = 1.0, respectively), but are negatively correlated with TIC (r = −0.66 and −0.70; $R^2$ = −0.78 and −0.84; $p$ < 0.010, respectively), and Ca (r = −0.62 and −0.71; $p$ < 0.050), respectively. Fe also shows a strong positive correlation with the lithophile elements Al, Si, Ti, and Li (r = 0.89–1.0) (Figure 10; Supplementary Figure S4).

All the RSTEs, except for Cu, covary with the major elements. They are particularly concurrent with peaks of elemental concentration at 1.42 m and 1.45 m, although slight relative enrichment also occurs beginning at 0.95 m level up to 1.3 m (Figure 11; Supplementary Tables S3, S4; Supplementary Figure S4). V has a moderately strong correlation with marlstone lithology (r = 0.52), TOC (r = 0.51), near perfect correlation with Th (r = 0.99) and Al (r = 1.0), but covariance was statistically significant only with Th ($p$ > 0.010). V and S were only moderately correlated (r = 0.78). Similarly, Mo shows enrichment at levels 0.30 m, 1.42 m and 1.45 m, and covaries positively with lithology yielding enhanced TOC, Al, whereas it is negatively correlated with TIC (r = −0.19, $p$ > 14.0). Ni is positively correlated with Ti, V, Cr, Cu, Mo, Th, Tl, and U (r > 0.90) and reveals strongest covariance with Al, P, Cr, Cu, Th, Tl, and U (r > 0.97) (Figures 10–12; Supplementary Figure S4).

### Redox elemental ratios

U/Th shows a moderate negative correlation with TOC (r = −0.42), but a moderate positive correlation with TIC (r = 0.32). Ni/Co correlated positively with sulfur content (r = 0.46), V/Cr showed a weak positive correlation with TOC (r = 0.18), Ni/Cu ratio shows a very weak positive correlation with TOC (r = 0.0045). Th/U tends to increase only slightly in limestone (r = 0.32) indicating a relative enrichment of thorium in calcareous sediments and negatively correlates weakly with marly-limestone (r = −0.27) and carbonaceous marls (r = −0.21). (Figures 11, 12; Supplementary Figure S4).

## Discussion

### Biochronology of the la Lata quarry lowermost section

Based on identified nannofossils, we point out the presence of Valanginian-lower Hauterivian nannofossils zones. The occurrence from the base of the studied succession of *Calcicalathina oblongata*, which the FO (first occurrence) is situated in the lower Valanginian (Applegate and Bergen, 1988; Bown, 2005; Melinte and Mutterlose, 2001; Aguado et al., 2018; Mutterlose et al., 2021) is indicative for the NC3 biozone. The LO (last occurrence) of *Rucinolithus wisei* delineates the boundary between NC3a and NC3b subzones., situated in the upper Valanginian (i.e., Applegate and Bergen, 1988; Bown, 2005).

The boundary between the NC3b and NC4a, nannofossil subzones that encompass the Valanginian-Hauterivian boundary interval, could not be identified, as it is marked by the LO of *Tubodiscus verenae* and/or LO of *Cyclagelosphaera deflandrei* (Bralower et al., 1989; Melinte and Mutterlose, 2001 and references therein), species not recorded in the studied succession. At La Charce, France (The Global Boundary Stratotype Section and Point (GSSP) for the base of the Hauterivian Stage), the LO of *E. windii* approximates the Valanginian–Hauterivian boundary,

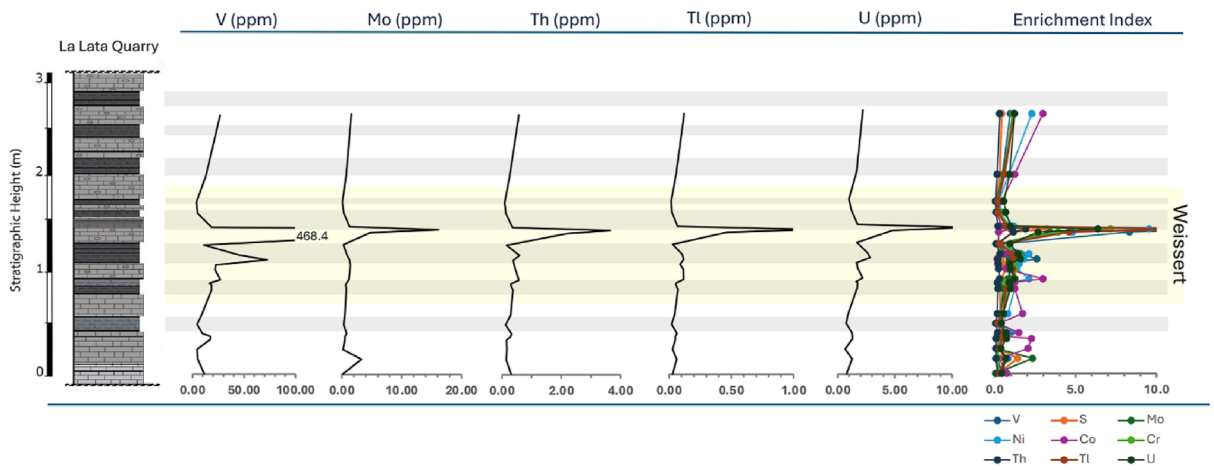


FIGURE 11
Stratigraphic variation in redox sensitive trace elements (RSTEs) correlated with lithology. The red dashed line corresponds to the average value from the dataset of this section (P for Pons, and B, for main background levels, which include data from the San Cayetano and Guasasa Fm in Sierra de los Órganos). The yellow shaded area highlights the Weissert horizons, with corresponding geochemical signatures. The grey shaded bars correspond to the carbonaceous, organic matter-rich lithologies. Refer to lithologic legend on Figures 3, 7.

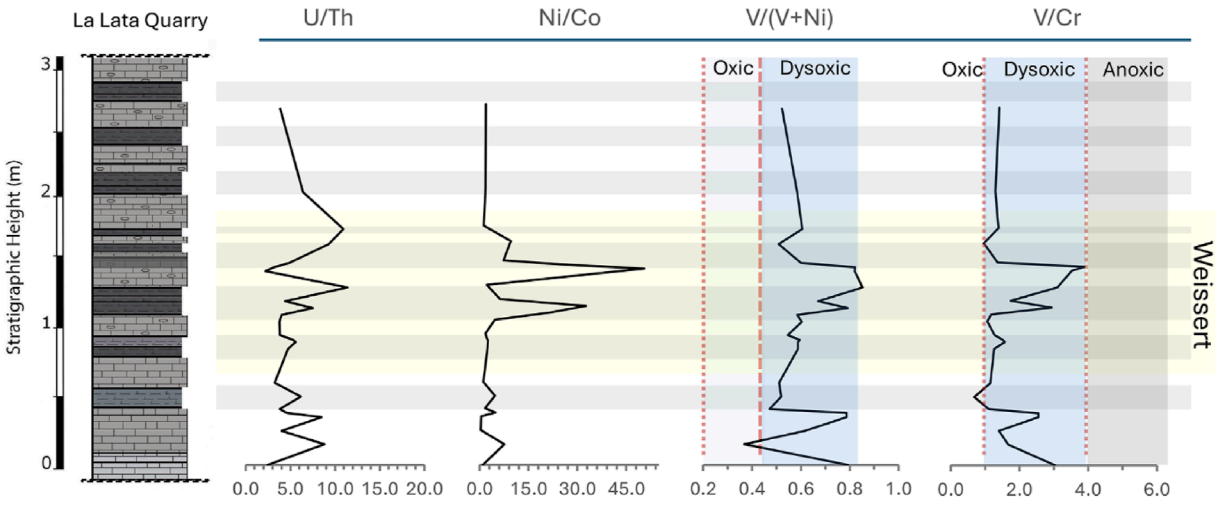


FIGURE 12
Stratigraphic variation in redox sensitive indexes correlated with lithology. The red dashed line corresponds to the average value from the dataset of this section plus background levels, which include data from the San Cayetano and Guasasa Fm in Sierra de los Órganos. The grey shaded bar corresponds to the organic matter-rich lithologies. The yellow shaded area highlights the interval of the Weissert Event, with corresponding geochemical signatures. Refer to lithologic legend on Figures 3, 7.

disappearing in the earliest Hauterivian (Mutterlose et al., 2021). *Eiffellithus windii* is present in the studied samples up to the top of the investigated succession, while the FO of *Lithraphidites bollii*, situated in the early Hauterivian, slightly above the LO of *E. windii* (i.e., Roth, 1978; Applegate and Bergen, 1988; Mutterlose et al., 2021), was not recorded. Nonetheless, the occurrence of *Calpionellites* cf. *darderi* up to 1.05 m, followed by the first record of *Calpionellites major* confirms that the lower part of the section straddles nannoplankton zones NK3a, NK3b and NC4a, which is consistent with a Valanginian-early Hauterivian age (Figures 2, 6, 13).

## Carbon isotope chemostratigraphy and biostratigraphic age correlation

Earth's two main carbon reservoirs, marine carbonates and biogenic organic matter, have notably different isotopic compositions. Marine carbonates are isotopically more positive ("heavier"), with an average $\delta^{13}C$ value around 0‰, whereas organic matter is more negative ("lighter"), averaging around −25‰. Carbonates become enriched in the heavier isotope $^{13}C$ through equilibrium exchange reactions within the inorganic carbon system, involving atmospheric $CO_2$, dissolved bicarbonate, and solid

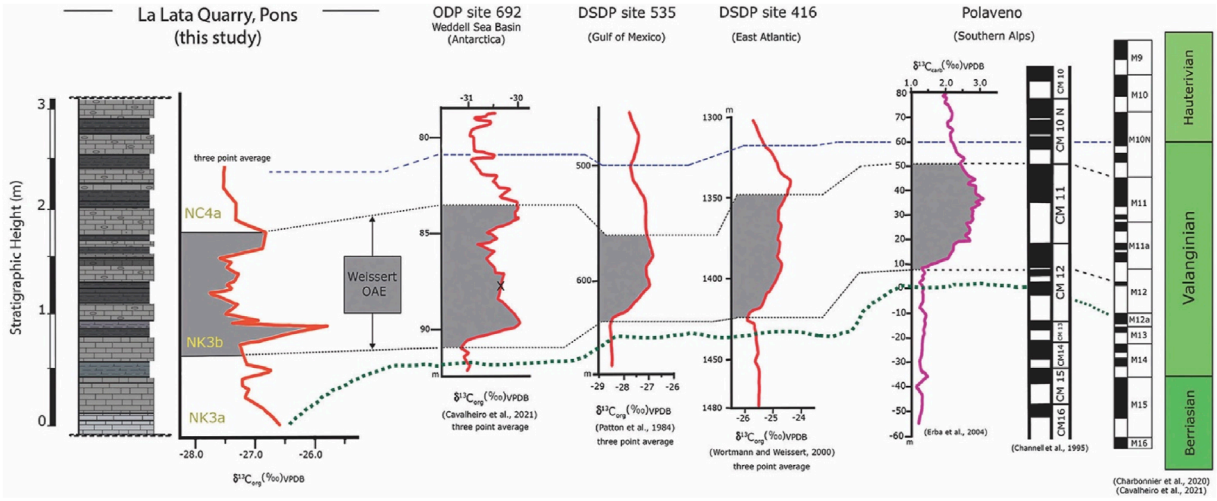


FIGURE 13
Integrated stratigraphic correlation of the Weissert Oceanic Anoxic Event across global sites. The stratigraphic column shows the La Lata Quarry section with respect to biozones NC4A, NK3b, NK3a, and a three-point moving average $\delta^{13}C_{org}$ isotope curve. Adjacent columns display data from ODP Site 692 (Weddell Sea Basin, Antarctica), DSDP Site 535 (Gulf of Mexico), and DSDP Site 416 (East Atlantic), each with a three-point moving average $\delta^{13}C_{org}$. The far-right column presents $\delta^{13}C_{org}$ data from one of the unofficial type-section for the Weissert Event at Polaveno (Southern Alps-northern Italy), along with M-series paleomagnetic chrons and a temporal scale from Berriasian to Hauterivian stages. Grey shading and black lines mark the Weissert interval as interpreted at different sites. The green dotted line indicates the correlation of the lowermost level of our section in relation to a time before the Weissert OAE and the upper blue after (early Hauterivian).

carbonate. By contrast, photosynthesis preferentially incorporates the more negative isotope $^{12}C$ into organic material due to kinetic fractionation (Clayton and Degens, 1959; Friedman and O'Neil, 1977; Saltzman et al., 2012; Hoefs, 2021). Carbonate rocks directly reflect shifts in dissolved inorganic carbon (DIC) in the ocean, as they directly precipitate from this pool (Schlanger et al., 1987; Menegatti et al., 1998; Hayes et al., 1999; Jahren et al., 2001; 2005; Reboulet et al., 2003; Oehlert and Swart, 2014; Swart and Oehlert, 2018). On the other hand, organic carbon signals are modulated by a complex interplay of biological productivity, preservation rates, and diagenetic alterations (Pedersen and Calvert, 1990; Hayes, 1993; Meyers, 1997; Higgins et al., 2018). This can lead to a temporal lag between changes in DIC and their manifestation in the organic carbon record.

The Valanginian stage was characterized, by pronounced positive carbon isotope excursions which have been recognized globally, thereby elevating their significance as reliable stratigraphic markers (Weissert, 1979; Lini et al., 1992; Channell et al., 1993; Erba et al., 2004; Jenkyns, 2010; Weissert et al., 2008; Gréselle et al., 2011; Sanchez-Hernandez and Maurrasse, 2016; Aguirre-Urreta et al., 2017a; Aguirre-Urreta et al., 2017b; Martinez et al., 2020; Martinez, et al., 2023 among others). Excursions of the carbon isotopes $\delta^{13}C$ from the organic fraction correlated with the Weissert Event have been observed in various geological settings worldwide (pelagic, neritic, and continental successions), including the southern Tethys, western North Atlantic, Gulf of Mexico, Colombia, and Pacific, emphasizing its role as a significant Early Cretaceous stratigraphic indicator (Cecca, 1998; Gröcke et al., 1999; 2005; Lini et al., 1992; Weissert et al., 1998; 2008; Bornemann and Mutterlose, 2008; Weissert and Erba, 2004; Silva-Tamayo et al., 2016; Joeckel et al., 2023).

Gréselle et al. (2011) proposed four distinct phases defining the Weissert Event. The first phase features stable, baseline values terminating in a negative deviation of ~0.5‰. The second phase is marked by a significant positive shift of ~2.0‰, representing the event's most substantial increase. The third phase includes a decrease of ~1‰, succeeded by a secondary peak. The fourth and final phase is characterized by a gradual decline, returning to values close to or at the pre-excursion levels. The $\delta^{13}C_{org}$ values from the lowermost section of La Lata quarry, Sierra de los Órganos, exhibit a similar trend (Figures 8, 13). The section starts from a small, above-average positive peak of ~ −26.7‰ (0 m datum) and decreases to below-average values upwards until reaching the largest excursion of ~ −25.6‰ at ~0.91 m. This peak is succeeded by a decreasing trend of 0.6‰–1.9‰ to a negative value of −27.7‰ at 1.2 m, reaching a second maximum at 1.62 and 1.73 m before returning to pre-excursion values. Additionally, an early Hauterivian $\delta^{13}C$ organic carbon peak observed in the La Lata section occurs just after the Weissert Event, reaching ~1.5‰ positive excursion. This CIE may represent a late phase or a local perturbation, similar to those seen at other globally recognized sites (e.g., DSDP holes 603B, 534A, 535, and ODP 692). The context of this excursion will be discussed in greater detail in an upcoming paper.

Overall, these patterns align with similar carbon curve patterns observed during the Weissert Event at sites such as ODP 692 at the Weddell Sea Basin, in Antarctica (Cavalheiro et al., 2021; Giraldo-Gómez et al., 2022), DSDP site 535 in the southwest Gulf of Mexico (Deroo et al., 1984; Cotillon and Rio, 1984; Patton et al., 1984; Lini et al., 1992), DSDP site 416 in the East Atlantic, ODP 1149B from the Pacific, and the Maiolica Formation sections in the Southern Alps, including Polaveno and Capriolo (Lini et al., 1992; Channell et al., 1993; Erba et al., 2004; Weissert et al., 2008)

(Figure 13). The values of site 692 are more negative, whereas those of site 416 are more positive. The $\delta^{13}C_{org}$ values from the lowermost section at La Lata quarry are most congruent with those of the Gulf of Mexico site 535, Rio Corona, and Polaveno in northern Italy (Cotillon and Rio, 1984; Patton et al., 1984; Lini et al., 1992; Marton and Buffler, 1999).

Both isotopic values, organic ($\delta^{13}C_{org}$) and inorganic ($\delta^{13}C_{carb}$) for different sites show slight discrepancies due to dissimilar fractionation, but they all fall within the *Calcicalathina oblongata* subzone. Additionally, the $\delta^{13}C_{org}$ curve from the La Lata quarry in the Sierra de los Órganos agrees with the correlations observed at sites 535 and 692 where the CIE is seen at the top of NK3a, at the base of NK3b (Figure 13).

The integration of the biostratigraphic data, particularly foraminifera, calpionellids, and nannofossil biostratigraphy and the isotopic data has been crucial for establishing a more comprehensive understanding of the temporal record of La Lata section. Correlation of key taxa, including *Globigerinelloides* cf. *paragottisi*, *Tintinnopsella* cf. *carpathica*, *Calpionellites* cf. *darderi* and *major*, along with calcareous nannofossils such as *Calcicalathina oblongata*, *Eiffellithus windii*, *Nannoconus* spp., and *Rucinolithis wisei*, with changes in $\delta^{13}C$ curves revealed that the studied interval of the section falls within the Calpionellites-Tintinnopsella biozones and the spans of nannofossil biozones NK3a up to the base of NC4A.

By comparison, in the Carpathians, the *Tintinnopsella* zone extends from the late Valanginian to the late Hauterivian (Reháková and Michalík, 1997; Lakova and Petrova, 2013). In Cuba, taxa representative of this biozone have been reported from the uppermost Tumbitas Member of the Guasasa Formation (lower Valanginian), which includes parts of the Calpionellites zone (Pszczółkowski, 1999b; López-Martínez et al., 2013; 2017). The observed delay between the last occurrence of *Calpionellites* cf. *darderi* (up to ~1.0 m) and the subsequent first appearance of *Calpionellites* cf. *major* coincides with the sub zonation within the Calpionellites biozone (Lakova and Petrova, 2013). Notably, these occurrences fall within the range of the Weissert Event (Figures 6, 13).

Both *Tintinnopsella* cf. *carpathica* and *Calpionellites* cf. *major* appear to have persisted into the upper Valanginian, and possibly into the Hauterivian of La Lata quarry. The presence of Nannoconids, *N. kamptneri,* and *bermudezii* throughout most of the studied interval, albeit rarely within the interval of the Weissert Event in the La Lata samples (Figure 6), supports the classification of these levels as Valanginian. The lack of *L. bolli* precludes the base of the Hauterivian, although the appearance of *Nannoconus bucheri* above the 1.5 m level coupled with the major CEI suggests that the lowermost Hauterivian is likely present. According to Thierstein (1973) and Erba (1989), *Nannoconus bucheri* appears in the early Hauterivian, and its First Appearance Datum (FAD) in the La Lata section, though slightly overlapping with the Weissert Event, and in association with *Tintinnopsella* spp., further indicates that the start of the Hauterivian may be represented in the uppermost levels. Overall, the micropaleontological findings of the La Lata Quarry section are compatible with previous findings (Fernández-Carmona and Díaz-Otero, 1977; Pszczółkowski, 1999b; Pszczółkowski and Myczyński, 1999; 2003; 2010; Pszczółkowski et al., 2013; López-Martínez et al., 2013).

Despite slight variations in absolute isotopic values across different sections, which may also depend on regional OM sources, a consistent worldwide concurrent pattern of fluctuations revealed significant isotopic excursions in the latest Valanginian and earliest Hauterivian indicative of the effects of global forcing factors (Cotillion and Rio, 1984; Arthur et al., 1985a; Arthur et al., 1985b; Lini et al., 1992; Channell et al., 1993). Initially, low $\delta^{13}C$ values around 1.3‰–1.5‰ in Berriasian and lowermost Valanginian sediments reached a peak to approximately 3‰ in the late/upper Valanginian, particularly within the *Calcicalathina oblongata* nannofossil zone. This positive excursion ended in the earliest Hauterivian, with values fluctuating between 1.5‰ and 2‰ within the *Lithraphidites bollii* nannofossil zone. Previous research established that this isotopic event, observable in various Tethyan and other global sections, was synchronous, predominantly occurring in the middle to upper part of the *C. oblongata* zone (Lini et al., 1992; Channell et al., 1993).

The integrated biostratigraphic and chemostratigraphic data of the lower 3 m of the La Lata Quarry section thus indicates that the onset of the Weissert Event shows somewhat stable, negative values during NK3a biozone, reaching the major positive C-isotope peak at the base of the NK3b, and later decreasing towards the NC4A, in agreement with previous works (e.g., Lini et al., 1992; Erba et al., 2004; Weissert et al., 2008; Cavalheiro et al., 2021). The magnetostratigraphic data further enabled the calibration of the C-isotope stratigraphy indicating that the positive C-isotope excursion commenced in the upper part of CM12 (now M11A) and peaked during CM11, before returning to pre-excursion levels from CM10N to CM8 (Weissert et al., 2008; Cavalheiro et al., 2021; Giraldo-Gómez et al., 2022). These new results thus allow for a refined correlation between the ammonite and magnetostratigraphy, compatible with the correlation proposed by Cavalheiro et al. (2021) but differing from earlier publications (Lini et al., 1992; Channell et al., 1993; Cecca, 1998; Erba et al., 2004). Thus, the carbon isotope geochemical and paleontological data of the studied lowermost La Lata Quarry section concur with an age between the earliest Valanginian and earliest Hauterivian, which encloses the Weissert Event.

## Weissert Event duration and sedimentation rates in La Lata quarry

Previous estimates of the duration of the Weissert Event vary, some researchers estimate it at ~2 Ma (Erba et al., 2004; Cavalheiro et al., 2021), and others at ~5 Ma (Sprovieri et al., 2006; Gréselle and Pittet, 2010). More recent astrochronological data placed the onset of the Weissert Event at ~ 134.50 Ma, with the positive $\delta^{13}C$ excursion extending to ~133.96 Ma, with a sustained elevated $\delta^{13}C$ plateau until 132.44 ± Ma, which yields a duration of ~2.06 Ma (Martinez et al., 2023). Studies in the Vocontian Basin suggest a duration of ~2.08 Ma, with the positive $\delta^{13}C$ excursion lasting 0.94 Ma and the $\delta^{13}C$ plateau ~1.14 Ma (Charbonnier et al., 2013) whereas a study of the Bersek Marl Formation in Hungary yielded ~1.4 Ma (Bajnai et al., 2017).

Sedimentation rate of the Valanginian deposits at Site 535 adjacent to northern Cuba is estimated to be approximately 28 m $Ma^{-1}$ (Buffler et al., 1984; Cotillon and

Rio, 1984; Schlanger et al., 1987) (see Supplementary Table S10; Supplementary Figure S1), while the Tumbitas Member (Guasasa Formation), spanning from the latest Berriasian to early Valanginian, yielded an estimated a rate of ~29 m $Ma^{-1}$ (Pszczółkowski and Myczyński, 2010; López-Martínez et al., 2013). Decompacted deposits from the Tumbitas Member of the Guasasa Formation indicated rates ranging between 46 and 60.5 m $Ma^{-1}$ (Pszczółkowski and Myczyński, 2010; López-Martínez et al., 2013).

Based on the biochronology combined with the paleomagnetic record the dry bulk accumulation rate for the 2.61 m of the section would range between 0.03 and 0.06 cm $ky^{-1}$ (0.3–06 m $Ma^{-1}$) which we consider are too low for such hemipelagic sediments (Seibold, 1975) and are drastically lower than estimates for the Sierra de los Órganos (2.0–4.0 m $Ma^{-1}$) and Sierra del Rosario (0.8–1.0 m $Ma^{-1}$) (Pszczółkowski et al., 1975; Pszczółkowski, 1987; Pszczółkowski and Myczyński, 2010) (Supplementary Figure S7). Although the accumulation rate may vary dependent upon the paleophysiographic settings of the Proto-Caribbean Basin, such extremely low sedimentation rates could be the results of stratigraphic condensation, compression, and/or the presence of hiatuses as is suggested by field observations (Figure 3; Supplementary Figures S3, S5, S7). Indeed, realignment of bioclasts and the deformation of the surrounding mud matrix, stylolites, microfractures, and the structural deformations observed in the outcrop (e.g., Figures 3, 4B5; Supplementary Figures S3, S5) are compatible with the presence of diastems or hiatuses brought about by the structural history of the region as demonstrated elsewhere (Sanchez-Hernandez and Maurrasse, 2014; 2016; Jankowska et al., 2020; Socorro and Maurrasse, 2022). We consider that our original sedimentation rate comparable to those estimated for DSDP site 535 in the Gulf of Mexico and Sierra de los Órganos (Schlager et al., 1984; Cotillon and Rio, 1984; Schenck, 2008; Pszczółkowski and Myczyński, 2010).

To further refine these estimates, future work will employ more precise decompaction models specific to the lithological variations at La Lata, alongside strontium isotope analysis. These steps will provide tighter constraints on sedimentation rates and help resolve whether the observed low rates reflect condensation, hiatuses, or other processes. Additionally, consideration of regional tectonic influences and paleogeographic factors will offer insight into sediment accommodation and preservation during the Weissert Event in the Proto-Caribbean basin.

## Organic carbon preservation and nutrient productivity dynamics

The lowermost succession at the La Lata quarry section exhibits intermittent high TOC levels, averaging ~3.7 wt%, indicating varying degrees of enhanced organic matter (OM) preservation during the latest Valanginian–early Hauterivian (Figure 8). At least three pronounced excursions in $\delta^{13}C_{org}$ do not fully align with TOC values greater than 1.7% ($r = 0.13$, $p = 0.028$), except during the largest carbon isotopic excursion (CIE), which reaches up to ~1.7‰ (Figure 8). This weak correlation between TOC and $\delta^{13}C_{org}$ suggests partial decoupling of local factors from global carbon cycle perturbations, as observed in other studies (Ponton and Maurrasse, 2006; Föllmi, 2012). While the relationship between TOC and $\delta^{13}C_{org}$ is statistically significant, the low correlation coefficient indicates a biologically weak connection, possibly due to OM diagenetic alteration, sediment mixing in carbonate platform or their provenance rather than global carbon cycle changes and processes (e.g., Swart, 2008; Swart et al., 2019). Indeed, the La Lata section shows that marlstone and argillaceous limestone OM-rich layers (excluding those within the Weissert Event), exhibit relatively more negative $\delta^{13}C_{org}$ values, ranging from −27.5‰ to −27.1‰, despite high TOC values (e.g., 10.82 wt% at 1.45 m and 10.23 wt% at 0.915 m). An ongoing study with biomarker analyses will provide us further means to clarify the depositional controls of La Lata sequence.

$\delta^{15}N$ values serve as tracers to distinguish the origins of OM, nutrient cycling, and the intricate relationship between carbon and nitrogen cycles (Williams et al., 1995; Farrell et al., 1995; Farrell et al., 1996; Farrell et al., 2011; Swart et al., 2019). Terrestrially sourced OM generally exhibits higher $\delta^{15}N$ due to nitrogen cycling in soils, whereas marine organic matter tends to show lower $\delta^{15}N$ values (Altabet and Deuser, 1985; Brownlow, 1979; Farrell et al., 1995; 1996; Hoefs, 2021). Simultaneous analysis of $\delta^{15}N$, TOC, and $\delta^{13}C_{org}$, particularly in settings with mixed terrestrial and marine inputs, helps determine the relative contributions of these sources to organic carbon deposition, shifts in nutrient availability, and organic carbon burial (Jenkyns and Clayton, 1986; Martin and Fitzwater, 1988; Jenkyns, 1999; Jenkyns, 2012; Jenkyns, 2018; Calvert et al., 1996; Nijenhuis et al., 1999; Emeis and Weissert, 2009; Derry, 2010). This methodology can address discrepancies in primary productivity signals, potentially influenced by terrestrial dilution or changes in bottom water oxygenation that impact the preservation of marine organic matter (Durand, 1980; Dean et al., 1986; Hansell and Carlson, 2014). $\delta^{15}N$ could also reflect nutrient utilization and nitrogen cycling during OAEs, where nitrogen limitation can significantly affect phytoplankton productivity and the nitrogen isotopic composition of organic matter (Williams et al., 1995; Tesdal et al., 2013; Swart et al., 2019; Hoefs, 2021). $\delta^{15}N$ measurements from bulk sediment worldwide exhibit a range from 2.5‰ to 16.6‰, with an average of 6.7‰ (Tesdal et al., 2013) and shifts towards more negative values may imply stronger terrestrial input, while values closer to zero or positive may indicate marine influences (Brownlow, 1979; Hoefs, 2021; Tesdal et al., 2013; Swart et al., 2019). Based on this standard of reference, since the La Lata Quarry section, $\delta^{15}N_{org}$ values show a positive shift (~−0.3‰) between 0.35 m and 0.41 m, significantly above the average (−1.9‰), they suggest marine influence (Figure 8). Furthermore, given that near-zero $\delta^{15}N$ values are often associated with nitrogen fixation in suboxic conditions, they could reflect such conditions in our case. The weak negative correlation between Fe and $\delta^{15}N_{org}$ ($r = -0.36$), and the weak correlation with K ($r = -0.26$; Supplementary Tables S1, S6–S8), rule out dust as a possible nitrogen source and suggests that nitrogen fixation, rather than upwelled nitrate, may have been a major source of nitrogen for organic production (Swart et al., 2019). Additionally, the decreasing trend in $\delta^{15}N_{org}$ values at 0.6 m, just before the Weissert Event, points to potential shifts in nitrogen cycling processes in the proto-Caribbean Basin.

RSTEs like Mo, V, and U, alongside the nitrogen isotopes help further clarify the nitrogen cycling pathways. For instance, Mo is essential for nitrogenase in nitrogen fixation, thus when elevated,

coupled with near-zero $\delta^{15}N_{org}$ values, implies nitrogen fixation under suboxic conditions. Similarly, higher V and U concentrations in reduced environments would support the interpretation of nitrogen cycling under low-oxygen conditions. However, in the La Lata section, the nitrogen isotope data ($\delta^{15}N_{org}$) and RSTEs (Mo, V, U) show a weak and non-significant correlation (r = −0.30 to 0.33, $p > 0.050$; Supplementary Tables S1, S6–S8). This weak correlation suggests that any relationship between nitrogen cycling, and redox conditions is minimal or potentially overshadowed by other local processes or diagenesis.

## Terrigenous inputs and elemental enrichment patterns

The temporal variability of major elements (Al, Si, Ti, Li, K, and Ca), biophilic elements (P, Fe), and RSTEs are proxies to infer source of sediment components, extant redox conditions, and productivity. Al and Ti are terrestrial and mainly derived from fluvial and/or eolian sources and are unaffected by biological processes or diagenesis (Brumsack, 2006; Blum and Hattier-Womack, 2009; Scholz et al., 2011). Thus, strong correlations between Fe, K, Ti, and Si oxides along with aluminum oxides ($Al_2O_3$ wt%) in marine sediments suggest co-sedimentation with or from terrigenous sources (Martin, 1992; Rowe et al., 2025). Conversely, a strong negative correlation with carbonate content (TIC and CaO) may indicate limited carbonate precipitation, dilution, or dissolution, and potentially reflecting oxygen deficient conditions, restricted environments, or both (Lerman, 1978; Schoonen, 2004). The La Lata quarry sediments show perfect positive correlation between Ti and Al (r = 1.0, $p = 1$), which corroborates a terrestrially sourced elements from terranes adjacent to the Proto-Caribbean basin.

P is a critical element for all living organisms across different trophic levels (Van Mooy et al., 2015) therefore it is important in sustaining productivity. In the ocean it occurs mostly as dissolved inorganic phosphorus (DIP) or orthophosphate ($PO_4^{3-}$) derived from chemically weathered phosphatic rocks (Golterman, 1995; 2001; Delaney, 1998; Compton et al., 2000; Filippelli, 2002; 2008; Martiny et al., 2019; Huang et al., 2012; 2016). Temporal distribution of P in the studied interval at the La Lata quarry shows no enrichment with respect to the Sierra de los Órganos background average (~0.23 mg/g, or 216–230 ppm), except at the onset of the Weissert Event and after its major CIE (~0.90–0.95 m). There is moderate positive correlation between P and TOC (r = 0.54, $R^2 = 0.41$, $p = 0.61$; Supplementary Figure S4), a near perfect correlation with Al (r = −0.99, $p = 0.65$) in contrast to a strong negative correlation with TIC (r = −0.85). P also has a pronounced positive correlation with Fe and Al, with a correlation coefficient exceeding 0.94. Fe temporal variation shows concentration that rarely exceeds the Sierra de los Órganos average background values (2.4 mg/g), albeit a significant enrichment level between 1.42 m–1.45 m (13.7 mg/g). Fe has moderate correlation with TOC (r = 0.50, $R^2 = 0.36$), a strong correlation with Al (r = 0.94, $R^2 = 0.50$) (Supplementary Figure S4).

These close relationships suggest a continuous nutrient supply originating from terrestrial sources enhancing OM production in the Proto-Caribbean Basin analogous to similar occurrences demonstrated elsewhere during the Weissert Event, as for instance the Lower Saxony Basin, Northern Germany (e.g., Thöle et al., 2020), and further supports the assertion that the Weissert event coincided with a significant global increase of terrigenous flux due to intensified hydrological cycle (Weissert, 1990; Kuhn et al., 2005; Duchamp-Alphonse et al., 2007; Westermann et al., 2010). Paleogeographic reconstructions of the Proto-Caribbean Basin justifies the potential terrigenous sources associated with the La Lata quarry sediments (Pindell, 1985; Pszczółkowski, 1976; 1999a; Cobiella Reguera, 1996; Cobiella Reguera, 2000; Cobiella Reguera, 2008; Schafhauser et al., 2003; Schenk, 2008; Pardo, 2009; Pindell and Kennan, 2009; Pszczółkowski and Myczyński, 2010; Pindell et al., 2020). We may also surmise that global settings associated with the main phase of the Paraná-Etendeka LIP (135.0 ± 0.6–133.2 ± 0.3 Ma) concurrent with the Valanginian stage (Renne et al., 1996; Silva Gomes and Vasconcelos, 2021) may have been a contributing factor that triggered the global event.

## Redox conditions indicators in relation to OM preservation

Studies of modern organic-rich deposits from oxygen-depleted ocean basins have established a correlation between higher concentrations of RSTEs and reducing conditions (Berner, 1974; Anderson and Raiswell, 2004; Brumsack, 2006; Dellwig et al., 2010; Ardakani er al., 2024). In undisturbed reducing sediments, trace metals can be strongly fixed into sulfidic minerals (Huerta-Diaz and Morse, 1990; 1992; Huerta-Diaz et al., 1998). However, if bottom waters are re-oxygenated (through enhanced circulation or decreased OM productivity), organic compounds and authigenic minerals can be reoxidized, releasing trace metals (Phillips and Xu, 2021; Dantas et al., 2022).

Elemental enrichments of Mo, U, V, Cr, Ni, Cu, Th, in marine sediments commonly serve as indicators of redox conditions because higher concentrations or relative enrichments of these elements coincide with regions associated with elevated accumulation of organic carbon coupled to sulfur cycling under reducing environment (e.g., Adams and Weaver, 1958; Wedepohl, 1971; Claypool et al., 1980; Breint and Wanty, 1991; Emerson and Huested, 1991; McManus et al., 2006; Yano et al., 2020). For instance, Mo originates from continental weathered deposits and is supplied to the oceans as molybdate anion ($MoO4^{2-}$) (Scott et al., 2008) where it remains in low concentration as a bioessential element in nitrogen fixation (Ruvalcaba Baroni et al., 2015; Fan et al., 2022). Due to its low biological uptake (Collier, 1985) Mo is considered a conservative element with long residence time (Sohrin et al., 1998; McManus et al., 2006) but it becomes enriched in sediments essentially associated with OM accumulation in oxygen depleted conditions. Similarly, V enrichment in sediments occurs under reducing conditions which appears to follow two distinct pathways, it can be reduced with $H_2S$ in euxinic environments, $V(IV) + H_2S \rightarrow V(OH)^3$ + clays (euxinic sediments), or V can adhere to organic particles in anoxic sediments, forming organic complexes (Breint and Wanty, 1991). Consequently, RSTEs as redox proxies are more reliable in environments with persistent, strong reducing conditions (anoxic/euxinic) and less predictable in phases with intermediate oxygen deficiency (Rimmer et al., 2004; Tribovillard et al., 2006).

Thus, the occurrence of reduced sulfur species such as pyrite ($FeS_2$) in sedimentary deposits typically signifies reducing conditions (Berner, 1970; Rickard and Morse, 2005), whereas oxidized forms like sulfate minerals point to oxidizing environments (Lerman, 1978; Berner and Raiswell, 1984; Schoonen, 2004). Based on this premise, RSTEs have been applied to infer paleoredox states in OM-rich deposits assumed to be associated with oxygen-depleted environments across various time scales (Brumsack, 1989; Ye et al., 2016; Yano et al., 2020). Records of such conditions are reported in the Caribbean region where previous studies indicate that during the Late Jurassic and Early Cretaceous, the northwestern Proto-Caribbean Basin developed dysoxic to anoxic conditions related to restricted water circulation in its deeper, narrower sections (Hatten, 1957; 1967; Pszczółkowski, 1978; 1999a; Moretti et al., 2003; Magnier et al., 2004; Cobiella Reguera, 2008; Pszczółkowski and Myczyński, 2010; López-Martínez et al., 2013). Since benthic foraminifera are absent in all the microfacies, except for very rare specimens in Microfacies D, and a bioturbation index below 3 (Figure 7) the record indicates that the La Lata quarry section accumulated under oxygen-poor (dysoxic) bottom water conditions. This is further supported by geochemical proxies such as Mo, U, and V concentrations and elemental redox ratios (Figure 7). Nonetheless, while the rarity of benthic fauna and low bioturbation index in some intervals may suggest such environments (Wignall and Myers, 1988), they are not definitive proof of persistent oxygen-poor conditions. Instead, the geochemical data provide the primary evidence for these settings, with brief reoxygenation episodes inferred from the redox-sensitive element ratios.

Indeed, maximum values of Ni/Co coeval with the interval of the Weissert Event (Figure 12; Supplementary Figure S8) reflect redox-controlled scavenging or fractionation processes, potentially linked to the differential solubility and transport of nickel and cobalt in such environments. Ni, Cr, and U values fluctuate with minor consistent enrichment (Figure 11), indicative of limited reducing conditions. These ratios covary with benthic foraminifera scarcity compatible with oxygen-deprived surrounding, although full anoxia was not achieved (Rhoads and Morse, 1971; Wignall and Myers, 1988; Tyson and Pearson, 1991). Also, the weak correlation of Ni and U with Al (Supplementary Tables S3, S4) further suggests that their presence may be linked to minor sulfides, as evidenced by dispersive pyrite (Figures 4, 9). By contrast, V is slightly depleted compared to Los Órganos background and Pons Fm levels, and its strong positive correlation with Al (r = 1.0; Supplementary Tables S3, S4) reveals a terrigenous origin.

Relative elemental enrichments of Mo, U and V in marine sediments can further serve as indicators of redox conditions (Adams and Weaver, 1958; Breint and Wanty, 1991; Emerson and Huested, 1991; McManus et al., 2006; Yano et al., 2020; Phillips and Xu, 2021). Higher concentrations or relative enrichments of Mo and U coincide with regions associated with elevated accumulation of organic carbon coupled to sulfur cycling under oxygen deficient settings (McManus et al., 2006).

Mo originates from weathered deposits and is supplied to oceans as molybdate anion ($MoO4^{2-}$) (Scott et al., 2008; Phillips and Xu, 2021). Despite its low concentration in seawater, its long residence time (Sohrin et al., 1998) and low biological uptake (Collier, 1985) make it a well-supplied trace metal in oceans (Anbar, 2004; Scott et al., 2008). At the La Lata quarry, Mo is weakly to moderately correlated with TOC (r = 0.52, $R^2$ = 0.37, $p$ = 0.35; Figures 11, 12; Supplementary Table S3; Supplementary Figure S4) but strong positive to Al (r = 0.96, $R^2$ = 0.93, $p$ = 0.40) and Fe (r = 0.98, $R^2$ = 0.97, $p < 0.010$). Mo and Fe covary at one level before the Weissert Event (0.15 m), and then during the event (levels ~0.90–~1.50 m) - perhaps indicative of complex interactions related to Fe-S phase (see below). Decoupling of Mo from Fe at the onset and after these Weissert levels suggests other factors influencing its presence, as both Fe and OM are scavenging agents (Helz et al., 1996). Mo significant increase is concurrent with V, Th, Tl, and U enhancement segments (1.42 m–1.45 m) aligns with minor reducing conditions (Figure 12; Supplementary Figures S4, S7). The ratio of Mo/TOC yielded a moderate positive correlation (r = 0.54, $p$ = 0.4) with most of the samples falling between the values of the recent euxinic sediments of the Black Sea (4.5 ± 1), and the Saanich Inlet (45 ± 5) (Özsoy and Ünlüata, 1997; Algeo and Lyons, 2006; Ardakani et al., 2024). Particularly, samples from the Weissert Event fell generally within the range of the modern values of the Black Sea (Figure 14B; Supplementary Figure S8).

U is released by weathering of landmasses and delivered to oceans (mostly U-238) where it occurs in low concentrations as soluble oxidized U(VI) under oxic conditions and as U(IV) in the reduced state where it is preserved in sediments. U(VI) is more soluble and dominates oxygen-rich surface waters, whereas U(IV) is less soluble and precipitates out of seawater in low-oxygen or reducing environments, such as those found in deep ocean sediments (Anderson et al., 1989; Klinkhammer and Palmer, 1991; Emerson and Huested, 1991; Zheng et al., 2002). The sediments analyzed from the lowermost La Lata section yielded U values moderately correlated with TOC (r = 0.54 and $R^2$ = 0.39, $p$ = 0.28, Supplementary Figure S4; Supplementary Tables S3–S8) and shows a stronger, near-perfect relationship with Al (r = 0.98, $p$ = 0.33), Li (r = 0.96, $p$ = 0.46), and other metals (r > 0.90), furthermore suggesting a detrital origin (Supplementary Figure S4).

V is essential for paleoredox evaluation due to its distinct behavior under varying redox conditions. In oxygenated environments, vanadium exists in a soluble form as vanadate ($V^{5+}$), but it forms insoluble compounds under low-oxygen conditions. V is incorporated into marine sediments through two main pathways, primarily governed by redox conditions (Brumsack, 1989; Calvert and Pedersen, 1993; Tribovillard et al., 2006). In euxinic environments, where anoxic and sulfidic conditions dominate, it is reduced by hydrogen sulfide ($H_2S$) and sequestered in sediments through the formation of insoluble compounds or adsorption onto organic matter. This behavior is like other redox-sensitive trace elements, such as Mo and U, which also precipitate under these conditions (Phillips and Xu, 2021; Dantas et al., 2022). V's transitioning between soluble and insoluble forms makes it a key proxy for reconstructing ancient redox environments, because under oxic conditions it remains soluble as vanadate, while in anoxic waters it is reduced to vanadyl ($V^{4+}$) and accumulates in sediments, offering valuable insights into past oxygen levels (Wignall and Twitchett, 1996; Socorro and Maurrasse, 2019; Ardakani et al., 2024).

At La Lata quarry, vanadium (V) shows a weak to moderate negative correlation with total organic carbon (TOC) (r = −0.51, $R^2$ = 0.38, $p < 0.010$; Figure 11; Supplementary Figures S4, S8; Supplementary Tables S3, S6, S7) but displays a perfect positive

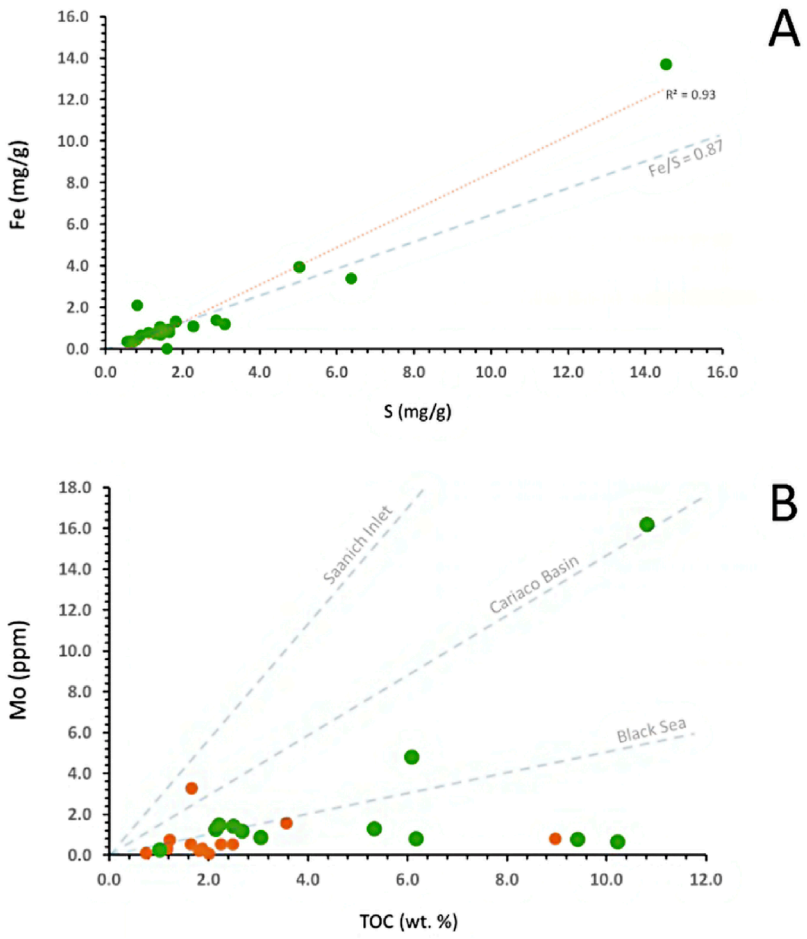


FIGURE 14
Cross-plots showing elemental relationships from samples at La Lata Quarry. **(A)** Plot of Fe versus S (mg/g), displaying a strong positive correlation ($R^2$ = 0.93), with reference ratios from other basins (dashed lines). **(B)** Plot of Mo (ppm) versus TOC (wt.%), comparing the sample data with reference trends from the Cariaco Basin, Black Sea, and Saanich Inlet (dashed lines) to highlight similarities in redox conditions across sites. Green and orange markers represent distinct sample groups. Figure adopted from Ardakani et al. (2024).

correlation with Al (r = 1, $R^2$ = 0.93, $p < 0.010$) and a strong positive correlation with iron (Fe) (r = 0.93, $R^2$ = 0.97, p < 0.010). V and Fe co-vary prominently at one major level before the Weissert Event (1.15 m) and again show a major relative enrichment peak towards the end of the event (between ~0.90 and ~1.50 m). The overall average V concentration is 46.9 ± 103.2 ppm (SD), with higher concentrations (~85 ppm) found in the more OM-rich layers, while the lighter limestone layers yield a much lower mean value of 12.9 ppm. Unusually high enrichment of V relative to Al would indicate that thermal loss of organic carbon (TOC) is not the dominant mechanism of V enrichment (Davies et al., 2000). Since under weak reducing conditions, V species may be partially blocked by sulfide complexation (Lewan, 1984; 1997; Killops and Killops, 2013), leading to enhanced Ni absorption, thus, the relatively higher Ni enrichment compared to background levels (Figure 11) is consistent with Ni absorption into organic compounds under weak reducing conditions (Morse and Luther III, 1999). Hence, V depletion further confirms the absence of strong reducing phases in this interval (Breint and Wanty, 1991; Lipinski et al., 2003).

The decoupling of V from Fe after the onset of the Weissert Event, as seen with Mo earlier, suggests that additional factors influence the behavior of V because both Fe and OM can act as scavenging agents (Helz et al., 1996). The negative correlation with TOC and the strong co-variance with Fe and Al reflects complex interactions between V, OM, and mineral phases under varying redox conditions, particularly during significant paleoenvironmental stress. A significant increase in vanadium occurs concurrently with elevated levels of S, Ni, Mo, Th, Tl, and U between 1.42 m and 1.45 m (Figure 11), suggesting increasingly reducing conditions (Figure 12; Supplementary Figure S8).

Additional redox proxies can also use S enrichment which occurs in marine sediments through the formation of sulfides, including pyrite and potentially molybdenum sulfides, particularly under euxinic conditions (Emerson and Huested, 1991; Helz et al., 1996; Phillips and Xu, 2021). Consequently, the S/Ca and S/TOC ratios can be valuable indicators of redox conditions and diagenetic processes (Claypool et al., 1980; Calvert and Pedersen, 1993). High S/TOC ratios often signal enhanced sulfate reduction and pyrite formation, indicative of anoxic conditions that favor

OM preservation (Hedges and Keil, 1995; Schoonen, 2004). In contrast, lower S/TOC ratios calcium-rich, possibly more oxic settings where carbonate minerals are prevalent (Nriagu, 1978; Claypool et al., 1980; Emerson et al., 1983). In the studied section, S/TOC ratios range from ~0.31 (1.65 mg/g S, 5.35% TOC) to 1.15 (1.40 mg/g S, 1.22% TOC), where the higher values correspond to anoxic, pyrite-forming conditions (Juncher et al., 2009; Yano et al., 2020). These findings fall within typical marine sediment ranges, implying that reactive iron was sufficiently available for sulfur incorporation (Jickells et al., 2005; Antler et al., 2014; Hülse et al., 2019), facilitating pyrite formation in reducing
environments.

Conversely, considering that low S/Ca ratios typically indicate calcium-rich, oxic environments where carbonate minerals dominate (Nriagu, 1978; Leventhal, 1983; Berner and Raiswell, 1984), a high S/Ca ratio of 0.014, corresponding to 1.90 mg/g S and 138.23 mg/g Ca at 2.61 m (Cu-PR-37, microfacies C), suggests a relative enrichment in sulfur. By contrast, the lower S/Ca ratio of 0.0021 in sample Cu-PR-30 (at 1.73 m, microfacies B), with 0.56 mg/g S and 268.32 mg/g Ca, reflects a calcium-rich environment Yano et al., 2020). Both levels occur after the Weissert event, further indicating potential shifts in redox conditions during deposition even in different organic-rich levels (Supplementary Table S9).

## Redox-sensitive trace element ratios as redox proxies

As previously discussed, the redox sensitive trace elements (RSTEs) typically show less enrichment in weakly reducing environments compared to anoxic/euxinic settings (Tribovillard et al., 2006). In this study, their use alongside elemental redox ratios (e.g., Ni/Co, U/Th, V/Cr, and V/(V + Ni)) compliment a robust assessment of paleoredox conditions (Figures 12, 14; Supplementary Figure S8). As shown in Figures 11, 12 the La Lata Quarry sediments yielded V/Cr ratios below 2 which suggest steady low oxygen conditions, but not complete or persistent anoxia (Jones and Manning, 1994; Hetzel et al., 2009). The strong correlation of V with Al (r = 1.0) and Li (r = 0.96), along with its increase in carbonaceous layers, implies a possible connection to terrigenous input rather than redox conditions alone (Hatch and Leventhal, 1992).

Overall, the various proxy's indicative of redox conditions during accumulation applied at La Lata indicate low oxygen settings but lack strong evidence for sulfidic phases that would drive significant RSTE enrichment. The geochemical and lithological variability suggests a complex history of variable redox conditions, diagenesis, and possible post-depositional alteration.

## Pyrite morphology and implications for redox conditions in the Proto-Caribbean Basin

Pyrite as a signal of redox conditions in ancient sediments and modern environments is widely asserted to indicate oxygen-deficient settings (Kremling, 1983; Wilkin et al., 1996; Wilkin et al., 1997; Donald and Southam, 1999; Juncher et al., 2009), but the natural geochemical mechanisms of pyrite morphology have been widely debated. Nonetheless, the critical role of hydrogen sulfide ($H_2S$) and OM-mediated by sulfate reducing bacteria (SRB) is well recognized (e.g., Jørgensen and Bak, 1991; Wilkin et al., 1996). Donald and Southam (1999) demonstrated the role of dissimilatory sulfate reducing bacteria in microcrystal and framboid pyrite formations, although similar processes have also been replicated - without bacteria-in laboratory experiments that led to the postulate that framboid can be formed due to rapid nucleation in euxinic water column without biological intervention (Butler and Rickard, 2000). It has also been established that in sedimentary deposits framboid formation predominantly occurs just beneath the $O_2$-$H_2S$ redox boundary due to the availability of reactants and relatively high Eh conditions (Wilkin et al., 1996; Wilkin et al., 1997; Butler and Rickard, 2000). With respect to size, Wilkin et al. (1996), Wilkin et al. (1997) indicated that framboid nucleation in water columns under anoxic/euxinic conditions is rapid, hence the unit sizes are smaller than framboid nucleation that takes place within anoxic/euxinic sediment pore water, even though the overlying water column may be oxic. Consequently, framboids are smaller in diameters (<6 μm) in deposits associated with anoxic/euxinic conditions, whereas in standard marine dysoxic settings framboids tend to be larger (>6–10 μm) (Wilkin et al., 1996; Bond and Wignall, 2010). Wignall and Newton (1998) further advanced the concept to apply the maximum framboid diameter (MFD) as an indicator of bottom water oxygen levels. This approach has proven effective in using framboid size distributions as a proxy to infer paleoredox states across geological time (e.g., Wilkin et al., 1996; Wignall and Newton, 1998; Bond and Wignall, 2010; Nielsen et al., 2011; Wang et al., 2012). In La Lata quarry succession, levels such as microfacies A, or limestone with low TOC show limited pyrite formation which is predominant in facies with higher TOC where framboid pyrite occurs with variable size ranges (Figures 4A–D, Figures 9A1-4; Supplementary Figure S3). We infer that where small framboid diameters (<10 μm) occur they imply nucleation in the water column under dysoxic conditions, whereas intermittent non-euxinic nucleation episodes in the pore waters formed the larger pyrite nodules (>14 μm).

This variability in framboid size further reflects rapid shifts between dysoxic, possibly euxinic, and less reducing conditions, indicating episodic redox fluctuations (Figures 12, 14; Supplementary Figure S8). The moderate correlation between S and TOC (r = 0.51) and the strong correlation between S and Fe (r = 0.96; $R^2$ = 0.93), though not statistically significant ($p$ = 1), suggest that sulfur sequestration through pyrite formation was prevalent (though not the greatest sulfur sink) (Figures 7, 14). The scattering of data points around the pyrite line (Fe/S = 0.87) (Figure 14) likely reflects variability in pyrite formation pathways suggesting that framboidal pyrite formed under more reactive, early depositional conditions taking place in the water column or sediment, whereas the larger pyrite nodules formed later as diagenetic products (Ardakani et al., 2024). This also corroborated by the textural perturbation caused by the pyrite crystal growth on the surrounding fabric as seen in thin sections (Figure 14; Supplementary Figure S3).

## Conclusion

This study characterizes the Weissert Event in the Sierra de los Órganos, Western Cuba. It integrates a multiproxy geochemical approach with a detailed sedimentary analysis to elucidate the complex interactions between regional oxygen depleted conditions and global perturbations of the carbon cycle during the Early Cretaceous. Our findings highlight the critical role of the Proto-Caribbean passive margins as a carbon sink during the Valanginian with evidence suggesting a broader influence on regional organic carbon sequestration both prior to and following that stage. The sedimentary record from western Cuba provides unique insights into the local response of marine ecosystems to local forcing factors, providing a valuable case study for understanding the Proto-Caribbean environments during the Early Cretaceous period.

The results reveal that OM preservation within the studied section was enhanced by a continuous influx of terrestrial material, which coincided with variable and prolonged low oxygen (dysoxic) conditions. Fully anoxic environments were not reached, as indicated by consistently low RSTE ratio, because the absence of a fully developed sulfidic phase limits the enrichment of redox-sensitive trace elements. Furthermore, OM preservation was enhanced by terrestrially sourced input showing a robust correlation with redox conditions favorable to carbon sequestration in the basin. While the primary source of the OM remains undetermined pending biomarker and pyrolysis analysis, the presence of diverse lithologies, micropaleontology, and varying geochemical signatures suggest that these sediments have recorded a complex history of deposition, diagenesis, and possibly post-depositional alteration.

These findings are particularly significant in the context of current global climate change, as they enhance our understanding of past oceanic conditions and provide valuable insights into potential future trends. The study also underscores the importance of terrestrial runoff and nutrient fertilization in driving bioproductivity and influencing OM production and preservation. The Valanginian Weissert Event in the Proto-Caribbean Basin, as recorded in the Sierra de los Órganos, underscores the impact of global climatic and oceanic shifts on regional marine ecosystems.

## Data availability statement

The original contributions presented in the study are included in the article/Supplementary Material, further inquiries can be directed to the corresponding author.

## Author contributions

JO: Conceptualization, Formal Analysis, Investigation, Visualization, Writing – original draft, Writing – review and editing. MCM: Formal Analysis, Investigation, Methodology, Resources, Writing – original draft, Writing – review and editing. FJ-MRM: Formal Analysis, Funding acquisition, Investigation, Methodology, Project administration, Resources, Supervision, Validation, Writing – original draft, Writing – review and editing.

## Funding

The author(s) declare that financial support was received for the research and/or publication of this article. Support for this project was partly covered by the Glenn Goodfriend memorial funds.

## Acknowledgments

Our heartfelt gratitude to the numerous individuals and organizations whose contributions have been invaluable to this project. Special appreciation is extended to Jorge A. Álvarez Licourt, Leonel Pérez Orozco, and Cándido Santana for their assistance with planning and fieldwork. Our thanks go to Jorge F. Garcell for his crucial help in securing the necessary exportation permits. We also extend our gratitude to the Office of the Conservator of Valle de Viñales, Pinar del Rio, and the director of La Lata Quarry for their cooperation and assistance. Extended thanks are due to the Cuban Registro Nacional de Bienes Culturales (RNBC) and Patrimonio for granting the necessary permits (LAH-23, No. 20152222, Fol. 0174644), which were essential for the successful completion of this project. We are deeply grateful to Carlos Herdocia, Vanesa Londoño, Andrei Pszczółkowski, Diane Pirie, Jander Socorro, Yosmel Sanchez, Tatiana Gaona, Jose Manuel Torres Parada, Jian Ping, Tom Beasley, Patrick Roman, Peter K. Swart, Amel Said, Ali Pourmand, and Yasmani Ceballos for their invaluable support, insights, and guidance trough the literature and in the laboratory. Also, to Helmut Weissert and Jorg Mutterlose for sharing their research. We also thank Project PNRR C9 - I8, code 97/15.11.2022, Contract No. 760115/23.05.2023, which provided the laboratory materials used to prepare the nannofossil samples. To François Fournier and two referees for their reviews.

## Conflict of interest

The authors declare that the research was conducted in the absence of any commercial or financial relationships that could be construed as a potential conflict of interest.

## Generative AI statement

The author(s) declare that no Generative AI was used in the creation of this manuscript.

## Publisher's note

All claims expressed in this article are solely those of the authors and do not necessarily represent those of

## Supplementary material

The Supplementary Material for this article can be found online at: https://www.frontiersin.org/articles/10.3389/feart.2025.1549274/full#supplementary-material

## References


Achterberg, E. P., van den Berg, C. M. G., Boussemart, M., and Davison, W. (1997). Speciation and cycling of trace metals in Esthwaite Water: a productive English lake with seasonal deep-water anoxia. *Geochimica Cosmochimica Acta* 61 (24), 5233–5253. doi:10.1016/S0016-7037(97)00316-5

Adams, J. A., and Weaver, C. E. (1958). Thorium-to-uranium ratios as indicators of sedimentary processes: example of the concept of geochemical facies. *AAPG Bull.* 42 (2), 387–430.

Aguado, R., Company, M., Castro, J., de Gea, G., Molina, J., Nieto, L., et al. (2018). A new record of the Weissert episode from the Valanginian succession of Cehegín (Subbetic, SE Spain): bio- and carbon isotope stratigraphy. *Cretac. Res.* 92, 122–137. doi:10.1016/j.cretres.2018.07.010

Aguirre Urreta, B., Lescano, M., Concheyro, A., Vennari, V., Tunik, M. A., Naipauer, M., et al. (2017a). "Geocronología y bioestratigrafía de alta resolución: el Cretácico Inferior de los Andes," in *XX congreso geológico argentino*.

Aguirre-Urreta, B., Schmitz, M., Lescano, M., Tunik, M., Rawson, P. F., Concheyro, A., et al. (2017b). A high precision U–Pb radioisotopic age for the agrio formation, neuquén basin, Argentina: implications for the chronology of the hauterivian stage. *Cretac. Res.* 75, 193–204. doi:10.1016/j.cretres.2017.03.027

Algeo, T. J., and Lyons, T. W. (2006). Mo–total organic carbon covariation in modern anoxic marine environments: implications for analysis of paleoredox and paleohydrographic conditions. *Paleoceanography* 21 (1). doi:10.1029/2004pa001112

Altabet, M. A., and Deuser, W. G. (1985). Seasonal variations in natural abundance of 15N in particles sinking to the deep Sargasso Sea. *Nature* 315 (6016), 218–219. doi:10.1038/315218a0

Álvarez, S. H., and Bernal, R. L. (2013). Las formaciones Pons y Peñas del Cretácicos de la Sierra de los Órganos (unpublished, available on Academia.edu).

Álvarez Sánchez, H. (1981). *Síntesis de la Evolución Geotectónica de la Sierra de los Órganos apoyada en el estudio de la Geología del Valle de Pons*, 272–108. (Unpublished). CUPR, Pinar del Río, Cuba.

Anbar, A. D. (2004). Molybdenum stable isotopes: observations, interpretations and directions. *Rev. Mineralogy Geochem.* 55 (1), 429–454. doi:10.2138/gsrmg.55.1.429

Anderson, R. F., Fleisher, M. Q., and Le Huray, A. P. (1989). Concentration, oxidation state, and particulate flux of uranium in the Black Sea. *Geochimica Cosmochimica Acta* 53, 2215–2224. doi:10.1016/0016-7037(89)90345-1

Anderson, T. F., and Raiswell, R. (2004). Sources and mechanisms for the enrichment of highly reactive iron in euxinic Black Sea sediments. *Am. J. Sci.* 304, 203–233. doi:10.2475/ajs.304.3.203

Antler, G., Turchyn, A. V., Herut, B., Davies, A., Rennie, V. C., and Sivan, O. (2014). Sulfur and oxygen isotope tracing of sulfate driven anaerobic methane oxidation in estuarine sediments. *Estuar. Coast. Shelf Sci.* 142, 4–11. doi:10.1016/j.ecss.2014.03.001

Applegate, J. L., and Bergen, J. A. (1988). Cretaceous calcareous nannofossil biostratigraphy of sediments recovered from the Galicia Margin, ODP Leg 103. *Proc. Ocean Drill. Program, Sci. Results* 103, 293–348.

Ardakani, O. H., Gadd, M. G., Hedhli, M., Petts, D., and Jensen, G. (2024). Organic matter the major sink of redox-sensitive trace elements in Upper Devonian black shale. *Chem. Geol.* 670, 122385. doi:10.1016/j.chemgeo.2024.122385

Arroyo, L., Trejos, T., Gardinalli, P. R., and Almirall, J. R. (2009). Optimization and validation of a laser ablation inductively coupled plasma mass spectrometry method for the routine analysis of soils and sediments. *Spectrochim. Acta Part B* 64, 16–25.

Arthur, M. A., Dean, W. E., and Claypool, G. E. (1985b). Anomalous $^{13}$C enrichment in modern marine organic carbon. *Nature* 315 (6016), 216–218. doi:10.1038/315216a0

Arthur, M. A., Dean, W. E., and Schlanger, S. O. (1985a). "Variations in the global carbon cycle during the Cretaceous related to climate, volcanism, and changes in atmospheric CO2,". *The carbon cycle and atmospheric CO2: natural variations archean to present*. Editors E. T. Sundquist, and W. S. Broecker (Geophysical Monographs, American Geophysical Union), 32, 504–529. doi:10.1029/gm032p0504

Arthur, M. A., and Premoli-Silva, I. (1982). "Development of widespread organic carbon-rich strata in the Mediterranean Tethys," in *Nature and origin of cretaceous carbon-rich facies*. Editors S. O. Schlanger, and M. B. Cita (London: Academic Press), 7–54.

Bajnai, D., Pálfy, J., Martinez, M., Price, G. D., Nyerges, A., and Főzy, I. (2017). Multi-proxy record of orbital-scale changes in climate and sedimentation during the Weissert event in the valanginian Bersek Marl Formation (gerecse mts., Hungary). *Cretac. Res.* 75, 45–60. doi:10.1016/j.cretres.2017.02.021

Bengtsson, L., and Enell, M. (1986). "Chemical analysis," in *Handbook of holocene palaeoecology and palaeohydrology*. Editor B. E. Berglund (Chichester: John Wiley & Sons Ldt.), 423–451.

Berner, R. A. (1970). Sedimentary pyrite formation. *Am. J. Sci.* 268 (1), 1–23. doi:10.2475/ajs.268.1.1

Berner, R. A. (1974). "Iron sulfides in Pleistocene deep Black Sea sediments and their paleoceanographic significance" in eds. E. T. Degens, and R. A. Ross *The Black Sea-geology, chemistry and biology*. (Memoir No. 20. American Association of Petroleum Geologists, Tulsa), 524–531.

Berner, R. A., and Raiswell, R. (1984). C/S method for distinguishing freshwater from marine sedimentary rocks. *Geology* 12 (6), 365–368. doi:10.1130/0091-7613(1984)12<365:cmfdff>2.0.co;2

Blum, M. D., and Hattier-Womack, J. (2009). "Climate change, sea-level change, and fluvial sediment supply to deepwater depositional systems" in eds B. Kneller, and O. J. Martinsen, *B. McCaffrey External controls on deep-water depositional systems* (SEPM Society for Sedimentary Geology),15–30).doi:10.2110/sepmsp.092.015

Bodin, S., Godet, A., Matera, V., Steinmann, P., Vermeulen, J., Gardin, S., et al. (2007). Enrichment of redox-sensitive trace metals (U, V, Mo, As) associated with the late Hauterivian Faraoni oceanic anoxic event. *Int. J. Earth Sci. Geol. Rundschau* 96, 327–341. doi:10.1007/s00531-006-0091-9

Bond, D. P., and Wignall, P. B. (2010). Pyrite framboid study of marine Permian–Triassic boundary sections: a complex anoxic event and its relationship to contemporaneous mass extinction. *Geol. Soc. Am. Bull.* 122 (7-8), 1265–1279. doi:10.1130/b30042.1

Bornemann, A., and Mutterlose, J. (2008). Calcareous nannofossil and $\delta^{13}$C records from the early cretaceous of the western atlantic ocean: evidence for enhanced fertilization across the berriasian–valanginian transition. *Palaios* 23 (12), 821–832. doi:10.2110/palo.2007.p07-076r

Bown, P. R. (2005). Early to mid-cretaceous calcareous nannoplankton from the northwest pacific ocean, leg 198, shatsky rise. *Proc. Ocean Drill. Program, Sci. Results* 198, 1–82.

Bown, P. R., Rutledge, D. C., Crux, J. A., and Gallagher, L. T. (1998). *Lower cretaceous in eds P.R. Bown calcareous nannofossil biostratigraphy*. London: British Micropalaeontological Society Publication Series, 86–131.

Bralower, T. J., Monechi, S., and Thierstein, H. R. (1989). Calcareous nannofossil zonation of the Jurassic-Cretaceous boundary interval and correlation with the geomagnetic polarity timescale. *Mar. Micropaleontol.* 14, 153–235. doi:10.1016/0377-8398(89)90035-2

Breint, G. N., and Wanty, R. B. (1991). Vanadium accumulation in carbonaceous rocks: a review of geochemical controls during deposition and diagenesis. *Chem. Geol.* 91, 83–97. doi:10.1016/0009-2541(91)90083-4

Brownlow, A. H. (1979). *Geochemistry*. New Jersey: Prentice Hall.

Brumsack, H. J. (1989). Geochemistry of recent TOC-rich sediments from the Gulf of California and the Black Sea. *Geol. Rundsch.* 78, 851–882. doi:10.1007/bf01829327

Brumsack, H. J. (2006). The trace metal content of recent organic carbon-rich sediments: implications for Cretaceous black shale formation. *Palaeogeogr. Palaeoclimatol. Palaeoecol.* 232, 344–361. doi:10.1016/j.palaeo.2005.05.011

Buffler, R. T., Schlager, W., Bowdler, J. L., Cotillon, P. H., Halley, R. B., Kinoshita, H., et al. (1984). "Initial reports, DSDP, 77," in *Initial reports of the deep-sea drilling project* (Washington: US Government Printing Office), 77, 25–218.

Butler, I. B., and Rickard, D. (2000). Framboidal pyrite formation via the oxidation of iron (II) monosulfide by hydrogen sulphide. *Geochimica Cosmochimica Acta* 64 (15), 2665–2672. doi:10.1016/s0016-7037(00)00387-2

Calvert, S. E., Bustin, R. M., and Ingall, E. D. (1996). Influence of water column anoxia and sediment supply on the burial and preservation of organic carbon in marine shales. *Geochimica Cosmochimica Acta* 60 (9), 1577–1593. doi:10.1016/0016-7037(96)00041-5

Calvert, S. E., and Pedersen, T. F. (1993). Geochemistry of recent oxic and anoxic marine sediments: implications for the geological record. *Mar. Geol.* 113 (1-2), 67–88. doi:10.1016/0025-3227(93)90150-t

Castro-Alfonso, L. (2015). "Geología de las sierras Pan de Azúcar, Celadas y Ancón. Rasgos favorables para la exploración petrolera," in *Memorias, trabajos y resúmenes, VI Convención Cubana de Ciencias de la Tierra Geociencias' 2015, Sociedad Cubana de Geología, La Habana*. CD-ROM.

Cavalheiro, L., Wagner, T., Steinig, S., Bottini, C., Dummann, W., Esegbue, O., et al. (2021). Impact of global cooling on Early Cretaceous high *p*CO2 world during the Weissert Event. *Nat. Commun.* 12 (1), 5411. doi:10.1038/s41467-021-25706-0

Cecca, F. (1998). Early Cretaceous (pre-Aptian) ammonites of the Mediterranean Tethys: palaeoecology and palaeobiogeography. *Palaeogeogr. Palaeoclimatol. Palaeoecol.* 138 (1-4), 305–323. doi:10.1016/s0031-0182(97)00126-0

Channell, J. E. T., Erba, E., and Lini, A. (1993). Magnetostratigraphic calibration of the late Valanginian carbon isotope event in pelagic limestones from Northern Italy and Switzerland. *Earth Planet. Sci. Lett.* 118 (1-4), 145–166. doi:10.1016/0012-821x(93)90165-6

Charbonnier, G., Adatte, T., Duchamp-Alphonse, S., Spangenberg, J. E., and Föllmi, K. B. (2020). "Global mercury enrichment in Valanginian sediments supports a volcanic trigger for the Weissert episode," in *Mass extinctions, volcanism, and impacts: new developments* (Geological Society of America). Chapter 4). doi:10.1130/2019.2544(04

Charbonnier, G., Boulila, S., Gardin, S., Duchamp-Alphonse, S., Adatte, T., Spangenberg, J. E., et al. (2013). Astronomical calibration of the Valanginian "Weissert" episode: the Orpierre marl–limestone succession (Vocontian Basin, southeastern France). *Cretac. Res.* 45, 25–42. doi:10.1016/j.cretres.2013.07.003

Charbonnier, G., Duchamp-Alphonse, S., Adatte, T., Föllmi, K. B., Spangenberg, J. E., Gardin, S., et al. (2016). Eccentricity paced monsoon-like system along the northwestern Tethyan margin during the Valanginian (Early Cretaceous): new insights from detrital and nutrient fluxes into the Vocontian Basin (SE France). *Palaeogeogr. Palaeoclimatol. Palaeoecol.* 443, 145–155. doi:10.1016/j.palaeo.2015.11.027

Charbonnier, G., Duchamp-Alphonse, S., Deconinck, J. F., Adatte, T., Spangenberg, J. E., Colin, C., et al. (2020). A global palaeoclimatic reconstruction for the Valanginian based on clay mineralogical and geochemical data. *Earth-Science Rev.* 202, 103092. doi:10.1016/j.earscirev.2020.103092

Charbonnier, G., Morales, C., Duchamp-Alphonse, S., Westermann, S., Adatte, T., and Föllmi, K. B. (2017). Mercury enrichment indicates volcanic triggering of Valanginian environmental change. *Sci. Rep.* 7 (1), 40808. doi:10.1038/srep40808

Claypool, G. E., Holser, W. T., Kaplan, I. R., Sakai, H., and Zak, I. (1980). The age curves of sulfur and oxygen isotopes in marine sulfate and their mutual interpretation. *Chem. Geol.* 28, 199–260. doi:10.1016/0009-2541(80)90047-9

Claypool, G. E., Holser, W. T., Kaplan, I. R., Sakai, H., and Zak, I. (1980). The age curves of sulfur and oxygen isotopes in marine sulfate and their mutual interpretation. *Chem. Geol.* 28, 199–260. doi:10.1016/0009-2541(80)90047-9

Clayton, R. N., and Degens, E. T. (1959). Use of carbon isotope analyses of carbonates for differentiating fresh-water and marine sediments. *AAPG Bull.* 43 (4), 890–897.

Cobiella Reguera, J. L. (1996). Estratigrafía y eventos jurásicos en la cordillera de Guaniguanico, Cuba Occidental. *Minería Geol.* 13 (3), 11–24.

Cobiella Reguera, J. L. (2000). Jurassic and Cretaceous geological history of Cuba. *Int. Geol. Rev.* 42 (7), 594–616. doi:10.1080/00206810009465102

Cobiella Reguera, J. L. (2008). Reconstrucción palinspástica del paleomargen mesozoico de América del Norte en Cuba occidental y el sudeste del Golfo de México: Implicaciones para la evolución del SE del Golfo de México. *Rev. Mex. Ciencias Geol.* 25 (3), 382–401.

Collier, R. W. (1985). Molybdenum in the northeast pacific ocean 1. *Limnol. Oceanogr.* 30 (6), 1351–1354. doi:10.4319/lo.1985.30.6.1351

Compton, J., Mallinson, D., Glenn, C., Filippelli, G., Föllmi, K., Shields, G., et al. (2000). "Variations in the global phosphorus cycle," in *SEPM special publications 66, marine authigenesis: from microbial to global*. Editors C. Glenn, L. Prévôt-Lucas, and J. Lucas, 21–34.

Cotillon, P., and Rio, M. (1984). Compared cyclicity of the lower cretaceous pelagic in the southern subalpine chains (SE France), the central atlantic (DSDP site 534), and the Gulf of Mexico (DSDP sites 535 and 540); paleoclimatic implications and application to trans-tethysian stratigraphic correlations. *Bull. la Société Géologique Fr.* 7 (1), 47–62.

Cramér, H. (1946). A contribution to the theory of statistical estimation. *Scand. Actuar. J.* 1946 (1), 85–94. doi:10.1080/03461238.1946.10419631

Danilewski, D. (1972). Esquema general de la composición tectónico-estructural de la zona de los mogotes en el área Pons-San Vicente (Sierra de los Órganos). Actas Academia de Ciencias de Cuba. *Inst. Geol. La Habana* 2, 42–44.

Dantas, R. C., Hassan, M. B., Cruz, F. W., and Jovane, L. (2022). Evidence for methane seepage in South Atlantic from the occurrence of authigenic gypsum and framboidal pyrite in deep-sea sediments. *Mar. Petroleum Geol.* 142, 105727. doi:10.1016/j.marpetgeo.2022.105727

Davies, S. C., Hughes, D. L., Janas, Z., Jerzykiewicz, L. B., Richards, R. L., Sanders, J. R., et al. (2000). Vanadium complexes of the $N(CH_2CH_2S)_3^{3-}$ and $O(CH_2CH_2S)_2^{2-}$ Ligands with coligands relevant to nitrogen fixation processes. *Inorg. Chem.* 39 (16), 3485–3498. doi:10.1021/ic9909476

Dean, W. E. (1974). Determination of carbonate and organic matter in calcareous sediments and sedimentary rocks by loss on ignition: comparison with other methods. *J. Sediment. Petrology* 44, 242–248.

Dean, W. E., Arthur, M. A., and Claypool, G. E. (1986). Depletion of 13C in Cretaceous marine organic matter: source, diagenetic, or environmental signal? *Mar. Geol.* 70, 119–157. doi:10.1016/0025-3227(86)90092-7

Delaney, M. L. (1998). Phosphorus accumulation in marine sediments and the oceanic phosphorus cycle. *Glob. Biogeochem. Cycles* 12 (4), 563–572. doi:10.1029/98gb02263

Dellwig, O., Leipe, T., März, C., Glockzin, M., Pollehne, F., Schnetger, B., et al. (2010). A new particulate Mn–Fe–P-shuttle at the redoxcline of anoxic basins. *Geochimica Cosmochimica Acta* 74 (24), 7100–7115. doi:10.1016/j.gca.2010.09.017

Deroo, G., Herbin, J. P., and Huc, A. Y. (1984). Organic geochemistry of Cretaceous black shales from deep sea drilling project site 530, leg 75, eastern south Atlantic. *Initial Rep. Deep-Sea Drill. Proj.* 75, 983–999.

Derry, L. A. (2010). A burial diagenesis origin for the Ediacaran Shuram–Wonoka carbon isotope anomaly. *Earth Planet. Sci. Lett.* 294 (1-2), 152–162. doi:10.1016/j.epsl.2010.03.022

Donald, R., and Southam, G. (1999). Low temperature anaerobic bacterial diagenesis of ferrous monosulfide to pyrite. *Geochimica Cosmochimica Acta* 63 (13/14), 2019–2023. doi:10.1016/s0016-7037(99)00140-4

Draper, G., and Barros, J. A. (1994). "Cuba. En," in *Caribbean geology: an introduction*. Editors K. S. Donovan, and T. A. y Jackson (Mona, Kingston, Jamaica: West Indies University Press).

Duchamp-Alphonse, S., Gardin, S., Fiet, N., Bartolini, A., Blamart, D., and Pagel, M. (2007). Fertilization of the northwestern Tethys (Vocontian basin, SE France) during the Valanginian carbon isotope perturbation: evidence from calcareous nannofossils and trace element data. *Palaeogeogr. Palaeoclimatol. Palaeoecol.* 243 (1-2), 132–151. doi:10.1016/j.palaeo.2006.07.010

Duque-Botero, F., and Maurrasse, F. J. M. (2005). Cyanobacterial productivity, variations in the organic carbon, and facies of the Indidura Formation (Cenomanian-Turonian), Northeastern Mexico. *J. Iber. Geol.* 31 (8).

Duque-Botero, F., and Maurrasse, F. J. M. (2008). Role of cyanobacteria in corg-rich deposits: an example from the indidura formation (Cenomanian-Turonian), northeastern Mexico. *Cretac. Res.* 29 (5-6), 957–964. doi:10.1016/j.cretres.2008.05.015

Durand, B. (1980). *Kerogen: insoluble organic matter from sedimentary rocks*. Bayeux, France: Editions Technip.

Emeis, K. C., and Weissert, H. (2009). Tethyan–Mediterranean organic carbon-rich sediments from Mesozoic black shales to sapropels. *Sedimentology* 56 (1), 247–266. doi:10.1111/j.1365-3091.2008.01026.x

Emerson, S., Jacobs, L., and Tebo, B. (1983). "The behavior of trace metals in marine anoxic waters: solubilities at the oxygen-hydrogen sulfide interface," in *Trace metals in sea water* (Springer), 579–608.

Emerson, S. R., and Huested, S. S. (1991). Ocean anoxia and the concentrations of molybdenum and vanadium in seawater. *Mar. Chem.* 34 (3-4), 177–196. doi:10.1016/0304-4203(91)90002-e

Erba, E. (1989). Upper jurassic to lower cretaceous Nannoconus distribution in some sections from northern and central Italy. *Mem. degli Ist. Geol. Mineral. dell'Universita Padova* 41, 255–261.

Erba, E. (1994). Nannofossils and superplumes: the Early Aptian "nannoconid crisis". *Paleoceanography* 9 (3), 483–501. doi:10.1029/94pa00258

Erba, E., Bartolini, A., and Larson, R. L. (2004). Valanginian Weissert oceanic anoxic event. *Geology* 32 (2), 149–152. doi:10.1130/g20008.1

Erba, E., and Tremolada, F. (2004). Nannofossil carbonate fluxes during the Early Cretaceous: phytoplankton response to nutrification episodes, atmospheric CO2, and anoxia. *Paleoceanography* 19 (1). doi:10.1029/2003PA000884

Fan, J., Duan, L., Yin, M., Yuan, H., and Li, X. (2022). Nonconservative behavior of dissolved molybdenum and its potential role in nitrogen cycling in the Bohai and Yellow Seas. *Front. Mar. Sci.* 9, 1094846. doi:10.3389/fmars.2022.1094846

Farrell, J. W., Pedersen, T. F., Calvert, S. E., and Nielsen, B. (1995). Glacialá¤-interglacial changes in nutrient utilization in the equatorial Pacific Ocean. *Nature* 377 (6549), 514–517. doi:10.1038/377514a0

Farrell, M., Hill, P. W., Farrar, J., Bardgett, R. D., and Jones, D. L. (2011). Seasonal variation in soluble soil carbon and nitrogen across a grassland productivity gradient. *Soil Biol. Biochem.* 43 (4), 835–844. doi:10.1016/j.soilbio.2010.12.022

Farrell, R. E., Sandercock, P. J., Pennock, D. J., and Van Kessel, C. (1996). Landscape-scale variations in leached nitrate: relationship to denitrification and natural nitrogen-15 abundance. *Soil Sci. Soc. Am. J.* 60 (5), 1410–1415. doi:10.2136/sssaj1996.03615995006000050017x

Fernández-Carmona, J., and Díaz-Otero, C. (1977). Importancia de los grupos de los grupos Calpionélidos y grupos Incertae Sedis en Cuba: intervalo Titoniano-Albiano. *La Minería Cuba* 3 (3), 52–57.

Filippelli, G. M. (2002). The global phosphorus cycle. *Rev. mineralogy Geochem.* 48 (1), 391–425. doi:10.2138/rmg.2002.48.10

Filippelli, G. M. (2008). The global phosphorus cycle: past, present, and future. *Elements* 4 (2), 89–95. doi:10.2113/gselements.4.2.89

Föllmi, K. B. (2012). Early Cretaceous life, climate and anoxia. *Cretac. Res.* 35, 230–257. doi:10.1016/j.cretres.2011.12.005

Föllmi, K. B., Weissert, H., Bisping, M., and Funk, H. (1994). Phosphogenesis, carbon-isotope stratigraphy, and carbonate-platform evolution along the Lower Cretaceous northern Tethyan margin. *Geol. Soc. Am. Bull.* 106 (6), 729–746. doi:10.1130/0016-7606(1994)106<0729:pcisac>2.3.co;2

Friedman, I., and O'Neil, J. R. (1977). Compilation of stable isotope fractionation factors of geochemical interest (No. 440-KK).

Giraldo-Gómez, V. M., Petrizzo, M. R., Bottini, C., Möller, C., Wagner, T., Cavalheiro, L., et al. (2022). Bottom water redox dynamics during the early cretaceous Weissert event in ODP hole 692B (Weddell Sea, Antarctica) reconstructed from the benthic foraminiferal assemblages. *Palaeogeogr. Palaeoclimatol. Palaeoecol.* 587, 110795. doi:10.1016/j.palaeo.2021.110795

Goddard, E. N., Trask, P. D., De Ford, R. K., Rove, O. N., Singewald, J. T., and Overbeck, R. M. (1963). *Rock-color chart*. Colorado, USA: Geological Society of America.Colorado

Golterman, H. L. (1995). The role of the ironhydroxide-phosphate-sulphide system in the phosphate exchange between sediments and overlying water. *Hydrobiologia* 297, 43–54. doi:10.1007/BF00033500

Golterman, H. L. (2001). Phosphate release from anoxic sediments or 'What did Mortimer really write? *Hydrobiologia* 450, 99–106. doi:10.1023/A:1017559903404

Gonfiantini, R., Stichler, W., and Rozanski, K. (1995). Standards and intercomparison materials distributed by the International Atomic Energy Agency for stable isotope measurements (No. IAEA-TECDOC–825).

González-Arreola, C., and Barragán, R. (2007). *Oosterella* (ammonoidea) from the taraises formation (upper valanginian), durango, northeast Mexico. *Cretac. Res.* 28 (3), 419–427. doi:10.1016/j.cretres.2006.06.006

Gréselle, B., and Pittet, B. (2010). Sea-level reconstructions from the Peri-Vocontian Zone (South-east France) point to Valanginian glacio-eustasy. *Sedimentology* 57 (7), 1640–1684. doi:10.1111/j.1365-3091.2010.01159.x

Gréselle, B., Pittet, B., Mattioli, E., Joachimski, M., Barbarin, N., Riquier, L., et al. (2011). The Valanginian isotope event: a complex suite of palaeoenvironmental perturbations. *Palaeogeogr. Palaeoclimatol. Palaeoecol.* 306 (1-2), 41–57. doi:10.1016/j.palaeo.2011.03.027

Gröcke, D. R., Hesselbo, S. P., and Jenkyns, H. C. (1999). Carbon-isotope composition of Lower Cretaceous fossil wood: ocean-atmosphere chemistry and relation to sea-level change. *Geology* 27, 155–158. doi:10.1130/0091-7613(1999)027<0155:cicolc>2.3.co;2

Gröcke, D. R., Price, G. D., Robinson, S. A., Baraboshkin, E. Y., Mutterlose, J., and Ruffell, A. H. (2005). The Upper Valanginian (Early Cretaceous) positive carbon–isotope event recorded in terrestrial plants. *Earth Planet. Sci. Lett.* 240 (2), 495–509. doi:10.1016/j.epsl.2005.09.001

Hammer, Ø., Harper, D. A. T., and Ryan, P. D. (2001). PAST: paleontological Statistic Software package for education and data analysis. *Palaeontol. Electron.* 4, 1–9. Available online at: http://palaeo-electronica.org/2001_1/past/issue1_01.htm.

Hansell, D. A., and Carlson, C. A. (2014). *Biogeochemistry of marine dissolved organic matter* (Academic Press).

Harris, G. P., Feldman, G. C., and Griffiths, F. B. (1993). "Global oceanic production and climate change," in *Ocean colour: theory and applications in a decade of CZCS experience* (Dordrecht Netherlands: Springer), 237–270.

Hatch, J. R., and Leventhal, J. S. (1992). Relationship between inferred redox potential of the depositional environment and geochemistry of the upper pennsylvanian (missourian) Stark shale member of the dennis limestone, wabaunsee county, Kansas, USA. *Chem. Geol.* 99 (1-3), 65–82. doi:10.1016/0009-2541(92)90031-y

Hatten, C. W. (1957). *Geology of Central Sierra de los Órganos. Pinar del Rio Province Cuba (unpublished report)*. Fondo Geológico Nacional. La Habana. Cuba.

Hatten, C. W. (1967). Principal features of Cuban geology: discussion. *AAPG Bull.* 51 (5), 780–789. doi:10.1306/5d25c0d1-16c1-11d7-8645000102c1865d

Hayes, J. M. (1993). Factors controlling $^{13}$C contents of sedimentary organic compounds: principles and evidence. *Mar. Geol.* 113 (1-2), 111–125. doi:10.1016/0025-3227(93)90153-m

Hayes, J. M., Strauss, H., and Kaufman, A. J. (1999). The abundance of $^{13}$C in marine organic matter and isotopic fractionation in the global biogeochemical cycle of carbon during the past 800 Ma. *Chem. Geol.* 161, 103–125. doi:10.1016/s0009-2541(99)00083-2

Hedges, J. I., and Keil, R. G. (1995). Sedimentary organic matter preservation: an assessment and speculative synthesis. *Mar. Chem.* 49 (2-3), 137–139. doi:10.1016/0304-4203(95)00013-h

Heiri, O., Lotter, A. F., and Lemcke, G. (2001). Loss on ignition as a method for estimating organic and carbonate content in sediments: reproducibility and comparability of results. *J. Paleolimnol.* 25, 101–110. doi:10.1023/a:1008119611481

Helz, G. R., Miller, C. V., Charnock, J. M., Mosselmans, J. F. W., Pattrick, R. A. D., Garner, C. D., et al. (1996). Mechanism of molybdenum removal from the sea and its concentration in black shales: EXAFS evidence. *Geochimica Cosmochimica Acta* 60 (19), 3631–3642. doi:10.1016/0016-7037(96)00195-0

Herdocia, C., and Maurrasse, F. J.-M. R. (2022). Chemostratigraphic characteristics of trace elements, biomarkers and clay mineralogy indicating environmental conditions within Aptian sediments of the Organyà Basin, North-east Spain, prior to the onset of OAE 1a. *Depositional Rec.* 8, 931–957. doi:10.1002/dep2.186

Herdocia, C., and Maurrasse, F. J.-M. R. (2023). Geochemical factors associated with deposition of lower Aptian organic-rich sediments during OAE1a in the Basque-Cantabrian Basin, northern Spain. *Front. Geochem.* 1, 1080169. doi:10.3389/fgeoc.2023.1080169

Herrera, N. M. (1961). Contribución a la estratigrafía de la Provincia de Pinar del Río. *Rev. Soc. Cubana Ing.* 5 (2), 2–24.

Herrle, J. O., Pross, J., Friedrich, O., Kößler, P., and Hemleben, C. (2003). Forcing mechanisms for mid-cretaceous black shale formation: evidence from the upper aptian and lower albian of the Vocontian Basin (SE France). *Palaeogeogr. Palaeoclimatol. Palaeoecol.* 190, 399–426. doi:10.1016/s0031-0182(02)00616-8

Hetzel, A., Böttcher, M. E., Wortmann, U. G., and Brumsack, H. J. (2009). Paleo-redox conditions during OAE 2 reflected in Demerara Rise sediment geochemistry (ODP Leg 207). *Palaeogeogr. Palaeoclimatol. Palaeoecol.* 273 (3-4), 302–328. doi:10.1016/j.palaeo.2008.11.005

Higgins, J. A., Blättler, C. L., Lundstrom, E. A., Santiago-Ramos, D. P., Akhtar, A. A., Ahm, A. C., et al. (2018). Mineralogy, early marine diagenesis, and the chemistry of shallow-water carbonate sediments. *Geochimica Cosmochimica Acta* 220, 512–534. doi:10.1016/j.gca.2017.09.046

Hoefs, J. (2021). *Stable isotope geochemistry*. Ninth Edition. Amsterdam: Springer.

Hoffman, D. W., and Rasmussen, C. (2022). Absolute carbon stable isotope ratio in the Vienna Peedee Belemnite isotope reference determined by 1H NMR spectroscopy. *Anal. Chem.* 94 (13), 5240–5247. doi:10.1021/acs.analchem.1c04565

Huang, J., Ji, M., Xie, Y., Wang, S., He, Y., and Ran, J. (2016). Global semi-arid climate change over last 60 years. *Clim. Dyn.* 46, 1131–1150. doi:10.1007/s00382-015-2636-8

Huang, J. P., Guan, X. D., and Ji, F. (2012). Enhanced cold season warming in semi-arid regions. *Atmos. Chem. Phys.* 12 (12), 5391–5398. doi:10.5194/acp-12-5391-2012

Huerta-Diaz, M. A., and Morse, J. W. (1990). A quantitative method for determination of trace metal concentrations in sedimentary pyrite. *Mar. Chem.* 29, 119–144. doi:10.1016/0304-4203(90)90009-2

Huerta-Diaz, M. A., and Morse, J. W. (1992). Pyritization of trace metals in anoxic marine sediments. *Geochimica Cosmochimica Acta* 56 (7), 2681–2702. doi:10.1016/0016-7037(92)90353-k

Huerta-Diaz, M. A., Tessier, A., and Carignan, R. (1998). Geochemistry of trace metals associated with reduced sulfur in freshwater sediments. *Appl. Geochem.* 13 (2), 213–233. doi:10.1016/s0883-2927(97)00060-7

Hülse, D., Arndt, S., and Ridgwell, A. (2019). Mitigation of extreme ocean anoxic event conditions by organic matter sulfurization. *Paleoceanogr. Paleoclimatology* 34 (4), 476–489. doi:10.1029/2018pa003470

Iturralde-Vinent, M. (1994). Cuban geology: a new plate tectonic synthesis. *J. Petroleum Geol.* 17 (1), 39–71. doi:10.1306/bf9ab732-0eb6-11d7-8643000102c1865d

Iturralde-Vinent, M., Garcia-Casco, A., Rojas Agramonte, Y., Proenza Fernández, J. A., Murphy, J. B., and Stern, R. J. (2016). The geology of Cuba: a brief overview and synthesis. *GSA Today* 26 (10), 4–10. doi:10.1130/gsatg296a.1

Iturralde-Vinent, M., and MacPhee, R. D. (1999). Paleogeography of the Caribbean region: implications for Cenozoic biogeography. *Bull. AMNH no. 238*.

Iturralde-Vinent, M., and Pszczółkowski, A. (2021). *Geología del terreno Guaniguanico. En: Geología de Cuba, Compendio, 2021*. La Habana, Cuba: DVD-Rom. Editorial CITMATEL. ISBN 978-959–237-352-5.

Iturralde-Vinent, M. A., Otero, C. D., García-Casco, A., and van Hinsbergen, D. J. (2008). Paleogene foredeep basin deposits of north-central Cuba: a record of arc-continent collision between the Caribbean and North American Plates. *Int. Geol. Rev.* 50 (10), 863–884. doi:10.2747/0020-6814.50.10.863

Jahren, A. H., Arens, N. C., Sarmiento, G., Guerrero, J., and Amundson, R. (2001). Terrestrial record of methane hydrate dissociation in the Early Cretaceous. *Geology* 29 (2), 159–162. doi:10.1130/0091-7613(2001)029<0159:tromhd>2.0.co;2

Jahren, A. H., Conrad, C. P., Arens, N. C., Mora, G., and Lithgow-Bertelloni, C. (2005). A plate tectonic mechanism for methane hydrate release along subduction zones. *Earth Planet. Sci. Lett.* 236, 691–704. doi:10.1016/j.epsl.2005.06.009

Jankowska, E., Nohl, T., Grohganz, M., Hohmann, N., Vandenbroucke, T. R. A., and Munnecke, A. (2020). Reconstructing depositional rates and their effect on paleoenvironmental proxies: the case of the Lau Carbon Isotope Excursion in Gotland, Sweden. *Paleoceanogr. Paleoclimatology* 35 (12), e2020PA003979. doi:10.1029/2020pa003979

Jarvis, I., Mabrouk, A., Moody, R. T., and de Cabrera, S. (2002). Late Cretaceous (Campanian) carbon isotope events, sea-level change, and correlation of the Tethyan and Boreal realms. *Palaeogeogr. Palaeoclimatol. Palaeoecol.* 188 (3-4), 215–248. doi:10.1016/s0031-0182(02)00578-3

Jenkyns, H. C. (1980). Cretaceous anoxic events: from continents to oceans. *J. Geol. Soc. Lond.* 137, 171–188. doi:10.1144/gsjgs.137.2.0171

Jenkyns, H. C. (1999). Mesozoic anoxic events and palaeoclimate. *Zentralblatt für Geol. Paläontologie* 1997 (7-9), 943–949.

Jenkyns, H. C. (2010). Geochemistry of oceanic anoxic events. *Geochem. Geophys. Geosystems* 11 (3), 1525–2027. doi:10.1029/2009gc002788

Jenkyns, H. C. (2018). Transient cooling episodes during cretaceous oceanic anoxic events with special reference to OAE 1a (early aptian). *Philosophical Trans. R. Soc. A Math. Phys. Eng. Sci.* 376 (2130), 20170073. doi:10.1098/rsta.2017.0073

Jenkyns, H. C., and Clayton, C. J. (1986). Black shales and carbon isotopes in pelagic sediments from the Tethyan Lower Jurassic. *Sedimentology* 33 (1), 87–106. doi:10.1111/j.1365-3091.1986.tb00746.x

Jenkyns, H. C., and Parente, M. (2012). Strontium isotope stratigraphy in the upper Cenomanian shallow-water carbonates of the southern Apennines: short-term perturbations of marine 87Sr/86Sr during the oceanic anoxic event 2. *Palaeogeogr. Palaeoclimatol. Palaeoecol.* 261, 15–29. doi:10.1016/j.palaeo.2008.01.003

Jickells, T. D., An, Z. S., Andersen, K. K., Baker, A. R., Bergametti, G., Brooks, N., et al. (2005). Global iron connections between desert dust, ocean biogeochemistry, and climate. *Science* 308 (5718), 67–71. doi:10.1126/science.1105959

Joeckel, R. M., Suarez, C. A., McLean, N. M., Möller, A., Ludvigson, G. A., Suarez, M. B., et al. (2023). Berriasian–valanginian geochronology and carbon-isotope stratigraphy of the yellow cat member, cedar mountain formation, eastern Utah, USA. *Geosciences* 13 (2), 32. doi:10.3390/geosciences13020032

Jones, B., and Manning, D. A. (1994). Comparison of geochemical indices used for the interpretation of palaeoredox conditions in ancient mudstones. *Chem. Geol.* 111 (1-4), 111–129. doi:10.1016/0009-2541(94)90085-x

Jørgensen, B. B., and Bak, F. (1991). Pathways and microbiology of thiosulfate transformations and sulfate reduction in a marine sediment (Kattegat, Denmark). *Appl. Environ. Microbiol.* 57 (3), 847–856. doi:10.1128/aem.57.3.847-856.1991

Juncher, J. C., Jacobsen, O. S., Elberling, B., and Aamand, J. (2009). Microbial oxidation of pyrite coupled to nitrate reduction in anoxic groundwater sediment. *Environ. Sci. & Technol.* 43 (13), 4851–4857. doi:10.1021/es803417s

Kerr, A. C. (1998). Oceanic plateau formation: a cause of mass extinction and black shale deposition around the Cenomanian–Turonian boundary? *J. Geol. Soc.* 155 (4), 619–626. doi:10.1144/gsjgs.155.4.0619

Khudoley, K. M., and Meyerhoff, A. A. (1971). *Paleogeography and geological history of greater antilles*, 129. Colorado, USA: Geological Society of America.

Killops, S. D., and Killops, V. J. (2013). *Introduction to organic geochemistry*. John Wiley & Sons.

Klinkhammer, G. P., and Palmer, M. R. (1991). Uranium in the oceans: where it goes and why. *Geochimica Cosmochimica Acta* 55 (7), 1799–1806. doi:10.1016/0016-7037(91)90024-y

Kremling, K. (1983). The behavior of Zn, Cd, Cu, Ni, Co, Fe, and Mn in anoxic Baltic waters. *Mar. Chem.* 13 (2), 87–108. doi:10.1016/0304-4203(83)90019-1

Kuhn, O., Weissert, H., Föllmi, K. B., and Hennig, S. (2005). Altered carbon cycling and trace-metal enrichment during the late Valanginian and early Hauterivian. *Eclogae Geol. Helvetiae* 98, 333–344. doi:10.1007/s00015-005-1172-7

Kujau, A., Heimhofer, U., Hochuli, P. A., Pauly, S., Morales, C., Adatte, T., et al. (2013). Reconstructing Valanginian (Early Cretaceous) mid-latitude vegetation and climate dynamics based on spore–pollen assemblages. *Rev. Palaeobot. Palynology* 197, 50–69. doi:10.1016/j.revpalbo.2013.05.003

Kujau, A., Heimhofer, U., Ostertag-Henning, C., Gréselle, B., and Mutterlose, J. (2012). No evidence for anoxia during the Valanginian carbon isotope event—an organic-geochemical study from the Vocontian Basin, SE France. *Glob. Planet. Change* 92, 92–104. doi:10.1016/j.gloplacha.2012.04.007

Lakova, I., and Petrova, S. (2013). Towards a standard tithonian to valanginian calpionellid zonation of the tethyan realm. *Acta Geol. Pol.* 63 (2), 201–222n. doi:10.2478/agp-2013-0008

Larson, R. L., and Erba, E. (1999). Onset of the Mid-Cretaceous greenhouse in the Barremian-Aptian: igneous events and the biological, sedimentary, and geochemical responses. *Paleoceanography* 14 (6), 663–678. doi:10.1029/1999pa900040

Leckie, R. M., Bralower, T. J., and Cashman, R. (2002). Oceanic anoxic events and plankton evolution: biotic response to tectonic forcing during the mid-Cretaceous. *Paleoceanography* 17 (3), 13–21. doi:10.1029/2001pa000623

Lerman, A. (1978). Chemical exchange across sediment-water interface. *Annu. Rev. Earth Planet. Sci.* 6 (1), 281–303. doi:10.1146/annurev.ea.06.050178.001433

Leventhal, J. S. (1983). An interpretation of carbon and sulfur relationships in Black Sea sediments as indicators of environments of deposition. *Geochimica Cosmochimica Acta* 47 (1), 133–137. doi:10.1016/0016-7037(83)90097-2

Lewan, M. D. (1984). Factors controlling the proportionality of vanadium to nickel in crude oils. *Geochimica Cosmochimica Acta* 48 (11), 2231–2238. doi:10.1016/0016-7037(84)90219-9

Lewan, M. D. (1997). Experiments on the role of water in petroleum formation. *Geochimica Cosmochimica Acta* 61 (17), 3691–3723. doi:10.1016/s0016-7037(97)00176-2

Lini, A., Weissert, H., and Erba, E. (1992). The Valanginian carbon isotope event: a first episode of greenhouse climate conditions during the Cretaceous. *Terra nova.* 4 (3), 374–384. doi:10.1111/j.1365-3121.1992.tb00826.x

Lipinski, M., Warning, B., and Brumsack, H. J. (2003). Trace metal signatures of jurassic/cretaceous black shales from the Norwegian shelf and the barents sea. *Palaeogeogr. Palaeoclimatol. Palaeoecol.* 190, 459–475. doi:10.1016/s0031-0182(02)00619-3

Llaguno, J. R. (2017). Environmental conditions of deposition, origin, and relative maturity of organic matter in uppermost Barremian-Lowest Aptian limestones of the Eastern Prada Quarry section, Organyà Basin, South-Central Pyrenees, Spain. *Fla. Int. Univ.*, 93. MS Thesis.

López-Martínez, R., Barragán, R., Bernal, J. P., Reháková, D., Gómez-Tuena, A., Martini, M., et al. (2017). Integrated stratigraphy and isotopic ages at the berriasian–valanginian boundary at Tlatlauquitepec (Puebla, Mexico). *J. S. Am. Earth Sci.* 75, 1–10. doi:10.1016/j.jsames.2016.12.003

López-Martínez, R., Barragán, R., Reháková, D., and Cobiella-Reguera, J. L. (2013). Calpionellid distribution and microfacies across the Jurassic/Cretaceous boundary in western Cuba (Sierra de los Órganos). *Geol. Carpathica* 64 (3), 195–208. doi:10.2478/geoca-2013-0014

Magnier, C., Moretti, I., López, J. O., Gaumet, F., López, J. G., and Letouzey, J. (2004). Geochemical characterization of source rocks, crude oils, and gases of Northwest Cuba. *Mar. Petroleum Geol.* 21 (2), 195–214. doi:10.1016/j.marpetgeo.2003.11.009

Martin, J. H. (1992). "Iron as a limiting factor in oceanic productivity," in *Primary productivity and biogeochemical cycles in the sea* (Boston, MA: Springer US), 123–137.

Martin, J. H., and Fitzwater, S. E. (1988). Iron deficiency limits phytoplankton growth in the north-east Pacific subarctic. *Nature* 331, 341–343. doi:10.1038/331341a0

Martinez, M., Aguado, R., Company, M., Sandoval, J., and O'Dogherty, L. (2020). Integrated astrochronology of the Barremian stage (early cretaceous) and its biostratigraphic subdivisions. *Glob. Planet. Change* 195, 103368. doi:10.1016/j.gloplacha.2020.103368

Martinez, M., Aguirre-Urreta, B., Dera, G., Lescano, M., Omarini, J., Tunik, M., et al. (2023). Synchrony of carbon cycle fluctuations, volcanism, and orbital forcing during the Early Cretaceous. *Earth-Science Rev.* 239, 104356. doi:10.1016/j.earscirev.2023.104356

Martinez, M., Deconinck, J. F., Pellenard, P., Riquier, L., Company, M., Reboulet, S., et al. (2015). Astrochronology of the Valanginian–Hauterivian stages (early cretaceous): chronological relationships between the paraná–etendeka large igneous province and the Weissert and the faraoni events. *Glob. Planet. Change* 131, 158–173. doi:10.1016/j.gloplacha.2015.06.001

Martiny, A. C., Lomas, M. W., Fu, W., Boyd, P. W., Chen, Y. L. L., Cutter, G. A., et al. (2019). Biogeochemical controls of surface ocean phosphate. *Sci. Adv.* 5 (8), eaax0341. doi:10.1126/sciadv.aax0341

Marton, G. L., and Buffler, R. T. (1999). Jurassic—early Cretaceous tectono-paleogeographic evolution of the southeastern Gulf of Mexico basin. *Sediment. basins world* 4, 63–91.

McManus, J., Berelson, W. M., Severmann, S., Poulson, R. L., Hammond, D. E., Klinkhammer, G. P., et al. (2006). Molybdenum and uranium geochemistry in continental margin sediments: paleoproxy potential. *Geochimica Cosmochimica Acta* 70 (18), 4643–4662. doi:10.1016/j.gca.2006.06.1564

Melinte, D. M., and Mutterlose, J. (2001). A Valanginian (Early Cretaceous) 'boreal nannoplankton excursion' in sections from Romania. *Mar. Micropaleontol.* 43, 1–25. doi:10.1016/s0377-8398(01)00022-6

Menegatti, A. P., Weissert, H., Brown, R. S., Tyson, R. V., Farrimond, P., Strasser, A., et al. (1998). High resolution $^{13}$C stratigraphy through the early aptian "livello selli" of the alpine Tethys. *Paleoceanography* 13 (5), 530–545. doi:10.1029/98pa01793

Meyers, P. A. (1997). Organic geochemical proxies of paleoceanographic, paleolimnologic, and paleoclimatic processes. *Org. Geochem.* 27 (5-6), 213–250. doi:10.1016/s0146-6380(97)00049-1

Michalík, J., Lintnerová, O., Reháková, D., Boorová, D., and Simo, V. (2012). Early Cretaceous sedimentary evolution of a pelagic basin margin (the Manín Unit, central Western Carpathians, Slovakia). *Cretac. Res.* 38, 68–79. doi:10.1016/j.cretres.2012.02.006

Moretti, I., Tenreyro, R., Linares, E., López, J. G., Letouzey, J., Magnier, C., et al. (2003). "Petroleum system of the Cuban northwest offshore zone" in editors C. Bartolini, R. T. Buffler, and J. Blickwede *The Circum-Gulf of Mexico and the Caribbean: hydrocarbon habitats, basin formation, and plate tectonics* (Tulsa, USA: AAPG Memoir 79), 675–696.

Morford, J. L., Russell, A. D., and Emerson, S. (2001). Trace metal evidence for changes in the redox environment associated with the transition from terrigenous clay to diatomaceous sediment, Saanich Inlet, BC. *Mar. Geol.* 174, 355–369. doi:10.1016/s0025-3227(00)00160-2

Morse, J. W., and Luther III, G. W. (1999). Chemical influences on trace metal-sulfide interactions in anoxic sediments. *Geochimica Cosmochimica Acta* 63, 3373–3378. doi:10.1016/s0016-7037(99)00258-6

Mukaka, M. M. (2012). Statistics corner: a guide to appropriate use of correlation coefficient in medical research. *Malawi Med. J.* 24 (3), 69–71.

Mutterlose, J., Rawson, P. F., Reboulet, S., with contributions by Baudin, F., Bulot, L., Emmanuel, L., et al. (2021). The global boundary stratotype section and point (GSSP) for the base of the hauterivian stage (lower cretaceous), La Charce, southeast France. *Episodes* 44 (2), 129–150. doi:10.18814/epiiugs/2020/020072

Myers, R. H., and Myers, R. H. (1990). *Classical and modern regression with applications*, 2. Belmont, CA: Duxbury press, 488.

Nielsen, S. G., Goff, M., Hesselbo, S. P., Jenkyns, H. C., LaRowe, D. E., and Lee, C. T. A. (2011). Thallium isotopes in early diagenetic pyrite–A paleoredox proxy? *Geochimica Cosmochimica Acta* 75 (21), 6690–6704. doi:10.1016/j.gca.2011.07.047

Nijenhuis, I. A., Bosch, H. J., Damsté, J. S., Brumsack, H. J., and De Lange, G. J. (1999). Organic matter and trace element rich sapropels and black shales: a geochemical comparison. *Earth Planet. Sci. Lett.* 169 (3-4), 277–290. doi:10.1016/s0012-821x(99)00083-7

Nriagu, J. O. (1978). Dissolved silica in pore waters of lakes ontario, erie, and superior sediments. *Limnol. Oceanogr.* 23 (1), 53–67. doi:10.4319/lo.1978.23.1.0053

Oehlert, A. M., and Swart, P. K. (2014). Interpreting carbonate and organic carbon isotope covariance in the sedimentary record. *Nat. Commun.* 5 (1), 4672. doi:10.1038/ncomms5672

Ogg, J. G., Ogg, G. M., and Gradstein, F. (2016). *A concise geologic time scale: 2016*. Elsevier.

Omaña, L., González-Arreola, C., and Núñez-Useche, F. (2017). The Berriasian–Valanginian boundary interval based on calpionellids from the Taraises Formation, Cuencamé de Ceniceros, Durango, NW Mexico: Biostratigraphic, paleoecologic and paleobiogeographic significance. *J. S. Am. Earth Sci.* 80, 589–600. doi:10.1016/j.jsames.2017.10.011

Orihuela, J., and Maurrasse, F. J.-M. R. (2022). The Pons formation of the Infierno Unit in north-western Cuba: its relation to Early Cretaceous anoxic events. *11th Int. Cretac. Symp.* Warsaw, Poland, August 22-26, 2022.

Orihuela, J., Maurrasse, F. J.-M. R., and Melinte-Dobrinescu, M. C. (2023a). "The Weissert oceanic anoxic event (Valanginian)," in *the Caribbean, Sierra de los Órganos, Western Cuba* (Lyon, France: Goldschmidt The Geochemical Society).

Orihuela, J., Melinte-Dobrinescu, M. C., and Maurrasse, F. J.-M. R. (2023b). "First record of an Oceanic Anoxic Event in the Proto-Caribbean Basin revealed by lowermost Cretaceous limestones from Sierra de los Órganos, Guaniguanico Terrain, Western Cuba," in *The 14th Romanian Symposium on Paleontology*. Bucharest, Romania, September 14-15, 2023.

Orihuela, J., Melinte-Dobrinescu, M. C., and Maurrasse, F. J.-M. R. (2024a). "Further chemostratigraphic characterization into the valanginian Weissert oceanic anoxic event in the Proto-Caribbean Basin," in *SEPM internation sedimentary geosciences congress*. Arizona, USA: Flagstaff.

Orihuela, J., Melinte-Dobrinescu, M. C., and Maurrasse, F. J.-M. R. (2024b). "Multiproxy characterization of the lower Valanginian-lower Aptian succession at the La Lata Quarry, Sierra de los Órganos, and its record of Oceanic Anoxic Events in the Proto-Caribbean," in *GSA connects 2024*. Geological Society of America. Anaheim, California, September 2024.

Özsoy, E., and Ünlüata, Ü. (1997). Oceanography of the Black Sea: a review of some recent results. *Earth-Science Rev.* 42 (4), 231–272. doi:10.1016/s0012-8252(97)81859-4

Pardo, G. (1975). "Geology of Cuba," in *The Gulf of Mexico and the caribbean* (Boston, MA: Springer), 553–615.

Pardo, G. (2009). *Geology of Cuba: AAPG studies in geology 58*, 58. Colorado, USA: AAPG.

Patton, J. W., Choquette, P. W., Guennel, G. K., Kaltenback, A. J., and Moore, A. (1984). Organic geochemistry and sedimentology of lower to mid-Cretaceous deep-sea carbonates, Sites 535 and 540, Leg 77. *Initial Rep. Deep. Drill. Proj.* 77, 417–443.

Pearson, K. (1896). VII. Mathematical contributions to the theory of evolution. —III. Regression, heredity, and panmixia. *Philosophical Trans. R. Soc. Lond. Ser. A, Contain. Pap. a Math. or Phys. character* (187), 253–318.

Pearson, K. (1900). I. Mathematical contributions to the theory of evolution. —VII. On the correlation of characters not quantitatively measurable. *Philosophical Trans. R. Soc. Lond. Ser. A, Contain. Pap. a Math. or Phys. Character* 195 (262-273), 1–47.

Pedersen, T., and Calvert, S. E. (1990). Anoxia vs. productivity: what controls the formation of organic-carbon-rich sediments and sedimentary rocks? *AAPG Bull.* 74 (4), 454–466. doi:10.1306/0c9b232b-1710-11d7-8645000102c1865d

Pendás-Amador, M. (2007). Modelos paleoambientales de los depósitos del Kimmerigdiano hasta el Eoceno inferior en el pozo Pinar 1, Sierra de los órganos; Pinar del Río. En: Memorias, Trabajos y Resúmenes. II Convención Cubana de Ciencias de la Tierra (Geociencias'2007). *Cent. Nac. Inf. Geol. Inst. Geol. Paleontol. Cuba, La Habana, CD-Rom*.

Percival, L. M., Matsumoto, H., Callegaro, S., Erba, E., Kerr, A. C., Mutterlose, J., et al. (2025). Cretaceous large igneous provinces: from volcanic formation to environmental catastrophes and biological crises. *Geol. Soc. Lond. Spec. Publ.* 544 (1), 299–342. doi:10.1144/sp544-2023-88

Percival, L. M. E., Ownsworth, E., Robinson, S. A., Selby, D., Goderis, S., and Claeys, P. (2023). Valanginian climate cooling and environmental change driven by Paraná-Etendeka basalt erosion. *Geology* 51, 753–757. doi:10.1130/g51202.1

Pérez, G. W., Cobiella Reguera, J. L., and Barragán, R. (2011). "Estudio de un corte del Cretácico temprano, en el miembro Tumbitas (Formación Guasasa), Sierra del Infierno, Sierra de los Órganos, Cuba Occidental," in *IX Congreso Cubano de Geología: Estratigrafía y Paleontología (Geo2-08)*. La Habana, Cuba.

Phelps, R. M., Kerans, C., Loucks, R. G., Da Gama, R. O., Jeremiah, J., and Hull, D. (2014). Oceanographic and eustatic control of carbonate platform evolution and sequence stratigraphy on the Cretaceous (Valanginian–Campanian) passive margin, northern Gulf of Mexico. *Sedimentology* 61 (2), 461–496. doi:10.1111/sed.12062

Phillips, R., and Xu, J. (2021). A critical review of molybdenum sequestration mechanisms under euxinic conditions: implications for the precision of molybdenum paleoredox proxies. *Earth-Science Rev.* 221, 103799. doi:10.1016/j.earscirev.2021.103799

Pindell, J. L. (1985). Alleghenian reconstruction and subsequent evolution of the Gulf of Mexico, Bahamas, and proto-caribbean. *Tectonics* 4 (1), 1–39. doi:10.1029/tc004i001p00001

Pindell, J. L., Graham, R., and Horn, B. W. (2020). "Role of outer marginal collapse on salt deposition in the eastern Gulf of Mexico," in *Campos, and Santo's basins* (London, UK: Geological Society)

Pindell, J. L., and Kennan, L. (2009). "Tectonic evolution of the Gulf of Mexico, Caribbean, and northern South America in the mantle reference frame: an update" in eds. K. H. James, M. A. Lorente, and J. L. Pindell *The origin and evolution of the caribbean plate* (London, UK: Geological Society, London, Special Publications, 328).1, 55. doi:10.1144/sp328.1

Pindell, J. L., Villagómez, D., Molina-Garza, R., Graham, R., and Weber, B. (2021a). *A revised synthesis of the rift and drift history of the Gulf of Mexico and surrounding regions in the light of improved age dating of the Middle Jurassic salt*, 504. Colorado Geological Society, London, Special Publications, 29–76. doi:10.1144/SP504-2020-43

Pindell, J. L., Weber, B., Hale-Erlich, W., Cossey, S., Bitter, M., Garza, R. M., et al. (2021b). "Strontium isotope dating of evaporites and the breakup of the Gulf of Mexico and proto–caribbean Seaway" in Editors U. Martens, and R. S. Molina *Garza southern and central méxico: basement framework, tectonic evolution, and provenance of mesozoic–cenozoic basins* Geological Society of America Special Paper 546,309–329. doi:10.1130/2020.2546(12)

Piotrowska, K. (1976). Tectonic style of the Sierra de los Órganos (Cuba). *Bull. Acad. Pol. Sc., Ser. Terre* 24 (314), 217–226.

Piotrowska, K. (1978). Nappe structures in the Sierra de los Órganos, western Cuba. *Acta Geol. Pol.* 28 (1), 97–170.

Piotrowska, K. (1993). Interrelationship of the terranes in western and central Cuba. *Tectonophysics* 219 (4), 273–282. doi:10.1016/0040-1951(93)90178-m

Ponton, C., and Maurrasse, F. J.-M. R. (2006). Aptian deposits of the Provencal Platform of Southern France: evidence for low-oxygen conditions and the influence of local physiography. *Geol. Soc. Am. Abstr. Programs* 38 (7), 492.

Ponton Guerrero, C. (2006). Barremian-aptian depositional environments and their sediments: the Mexican versus the provencal (France) platforms, paleotectonic and paleoclimatic implications. *Fla. Int. Univ.*, 113. MS Thesis.

Price, G. D., Bajnai, D., and Fiebig, J. (2020). Carbonate clumped isotope evidence for latitudinal seawater temperature gradients and the oxygen isotope composition of Early Cretaceous seas. *Palaeogeogr. Palaeoclimatol. Palaeoecol.* 552, 109777. doi:10.1016/j.palaeo.2020.109777

Price, G. D., Ruffell, A. H., Jones, C. E., Kalin, R. M., and Mutterlose, J. (2000). Isotopic evidence for temperature variation during the early Cretaceous (late Ryazanian–mid-Hauterivian). *J. Geol. Soc.* 157 (2), 335–343. doi:10.1144/jgs.157.2.335

Pszczółkowski, A. (1971). Jurassic, Cretaceous and Paleogene deposits of Sierra del Rosario (Cuba). Bulletin of the Polish Academy of Sciences. *Earth Sci.* 19, 249–259.

Pszczółkowski, A. (1978). Geosynclinal sequences of the Cordillera de Guaniguanico in western Cuba; their lithostratigraphy, facies development, and paleogeography. *Acta Geol. Pol.* 28 (1), 1–96.

Pszczółkowski, A. (1987). Paleogeography and tectonic evolution of Cuba and adjoining areas during the Jurassic-Early Cretaceous. *Ann. Soc. Geol. Pol.* 57, 127–142.

Pszczółkowski, A. (1999a). New data on the Lower Cretaceous microfossil and nannoconid stratigraphy in the Guaniguanico terrane of western Cuba. *Stud. Geol. Pol.* 114, 7–33.

Pszczółkowski, A. (1999b). "The exposed passive margin of North America in western Cuba,". *Sedimentary basins of the world*. Editors C. Bartolini, R. Buffler, and J. C. Pashin (Elsevier), 4, 93–121.

Pszczółkowski, A., García Delgado, D., and Gil González, S. (2013). "Planktonic foraminifers and nannoconid assemblages from the Late Aptian and Late Albian limestones of the Pons Formation (Sierra de los Órganos, western Cuba)," in *V Convención de Ciencias de la Tierra (Geociencias' 2013), 1 al 5 de abril de 2013. X Congreso Cubano de Geología (Geología'2013)*, 10. Memorias en CD-Rom, GE02.

Pszczółkowski, A., and Myczyński, R. (1999). Nannoconid assemblage in upper Hauterivian-lower Aptian limestones of Cuba: their correlation with ammonites and some planktonic foraminifers. *Stud. Geol. Pol.* 114, 35–75.

Pszczółkowski, A., and Myczyński, R. (2003). "Stratigraphic constraints on the late Jurassic-cretaceous paleotectonic interpretations of the placetas belt in Cuba,". *The circum-Gulf of Mexico and the Caribbean; hydrocarbon habitats, basin formation, and plate tectonics*. Editors C. Bartolini, R. T. Buffler, and J. F. Blickwede (American Association of Petroleum Geologists Memoir), 79, 545–581.

Pszczółkowski, A., and Myczyński, R. (2010). Tithonian-early Valanginian evolution of deposition along the proto-Caribbean margin of North America recorded in Guaniguanico successions (western Cuba). *J. S. Am. Earth Sci.* 29, 225–253. doi:10.1016/j.jsames.2009.07.004

Pszczółkowski, A., Piotrowska, K., Mycznski, R., Piotrowski, J., Skupinski, A., Grodzicki, J., et al. (1975). Texto explicativo al mapa geológico a escala 1:250 000 de la provincia de Pinar del Río. *Brigada Cubano-Polaca, Inst. Geol. Paleont., Minist. Indust. Bas., La Habana (Unedited)*.

Reboulet, S., Mattioli, E., Pittet, B., Baudin, F., Olivero, D., and Proux, O. (2003). Ammonoid and nannoplankton abundance in Valanginian (early Cretaceous) limestone–marl successions from the southeast France Basin: carbonate dilution or productivity? *Palaeogeogr. Palaeoclimatol. Palaeoecol.* 201 (1-2), 113–139. doi:10.1016/s0031-0182(03)00541-8

Reháková, D., and Michalík, J. (1997). Evolution and distribution of calpionellids—the most characteristic constituents of Lower Cretaceous Tethyan microplankton. *Cretac. Res.* 18 (3), 493–504. doi:10.1006/cres.1997.0067

Renne, P. R., Glen, J. M., Milner, S. C., and Duncan, A. R. (1996). Age of Etendeka flood volcanism and associated intrusions in southwestern Africa. *Geology* 24 (7), 659–662. doi:10.1130/0091-7613(1996)024<0659:aoefva>2.3.co;2

Rhoads, D. C., and Morse, J. W. (1971). Evolutionary and ecologic significance of oxygen-deficient marine basins. *Lethaia* 4 (4), 413–428. doi:10.1111/j.1502-3931.1971.tb01864.x

Rickard, D., and Morse, J. W. (2005). Acid volatile sulfide (AVS). *Mar. Chem.* 97 (3-4), 141–197. doi:10.1016/j.marchem.2005.08.004

Rigassi-Studer, D. (1963). Sur le géologie de la Sierra de los Órganos, Cuba. *Archives des Sci. Physique d'Histoire Naturelle Geneve* 16 (2), 339–350.

Rimmer, S. M., Thompson, J. A., Goodnight, S. A., and Robl, T. L. (2004). Multiple controls on the preservation of organic matter in Devonian–Mississippian marine black shales: geochemical and petrographic evidence. *Palaeogeogr. Palaeoclimatol. Palaeoecol.* 215, 125–154. doi:10.1016/s0031-0182(04)00466-3

Rocha, B. C., Davies, J. H., Janasi, V. A., Schaltegger, U., Nardy, A. J., Greber, N. D., et al. (2020). Rapid eruption of silicic magmas from the Paraná magmatic province (Brazil) did not trigger the Valanginian event. *Geology* 48 (12), 1174–1178. doi:10.1130/g47766.1

Roth, P. H. (1978). Calcareous nannoplankton biostratigraphy and oceanography of the northwestern Atlantic ocean. *Initial Rep. Deep-Sea Drill. Proj.* 44, 731–760.

Roth, P. H. (1983). Jurassic and lower cretaceous calcareous nannofossils in the western North Atlantic (site 534): biostratigraphy, preservation, and some observations on biogeography and palaeoceanography. *Initial Rep. Deep-Sea Drill. Proj.* 76, 587–621.

Rowe, O. F., Paczkowska, J., Brutemark, A., Brugel, S., Traving, S. J., Lefébure, R., et al. (2025). Climate change–induced terrestrial matter runoff may decrease food web production in coastal ecosystems. *Limnol. Oceanogr.* 9999, 1–13. doi:10.1002/lno.12762

Ruvalcaba Baroni, I., Van Helmond, N. A. G. M., Tsandev, I., Middelburg, J. J., and Slomp, C. P. (2015). The nitrogen isotope composition of sediments from the proto-North Atlantic during Oceanic Anoxic Event 2. *Paleoceanography* 30 (7), 923–937. doi:10.1002/2014pa002744

Saltzman, M. R., Thomas, E., Gradstein, F. M., Ogg, J. G., and Schmitz, M. (2012). Carbon isotope stratigraphy. *Geol. time scale* 1, 207–232. doi:10.1016/b978-0-444-59425-9.00011-1

Sanchez-Hernandez, Y., and Maurrasse, F. J.-M. R. (2014). Geochemical characterization and redox signals from the latest Barremian to the earliest Aptian in a restricted marine basin: el Pui section, Organyà Basin, south-central Pyrenees. *Chem. Geol.* 372, 12–31. doi:10.1016/j.chemgeo.2014.02.011

Sanchez-Hernandez, Y., and Maurrasse, F. J.-M. R. (2016). The influence of regional factors in the expression of oceanic anoxic event 1a (OAE1a) in the semi-restricted Organyà Basin, south-central Pyrenees, Spain. *Palaeogeogr. Palaeoclimatol. Palaeoecol.* 441, 582–598. doi:10.1016/j.palaeo.2015.06.031

Schafhauser, A., Stinnesbeck, W., Holland, B., Adatte, T., and Remane, J. (2003). Lower Cretaceous pelagic limestones in southern Belize: proto-Caribbean deposits on the southeastern Maya block. *AAPG Spec.*, 624–637.

Schenck, C. J. (2008). *Jurassic-cretaceous composite total petroleum system and geologic models for oil and gas assessment of the North Cuba basin, Cuba. US geological survey North Cuba basin assessment team, Jurassic-Cretaceous composite total petroleum system and geologic assessment of oil and gas resources of the North Cuba basin*, 94. Washington D.C., USA: Cuba: US Geological Survey Digital Data Series DDS-69-M. doi:10.3133/ds69M

Schlager, W., Buffler, R. T., Angstadt, D., Bowdler, J. L., Cotillon, P. H., Dallmeyer, R. D., et al. (1984). Deep sea drilling project, leg 77, southeastern Gulf of Mexico. *Geol. Soc. Am. Bull.* 95 (2), 226–236. doi:10.1130/0016-7606(1984)95<226:dsdpls>2.0.co;2

Schlanger, S. O., Arthur, M. A., Jenkyns, H. C., and Scholle, P. A. (1987). The Cenomanian-Turonian Oceanic Anoxic Event, I. Stratigraphy, and distribution of organic carbon-rich beds and the marine δ13C excursion. *Geol. Soc.* 26 (1), 371–399. doi:10.1144/gsl.sp.1987.026.01.24

Schlanger, S. O., and Jenkyns, H. (1976). Cretaceous oceanic anoxic events: causes and consequences. *Geol. Mijnb.* 55 (3-4).

Scholle, P. A., and Arthur, M. A. (1980). Carbon isotope fluctuations in Cretaceous pelagic limestones: potential stratigraphic and petroleum exploration tool. *AAPG Bull.* 64 (1), 67–87. doi:10.1306/2f91892d-16ce-11d7-8645000102c1865d

Scholz, F., Hensen, C., Noffke, A., Rohde, A., Liebetrau, V., and Wallmann, K. (2011). Early diagenesis of redox-sensitive trace metals in the Peru upwelling area–response to ENSO-related oxygen fluctuations in the water column. *Geochimica Cosmochimica Acta* 75 (22), 7257–7276. doi:10.1016/j.gca.2011.08.007

Schoonen, M. A. (2004). *Mechanisms of sedimentary pyrite formation*. Special papers-Geological Society of America, 117–134.

Schubert, C. J., and Nielsen, B. (2000). Effects of decarbonation treatments on $\delta^{13}C$ values in marine sediments. *Mar. Chem.* 72 (1), 55–59. doi:10.1016/s0304-4203(00)00066-9

Scott, C., Lyons, T. W., Bekker, A., Shen, Y. A., Poulton, S. W., Chu, X. L., et al. (2008). Tracing the stepwise oxygenation of the proterozoic ocean. *Nature* 452 (7186), 456–459. doi:10.1038/nature06811

Seibold, E. (1975). Der Meeresboden Forschungsstand und Zukunftsaufgaben. *Naturwissenchaften* 62, 321–330. doi:10.1007/bf00608892

Silva Gomes, A., and Vasconcelos, P. M. (2021). Geochronology of the Paraná-Etendeka large igneous province. *Earth-Science Rev.* 220, 103716. doi:10.1016/j.earscirev.2021.103716

Silva-Tamayo, J. C., Ramirez, C., Lara, M., Sial, A. N., Trujillo, D., and Salazar, E. (2016). Sedimentology and chemostratigraphy of a valanginian carbonate succession from the baja guajira basin, northern Colombia. *Braz. J. Geol.* 46, 163–180. doi:10.1590/2317-488920160030294

Socorro, J., and Maurrasse, F. J. M. (2020). Regional palaeoenvironmental influence on organic matter sequestration and characteristics of carbon isotope segment C5 in a hemipelagic sequence, Organyà Basin, northeast Spain. *Depositional Rec.* 6 (3), 552–580. doi:10.1002/dep2.111

Socorro, J., and Maurrasse, F. J.-M. R. (2019). Continuous accumulation of organic matter-rich sediments associated with Oceanic Anoxic Event 1a in the El Pujal section, Organyà Basin, Catalunyà Spain and its relation to episodic dysoxia. *Cretac. Res.* 95, 225–251. doi:10.1016/j.cretres.2018.11.009

Socorro, J., and Maurrasse, F. J.-M. R. (2022). Demise of organic matter–rich facies and changing paleoenvironmental conditions associated with the end of carbon isotope segment C5 of oceanic anoxic event 1a in the north and northeastern iberian Peninsula. *J. Geol.* 130 (2), 133–170. doi:10.1086/718834

Sohrin, Y., Iwamoto, S. I., Akiyama, S., Fujita, T., Kugii, T., Obata, H., et al. (1998). Determination of trace elements in seawater by fluorinated metal alkoxide glass-immobilized 8-hydroxyquinoline concentration and high-resolution inductively coupled plasma mass spectrometry detection. *Anal. Chim. Acta* 363 (1), 11–19. doi:10.1016/s0003-2670(98)00074-9

Sprovieri, M., Coccioni, R., Lirer, F., Pelosi, N., and Lozar, F. (2006). Orbital tuning of a lower Cretaceous composite record (Maiolica Formation, central Italy). *Paleoceanography* 21 (4), PA4212. doi:10.1029/2005PA001224

Swart, P. K. (2008). Global synchronous changes in the carbon isotopic composition of carbonate sediments unrelated to changes in the global carbon cycle. *Proc. Natl. Acad. Sci.* 105 (37), 13741–13745. doi:10.1073/pnas.0802841105

Swart, P. K., Blättler, C. L., Nakakuni, M., Mackenzie, G. J., Betzler, C., Eberli, G. P., et al. (2019). Cyclic anoxia and organic rich carbonate sediments within a drowned carbonate platform linked to Antarctic ice volume changes: late Oligocene-early Miocene Maldives. *Earth Planet. Sci. Lett.* 521, 1–13. doi:10.1016/j.epsl.2019.05.019

Swart, P. K., and Oehlert, A. M. (2018). Revised interpretations of stable C and O patterns in carbonate rocks resulting from meteoric diagenesis. *Sediment. Geol.* 364, 14–23. doi:10.1016/j.sedgeo.2017.12.005

Taylor, A. M., and Goldring, R. (1993). Description and analysis of bioturbation and ichnofabric. *J. Geol. Soc.* 150 (1), 141–148. doi:10.1144/gsjgs.150.1.0141

Tesdal, J. E., Galbraith, E. D., and Kienast, M. (2013). Nitrogen isotopes in bulk marine sediment: linking seafloor observations with subseafloor records. *Biogeosciences* 10 (1), 101–118. doi:10.5194/bg-10-101-2013

Thierstein, H. R. (1973). Lower cretaceous calcareous nannoplankton biostratigraphy. *Abh. Geol. Bundesanst.* 29, 3–52.

Thöle, H., Bornemann, A., Heimhofer, U., Luppold, F. W., Blumenberg, M., Dohrmann, R., et al. (2020). Using high-resolution XRF analyses as a sequence stratigraphic tool in a mudstone-dominated succession (Early Cretaceous, Lower Saxony Basin, Northern Germany). *Depositional Rec.* 6 (1), 236–258. doi:10.1002/dep2.83

Tribovillard, N., Algeo, T. J., Lyons, T., and Riboulleau, A. (2006). Trace metals as paleoredox and paleoproductivity proxies: an update. *Chem. Geol.* 232 (1-2), 12–32. doi:10.1016/j.chemgeo.2006.02.012

Tribovillard, N. P. (1998). Cyanobacterially generated peloids in laminated, organic-matter rich, limestones, an unobtrusive presence. *Terra nova.* 10, 126–130. doi:10.1046/j.1365-3121.1998.00177.x

Turekian, K. K., and Wedepohl, K. H. (1961). Distribution of the elements in some major units of the Earth's crust. *Geol. Soc. Am. Bull.* 72, 175–192. doi:10.1130/0016-7606(1961)72[175:doteis]2.0.co;2

Tyson, R. V., and Pearson, T. H. (1991). "Modern and ancient continental shelf anoxia: an overview" in eds. R. V. Tyson, and T. H. Pearson *Modern and ancient continental shelf anoxia* (London, UK: Geological Society of London Special Publication, 58), 1–24. doi:10.1144/gsl.sp.1991.058.01.01

Van der Weijden, C. H. (2002). Pitfalls of normalization of marine geochemical data using a common divisor. *Mar. Geol.* 184 (3-4), 167–187. doi:10.1016/s0025-3227(01)00297-3

Van Mooy, B. A. S., Krupke, A., Dyhrman, S. T., Fredricks, H. F., Friischkorn, K. R., Ossolinski, J. E., et al. (2015). Major role of planktonic phosphate reduction in the marine phosphorus redox cycle. *Science* 348, 783–785. doi:10.1126/science.aaa8181

Vázquez Torres, M., Pino Torga, R., Hernández Mesa, Y., Ramírez Hernández, R., and Núñez Mantilla, H. (2020). *Mapa Geológico de la República de Cuba a Escala 1:50 000, hoja explicativa 3483-IV Minas de Matahambre*. La Habana, Cuba: Empresa Geominera de Pinar del Rio, Instituto de Geología y Paleontología Servicio Geológico de Cuba.

Wang, L., Shi, X., and Jiang, G. (2012). Pyrite morphology and redox fluctuations recorded in the Ediacaran Doushantuo Formation. *Palaeogeogr. Palaeoclimatol. Palaeoecol.* 333, 218–227. doi:10.1016/j.palaeo.2012.03.033

Wedepohl, K. H. (1971). Environmental influences on the chemical composition of shales and clays. *Phys. Chem. Earth* 8, 307–333. doi:10.1016/0079-1946(71)90020-6

Weissert, H. (1979). Die Paläozeanographie der Südwestlichen Tethys in der Unterbeide. *Mitt. Geol. Inst. Eidg. Tech. Hochsch. Univ. Zürich* 226, 174.

Weissert, H. (1981). *The environment of deposition of black shales in the early Cretaceous: an ongoing controversy*, 32. SPEM Special Publication, 547–560.

Weissert, H. (1989). C-isotope stratigraphy, a monitor of paleoenvironmental change: a case study from the Early Cretaceous. *Surv. Geophys.* 10 (1), 1–61. doi:10.1007/bf01901664

Weissert, H. (1990). Siliciclastics in the early cretaceous Tethys and North Atlantic oceans – documents of periodic greenhouse climate conditions. *Mem. della Soc. Geol. Ital.* 44, 59–69.

Weissert, H. (2019). Mesozoic C-cycle perturbations and climate: evidence for increased resilience of the Cretaceous biosphere to greenhouse pulses. *Can. J. Earth Sci.* 56 (12), 1366–1374. doi:10.1139/cjes-2018-0227

Weissert, H., and Erba, E. (2004). Volcanism, $CO_2$, and paleoclimate: a Late Jurassic–Early Cretaceous carbon oxygen isotope record. *J. Geol. Soc. Lond.* 161, 1–8.

Weissert, H., Joachimski, M., and Sarnthein, M. (2008). Chemostratigraphy. *Newsl. Stratigr.* 42 (3), 145–179. doi:10.1127/0078-0421/2008/0042-0145

Weissert, H., Lini, A., Föllmi, K. B., and Kuhn, O. (1998). Correlation of Early Cretaceous carbon isotope stratigraphy and platform drowning events: a possible link? *Palaeogeogr. Palaeoclimatol. Palaeoecol.* 137 (3-4), 189–203. doi:10.1016/s0031-0182(97)00109-0

Weissert, H., McKenzie, J. A., and Channell, J. E. T. (1985). Natural variations in the carbon cycle during the Early Cretaceous. *carbon cycle Atmos. $CO_2$ Nat. Var. Archean Present* 32, 531–545. doi:10.1029/gm032p0531

Westermann, S., Föllmi, K. B., Adatte, T., Matera, V., Schnyder, J., Fleitmann, D., et al. (2010). The Valanginian δ13C excursion may not be an expression of a global oceanic anoxic event. *Earth Planet. Sci. Lett.* 290 (1-2), 118–131. doi:10.1016/j.epsl.2009.12.011

Wignall, P. B., and Myers, K. J. (1988). Interpreting benthic oxygen levels in mudrocks: a new approach. *Geology* 16, 452–455. doi:10.1130/0091-7613(1988)016<0452:ibolim>2.3.co;2

Wignall, P. B., and Newton, R. (1998). Pyrite framboid diameter as a measure of oxygen deficiency in ancient mudrocks. *Am. J. Sci.* 298 (7), 537–552. doi:10.2475/ajs.298.7.537

Wignall, P. B., and Twitchett, R. J. (1996). Oceanic anoxia and the end Permian mass extinction. *Science* 272, 1155–1158. doi:10.1126/science.272.5265.1155

Wilkin, R. T., Arthur, M. A., and Dean, W. E. (1997). History of water-column anoxia in the Black Sea indicated by pyrite framboid size distributions. *Earth Planet. Sci. Lett.* 148, 517–525. doi:10.1016/s0012-821x(97)00053-8

Wilkin, R. T., Barnes, H. L., and Brantley, S. L. (1996). The size distribution of framboidal pyrite in modern sediments: an indicator of redox conditions. *Geochimica Cosmochimica Acta* 60 (20), 3897–3912. doi:10.1016/0016-7037(96)00209-8

Williams, L. B., Ferrell, Jr. R. E., Hutcheon, I., Bakel, A. J., Walsh, M. M., and Krouse, H. R. (1995). Nitrogen isotope geochemistry of organic matter and minerals during diagenesis and hydrocarbon migration. *Geochimica Cosmochimica Acta* 59 (4), 765–779. doi:10.1016/0016-7037(95)00005-k

Yano, M., Yasukawa, K., Nakamura, K., Ikehara, M., and Kato, Y. (2020). Geochemical features of redox-sensitive trace metals in sediments under oxygen-depleted marine environments. *Minerals* 10 (11), 1021. doi:10.3390/min10111021

Ye, Y. T., Wu, C. D., Zhai, L. N., and An, Z. Z. (2016). Pyrite morphology and episodic euxinia of the ediacaran doushantuo Formation in south China. *Sci. China Earth Sci.* 60, 102–113. doi:10.1007/s11430-016-0066-0

Zheng, Y., Anderson, R. F., van Geen, A., and Fleisher, M. Q. (2002). Remobilization of authigenic uranium in marine sediments by bioturbation. *Geochimica Cosmochimica Acta* 66 (10), 1759–1772. doi:10.1016/s0016-7037(01)00886-9